UARL F910336-24

FINAL REPORT

INVESTIGATION OF THE IGNITION
AND COMBUSTION OF METAL WIRES

by

D. K. Kuehl and M. L. Zwillenberg

prepared for

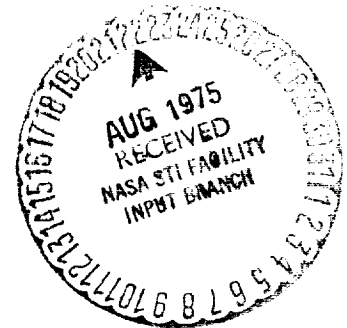NATIONAL AERONAUTICS AND SPACE ADMINISTRATION

May, 1967

CONTRACT NAS 7-353

United Aircraft Research Laboratories

U

UNITED AIRCRAFT CORPORATION

A

EAST HARTFORD, CONNECTICUT

United Aircraft Research Laboratories

U
UNITED AIRCRAFT CORPORATION
A

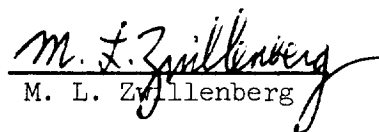### EAST HARTFORD, CONNECTICUT

Report F910336-24

Investigation of the Ignition
and Combustion of Metal Wires

Final Report Contract NAS 7-353

REPORTED BY _____

D. K. Kuehl

_____

M. L. Zwillenberg

APPROVED BY _____

W. G. Burwell, Chief
Kinetics & Thermal Sciences

DATE May 1967

NO. OF PAGES 138

COPY NO. 31

FOREWARD

The work described herein was performed by United Aircraft Research Laboratories for the National Aeronautics and Space Administration under Contract NAS 7-353 initiated March 16, 1965. This program has involved experimental and theoretical studies to investigate the ignition and combustion characteristics of beryllium and aluminum.

Included among those who cooperated in performance of the work under Contract NAS 7-353 were Mr. D. K. Kuehl, Principal Investigator; Mr. M. L. Zwillenberg, Research Scientist; Dr. W. G. Burwell, Chief, Kinetics and Thermal Sciences Section; Mrs. I. S. Lukas, Engineering Assistant, and Miss D. Dimonaco, Mr. D. Kasper, Miss B. Howe, and Mrs. P. Larson, Engineering Aides of the UARL.

This work was conducted under the program management of Mr. R. W. Ziem, Chemical Propulsion Division, NASA Headquarters, Washington, D. C., and the Project Manager was Mr. W. Dowler, Jet Propulsion Laboratory, Pasadena, California.

This document is unclassified in its entirety.

Investigation of the

Ignition and Combustion of Metal Wires

by

D. K. Kuehl and M. L. Zwillenberg

ABSTRACT

This report presents a summary of the results of theoretical and experimental studies on metal ignition and combustion conducted at the United Aircraft Research Laboratories under NASA Contract NAS 7-353.

Experimental measurements were made of the ignition temperatures of aluminum and beryllium, using electrically-heated wires in cool static oxidizing atmospheres including simulated products of solid propellant combustion. The results obtained indicate that the ignition temperatures are dependent on the metal species, the pressure, and the oxidizer species and concentration. The purity of the metal and the surface treatment or condition of the metal are of particular importance in obtaining ignition. The ignition temperatures of both aluminum and beryllium can be significantly below the melting points of their respective oxides, especially in oxidizing environments not containing oxygen gas.

The burning times of spherical metal particles have been predicted using a computer program based on quasi-steady-state vapor-phase combustion. This program has been applied to the burning of aluminum and beryllium in oxygen, and mixtures of oxygen with inert gases. Improved correlation between experimental data and theoretical calculations was obtained by incorporating back diffusion of oxide from the flame to the particle in the theoretical model on which calculations were based.

CONCLUSIONS

Based on the experimental and analytical studies reported herein a number of useful conclusions may be made. These conclusions are presented below divided into three major categories: (A) those based on experiments with aluminum wires, (B) those based on experiments with beryllium wires, and (C) those based on the results of the analytical studies.

A. Aluminum Experiments

1. Aluminum ignites reproducibly in oxygen (O_2) and oxygen/argon (O_2/Ar) mixtures.

2. Above a critical ignition pressure in the range, 2-10 psia, the ignition temperature of aluminum in O_2 or O_2/Ar is approximately equal to the melting point of aluminum oxide (i.e., 2318 K). Below the critical ignition pressure, the ignition temperature of aluminum in O_2 or O_2/Ar decreases with decreasing pressure.

3. The pressure range in which aluminum ignition occurs in O_2 or O_2/Ar is reduced with decreasing oxygen mole fraction; i.e., the lower pressure limit of ignition was 0.25 psia at 100% O_2, 0.5 psia at 50% O_2, 5 psia at 30% O_2, and 16 psia at 10% O_2, while the upper pressure limit exceeded 1000 psia at 100% O_2, and was 250 psia at 50% O_2, and 125 psia at 20% O_2.

4. The ignition of aluminum wire in O_2/inert mixtures requires more energy as the inert gas has higher thermal conductivity, and application of the energy is more likely to break the wire than to cause ignition.

5. High purity (99.99 percent) aluminum ignites more readily (i.e., a greater percentage of the high purity test specimens were ignited) than less pure (99.7 percent or lower) aluminum, but at the same ignition temperature.

6. Aluminum will ignite (ca 1380 K) in pure nitrogen at pressures of 400 psia or higher.

7. Aluminum ignites below its melting point (i.e., 933 K) in chlorine tri-fluoride (CTF).

8. At low pressures aluminum burns with a voluminous vapor phase flame in oxygen containing atmospheres.

9. At high pressure and low oxygen concentrations aluminum burns on or near the surface.

10. At high pressure and high oxygen concentrations aluminum tends to fragment during combustion.

11. Vapor phase combustion produces very fine oxide particles (smoke).

12. Surface combustion produces large accumulations of oxide on the end of aluminum wire.

13. Fragmentation followed by droplet combustion produces both smoke and moderately sized oxide spheres, which are most probably caused by back diffusion of oxide from the flame to the ejected particles of aluminum.

B.   Beryllium Experiments

1. Beryllium is difficult to ignite in pure oxygen, igniting only above 16 psia and nonreproducibly.

2. The ignition temperature of beryllium in oxygen is within approximately 400 K deg of the melting point of beryllium oxide (2820 K), and is higher than the ignition temperature of aluminum.

3. The extensive pre-ignition reaction of beryllium in oxygen proves that beryllium oxide is not completely protective at high temperatures below the oxide melting point.

4. Beryllium wire clad with nickel ignites consistently in oxygen whereas no other surface treatment employed in this study produced consistent ignition.

5. Beryllium ignites below, but near, the beryllium melting point (1551 K) in gases containing water vapor.

6. In CTF, beryllium ignites at about 1100 K which is below the melting point of beryllium.

7. Beryllium ignites in pure nitrogen at 500 psia at a temperature of about 2350 K.

8. The presence of CTF mixed with the combustion products of a solid propellant should significantly affect the ignition and combustion of beryllium included in the propellant, reducing the ignition temperature and hence ignition delay of the beryllium, and oxidizing a significant portion of the beryllium to the halide rather than the oxide.

9. Beryllium wire burns in a more erratic manner than aluminum, and also more slowly overall, alternately burning cigarette fashion and then fragmenting the accumulated beryllium on the end of the wire.

10. Burning beryllium fragments more frequently than burning aluminum.

11. Beryllium cannot support self-sustaining combustion in cool simulated combustion products where the theoretical combustion temperature of the beryllium is less than the melting point of beryllium oxide, regardless of the surface treatment.

12. Beryllium will support self-sustaining combustion in cool simulated combustion products containing sufficient water that the combustion temperature of the beryllium is higher than the melting point of beryllium oxide.

C. Analytical Studies

1. Burning times, particle temperatures, and flame diameters of aluminum and beryllium particles can be predicted with satisfactory accuracy by means of a mathematical model which is based on quasi-steady-state combustion of spherical metal particles, and which includes the back diffusion of metal oxide to the particle.

2. Predicted flame temperatures and particle temperatures increase with increasing pressure, but are almost independent of the ambient temperature.

3. The predicted burning rates of aluminum and beryllium increase slightly with increasing pressure and increasing oxygen mole fraction.

4. The predicted burning rates of aluminum and beryllium are essentially independent of ambient gas temperature, up to and including 3000 K.

5. At low pressures (below 10 atm), the combustion of beryllium particles is predicted as erratic due to the condensation of solid beryllium oxide on the particles through back diffusion.

6. The predicted burning times of both aluminum and beryllium particles indicate that both should obey the "d^2" law for a wide range of particle sizes.

Investigation of the

Ignition and Combustion of Metal Wires

TABLE OF CONTENTS

LIST OF FIGURES

LIST OF TABLES

INTRODUCTION

Metals are being utilized as sources of energy through chemical reaction in a large number of applications. Specific metals such as aluminum and beryllium are of interest as ingredients in propellant formulations primarily because of their high heats of combustion in combination with conventional oxidizers. In order to attain the benefit of these energies in a variety of practical propellant systems, techniques must be found by which these metals can be easily and predictably ignited and burned with a high efficiency. Late (delayed) ignition or incomplete combustion of the metal in rocket motors are probable sources of degradations in the delivered performance of systems employing metalized propellants (Ref. 1). Beryllium could be especially difficult to ignite in rocket motors, but because of the high performance potential this material offers, a thorough study of its ignition and combustion characteristics has been warranted (Ref. 1).

Both analytical and experimental studies (Refs. 2 through 13) have been conducted in the past in efforts to understand and improve the ignition and combustion processes of metals. These efforts have not proved entirely satisfactory. Early efforts to compute ignition delay times and combustion rates were deficient because of the use of inaccurate theoretical models and incorrect ignition criteria. Limiting assumptions have been applied even when incorrect because these were necessary for mathematical convenience in obtaining solutions. The best theoretical model available previously is believed to be that of Brzustowski (Ref. 12). Experimental results have been strongly dependent on experimental conditions and techniques. The combustion of metals as studied by many investigators under a wide variety of experimental situations has been described (Refs. 2 through 11) alternatively as occurring on the surface, in the vapor phase, or in special cases, explosively, causing fragmentation of the metal. Although similar phenomena have been reported for many metals in a number of initial physical forms (particles, foil, wire), the conditions under which the specific phenomena have been reported are not consistent. It is important to know the mechanisms and physical parameters influential in the kinetics of metal combustion in order to predict and generate those conditions which will lead to improved ignition characteristics and increased combustion efficiency in the practical confines of combustion chambers.

Fully consistent quantitative information has been generally lacking on the ignition temperatures, reaction modes, and burning rates of aluminum and beryllium. Therefore, one of the specific objectives of the present program was to measure quantitatively the ignition temperatures of aluminum and beryllium as functions of pressure, oxidizer species and concentration, and both metal purity and surface character. A second objective was to characterize the combustion modes of aluminum and beryllium to define the regimes in which different types of burning would occur, and to use this information to confirm the validity of a theoretical model developed in previous studies and based on Brzustowski's analysis, and to modify that model.

A third objective was to calculate burning rates of both aluminum and beryllium and to compare theoretical predictions of metal combustion behavior with experimentally observed results.

During the first year of this contract, ignition and combustion of aluminum and beryllium in oxygen and oxygen-inert mixtures were studied as reported in detail in Ref. 14. During the current year, gaseous mixtures simulating solid propellant combustion products were used as the environment for experimental measurements of ignition temperatures and investigations of combustion characteristics, in order to more closely simulate the actual conditions present in metalized rocket motors. This simulation is especially important since theoretical considerations suggest that the use of mixed gas systems and oxidizers other than oxygen will greatly modify the ignition and combustion phenomena, as a thick protective oxide coating is less likely to form prior to ignition when free oxygen is absent.

In this report, "ignition" is intended to signify the phenomenon and time when the reaction rate produces more heat than is lost through conduction, convection, and radiation and both temperature and reaction rate increase abruptly with following self sustained reaction. "Combustion" is intended to signify the self sustained reaction which follows ignition. In some cases reaction occurs while electrical energy is being supplied to the wire, but does not continue when externally supplied energy is no longer applied. This is sometimes called "pre-ignition reaction" if it is followed by ignition, or as just "reaction" when no ignition as defined above occurs.

EXPERIMENTAL STUDIES

Apparatus and Procedure

Combustion Chamber and Exhaust System

Experimental studies of metal ignition and combustion in gaseous oxidizers were performed in the apparatus shown schematically in Fig. 1. In this apparatus, wires 2 to 4 in. long and having diameters between 0.004 and 0.040 in. were heated electrically in a controlled near-ambient-temperature atmosphere. Valving and gauges on the main control panel were arranged for metering up to three different gases such as N_2, Ar, CO_2, O_2, or He into the test chamber. Additional facilities were available for adding directly to the chamber such corrosive gases as HCl and ClF_3. Steam was added to the gaseous content of the chamber by boiling water in the thermostatically controlled (293 to 473 K) unit shown in Figs. 2 and 3, which was located inside the chamber. This heater supplied steam at partial pressures up to approximately 200 psia. During runs with water, it was necessary to heat the windows of the chamber to prevent condensation. Windows were normally constructed of tempered glass but quartz windows were used for operation with CTF to reduce etching problems, which were more severe when CTF and HCl were used simultaneously than when CTF was used alone or with an inert.

Gas pressures in the test chamber were maintained constant during each test and were varied between 0.25 and 1000 psia during the test program. A fan mounted in the test chamber allowed stirring of oxidizing gas mixtures for uniformity prior to selected experimental runs. Severe corrosion of fan bearings and shaft during CTF and HCl tests forced discontinuance of the mixing procedure, but no changes in ignition or combustion characteristics were observed to result from this change in procedure.

The test chamber and an exhaust system were maintained in a hood with a filtered exhaust (Fig. 4). Gases vented from the chamber were passed through a sodium hydroxide trap (water cooled) to remove corrosive acids or halogens. An "Ultipore .15" filter ensured a minimum of condensed contaminants in the gases vented from the chamber and either by-passing or going through the NaOH trap. During pumpdown sequences, a liquid nitrogen trap prevented either water from the test chamber or water generated in the NaOH trap from entering the vacuum pump. In spite of these precautions, frequent vacuum pump oil changes were necessary as well as periodic factory maintenance and repair of "frozen" pumps.

During tests without water, a tray placed in the test chamber above the fan, but below the wire specimen, caught most of the solid products of combustion. Microscope slides placed in this tray provided product samples conveniently accessible for microscopic examination. The relatively cold brass electrodes within the chamber also served as heat sinks for the condensation of gaseous products of

combustion, available for subsequent examination. The contact surfaces of these brass electrodes were periodically coated with Viking 232 to reduce their contact resistance with the sample wires.

Ignition Systems

The electrical ignition system shown schematically in Fig. 5 was designed to supply 60 cps voltage as a ramp function to 1/2-in. dia brass electrodes in the test chamber. Voltage gradients of 1/25 to 10 volts per second could be obtained. Both current and voltage (rectified) were recorded on a CEC oscillograph together with the output from two photocells which viewed the wire sample (one through an optical filter). The photocells provided brightness temperature (integrated over the length of the wire).

An alternative technique for obtaining wire ignition was also utilized in the course of the experimental program. This technique employed a high voltage supply, R-L-C circuit and electronic switching circuits to provide a short current pulse which heated the wire to its ignition temperature (Fig. 6). The pulse length was controlled by varying circuit capacitance and resistance, while pulse energy was determined by the (variable) voltage to which the capacitor was charged. The present apparatus was used to supply current pulses from 0.2 to 10 milliseconds in length. Instantaneous wire current and voltage were measured from oscillo-scope photographs, allowing the calculation of instantaneous power input to the wire. By integrating the power input, and correcting for heat losses (which were small because of the short heating time), the temperature history of the wire could be computed.

The two heating circuits described above are shown in Fig. 7. Both circuits could be controlled remotely, and the pulse heating circuit could also be initiated automatically by means of internal switches in the high speed cameras, to ensure proper filming rate at the time of ignition. In addition to providing a linear rate of increase of voltage, the slow heating (60 cps) circuit could also be operated to maintain a constant temperature (less than ignition) by using an indi-cating pyrometer and manual control.

Wire Temperature Measurement

In both the slow heating mode of ignition and the pulse ignition technique, the temperatures of wires which heated uniformly were estimated from the deflection of the photocell outputs on either the CEC oscillograph or a Tektronix Type 545 high-speed oscilloscope. Calibration of the photocells was based on measurements with a two-color ratio pyrometer (Milletron Therm-0-Scope) using a heated tungsten wire as the radiating source. The accuracy of such photocell measurements was estimated to result in a standard deviation of ± 20 deg K. Selected measurements made with a two-color ratio pyrometer at the melting point of aluminum oxide also verified the accuracy of these temperature measurements.

For use in estimating local temperatures in wires which did not heat uniformly (typically beryllium) a simple system was installed in which a reproducibly heated tungsten reference wire was projected through a step filter to produce an optically graded image in the plane of the test wire. Simultaneous exposure of both wires on the photographic record of the ignition tests allowed visual or microdensito- metric comparisons of the exposures obtained just prior to ignition. From this comparison, local temperatures at ignition could be estimated to better than $\pm$ 100 deg K.

The temperature of wires reacting slowly and producing surface deposits of oxide were measured directly with a 2-color ratio pyrometer, with the time- temperature history recorded on an X-Y recorder. Temperatures during reaction could be estimated to within $\pm$ 50 deg K or better in the range 1300 K to 3000 K, for reacting wires whose temperatures were changing only slowly. The temperatures at ignition of wires igniting below the melting point of the metal were also estimated from the resistance of the sample just prior to ignition. Qualitative changes in resistance occurring at the melting point of the metal provided quali- tative information as to whether this technique could be used. During pulse ignition runs, the total energy applied to the wire could be calculated from the electrical constants of the circuit and the voltage applied to the condensers. From this information and the thermal properties of the wire, calculation of the heat balance allowed estimation of the maximum temperature which could be attained without chemical reaction, and therefore the ignition temperature approximated by determining the minimum voltage required for ignition.

Ancillary Instrumentation

In addition to the electronic data acquisition system represented by the CEC oscillograph, and the oscilloscope used with the pulse ignition technique, a num- ber of other pieces of equipment were utilized in the experimental program. Both high-speed (Hycam, Fastax and Milliken) cameras and lower speed cameras (Pathé) were used to record photographically the ignition transients and behavior during combustion, as well as to aid in estimating local hot spot temperatures as des- cribed above. A timing and synchronizing unit was integrated into the high-speed camera-pulse ignition system to permit accurate measurement of framing speed on movies and to permit synchronization of high-speed films and oscilloscope traces taken during pulse ignition tests. This system placed either a 1000 pulse per second or 120 pulse per second marker on one edge of the film, and a continuous marker on the other edge which was stopped when the fast acting vacuum switch in the pulse circuit fired. This second marker was reactivated when the oscilloscope sweep was triggered, giving a precise identification to the timing sequence during the pulse discharge.

The clarity and usefulness of camera records were increased by use of anti- halation film (Kodak 7278) and by use of an intensity control device incorporating a Kerr Cell. The Kerr Cell was used as an electrically variable neutral density

filter to keep the light intensity reaching the camera from the igniting wires at a relatively constant level. The electronic and optical schematics showing the function of the exposure control system are shown in Figs. 8 and 9. The transmission and optical density of the Kerr Cell as functions of the applied voltage are shown in Fig. 10. The Kerr Cell and associated equipment are shown in Fig. 11. The Kerr cell (on the right) was adjusted for the normally transparent mode with 12.5 kilovolts applied, and the three photodiodes (on the left) were illuminated by the light from the wire. A light shining on the photocells could reduce the transmittance of the cell by a factor of 100 or more, with the opacity of the cell proportional to the intensity of the incident light. The response of the photocells was adjusted to produce a voltage change of up to 10 kilovolts when illuminated by a burning wire. This system allowed photographic recording of pre-ignition as well as post-ignition events, allowing clear observation of both bright and dim portions of the ignition transient as shown in Fig. 12. The rise time of the Kerr Cell system (from maximum transmission to minimum transmission) as determined from oscilloscope records was less than 200 microseconds.

A 1.5 meter ARL-Dietert grating spectrograph was used to obtain spectra of burning metal wires. However, the requirement of keeping the image of the burning wire optically focused on the entrance slit was not reproducibly fulfilled. Therefore, a converging light conduit fabricated from a bar of lucite was installed which optically coupled the combustion chamber window and the spectrograph slit. Flame spectra were also obtained, at lower resolution, with an F/4 Hilger-Watts prism spectrograph with quartz optics. A Jarrel-Ash automatic scanning and recording microdensitometer was utilized to increase the discrimination and assist in identification of lines observed in typical Al and Be flames.

Chemical Analysis

The purity of wires used in these ignition and combustion tests was characterized by both spectral analysis and wet-chemical analysis. Most aluminum wires were 99.99 percent Al or purer. Beryllium wires as obtained from a number of sources varied widely in their chemical composition, at least in part due to their surface treatment. The wires used, and their chemical composition and/or special treatment are identified in Table I. Samples of beryllium wire (0.020-in. dia) were analyzed using three techniques: (a) the wire was dissolved in acid and the hydrogen evolution was used to estimate the total metal (as Be) present, (b) the wire was selectively dissolved in alcoholic bromine and alcoholic HCl and the residue (insoluble BeO) was determined gravimetrically, and (c) the wire was examined spectrographically for other metallic impurities. It is postulated that the insoluble BeO is distributed in the bulk of the metal while any surface BeO is soluble in the selective solvents used. The surface oxide (or lubricant residue in the case of as-drawn wire) may thus be estimated by difference, based on the Be plus insoluble BeO, as shown in Table I. The trace impurities are also indicated in Table I.

Surface Treatment of Wires

Pickled wires (Type H) were prepared by immersion for 120 sec in 1 N H_2SO_4. Gold plated wires (Type I) were made from pickled wires (Type H) by electroplating. Amalgamated wires (Type J) were first pickled and then immersed in 5 percent alcoholic mercuric chloride followed by an ethyl ether rinse. Anodized wires (Type K) were prepared by treating first for 120 sec in 1 N H_2SO_4 and then anodizing at 10 milliamps per square centimeter for 20 sec in a bath consisting of 10 gm CrO_3 dissolved in 50 cc of 10 percent HNO_3. Specifications of other selected raw materials are listed in Table II.

Background Information

It has been commonly supposed that metals forming protective oxides, including both aluminum and beryllium, will ignite only after the protective oxide becomes molten, or after the metal is broken in such a way as to expose an unprotected surface to a hot oxidizing atmosphere. It has also been postulated that the metal will react and ignite at a very low temperature if it is not prevented from doing this by an impervious protective oxide. In light of these considerations an analysis of the metal vapor pressure/metal oxide melting point relationship of Al (Fig. 13) is helpful in explaining some of the results that were obtained in the measurements of the ignition temperatures of Al and Be. The pressure at which the oxide melting point coincides with the metal boiling point can be called the critical ignition pressure (Ref. 11). At pressures above the critical ignition pressure, the liquid metal and gaseous oxidizer cannot react unless the oxide coating is melted or broken. Since at these pressures the vapor pressure of the metal cannot exceed the total pressure without melting the oxide, melting will occur before internal pressures can break through the oxide coating, and the oxide melting point should be identified as the ignition temperature (A in Fig. 13). Below the critical ignition pressure, one of three mechanisms may occur. If the oxide coating is thin and weak but impervious, it will break when the internal pressure (of metal vapor) exceeds the ambient pressure by a small amount. In this case the ignition temperature-pressure (T_{ig} - P) relationship will follow the vapor pressure curve (B in Fig. 13). If the oxide coating is thin and permeable, sufficient metal vapor will diffuse through the oxide coating to cause ignition in the vapor phase external to the unbroken oxide coating, and the T_{ig} - P curve will be that of C in Fig. 13. If the oxide coating is thick, strong, and impervious, a higher than ambient vapor pressure will be needed to break the oxide coating, and the T_{ig} - P curve will be that of D in Fig. 13. Brzustowski (Ref. 4) noted a decrease in the brightness temperature at ignition for aluminum wire in the range of 1 atm down to 50 mm Hg. Although he postulated that a change in emissivity accounted for the reduction in observed temperature, it is probable that the effect noted was the same as that suggested in Fig. 13. Since Brzustowski's (Ref. 4) wire was anodized in most cases, his results might be classified as falling in the region typified by Curve D

of Fig. 13. It was also observed (Ref. 11) that, in the region below the critical ignition pressure, the ignition temperature was also responsive to oxygen partial pressure, being slightly higher at higher oxygen concentrations (30 to 100 percent oxygen were tested). It was postulated that higher oxygen concentrations caused a thicker oxide buildup in the preignition reaction, thereby retarding escape of metal vapor until a greater partial pressure differential was achieved by raising the temperature. The failure of beryllium to follow closely the predictions of a vapor pressure-BeO melting point relationship similar to Fig. 13, lead to the general suspicion that BeO is not truly a protective oxide, at least at high temperatures. No comparison with this type of predicted behavior can be suggested with metals not forming protective oxides, or in oxidizers not forming protective products.

The composition of gases used to simulate solid propellant combustion products was selected based on calculations described subsequently in Appendix 1.

Test Results

Most of the experiments reported herein were conducted in gaseous mixtures containing oxygen, or in gases simulating the products of solid propellant combustion. Selected tests were also conducted in either inert gases (Ar, N_2) or other oxidizers (N_2, H_2O, CTF), or with these as additives. Since each of the various metals tested in the form of wire during this program gave different responses to different environments, each metal will be reported separately, with a general comparison following. The gas compositions which were used to simulate combustion chamber conditions were determined by calculating equilibrium compositions of a 12 PBAN/88 AP mixture, and then expanding with shifting equilibrium to an exhaust pressure corresponding to a gas temperature of about 300-310 K using an existing UARL computer program. Experiments were run using volume ratios of all components so calculated except methane and water, and varying the percentage of water from zero to the equilibrium value. The results of the equilibrium composition calculations are presented and discussed in a later section of this report (Appendix I).

Selected typical examples have been extracted from Ref. 14 for presentation here rather than verbatim treatment of the large amount of previously reported results. For additional background information, or more complete description of similar tests to those reported here as examples, Ref. 14 is recommended.

Aluminum Ignition

The majority of tests were conducted with aluminum which was 99.99 percent pure. This high purity aluminum ignited consistently and reproducibly, while aluminum of 99.7 percent purity was more difficult to ignite. Preliminary tests with wires ranging from 0.010-in. dia to 0.080-in. dia were conducted. These

showed that for large wires a very slow heating rate was required in order that sufficient Al_2O_3 could be formed on the surface of the wire to support the weight of the sample when the aluminum reached its melting point. For this reason most of the tests reported here were conducted with 20-mil Al wire (99.99 percent Al) with some tests using 35-mil wire (99.7 percent Al). Tests were conducted in argon, oxygen, nitrogen, and argon/oxygen and nitrogen/oxygen mixtures, and in CTF and simulated solid propellant combustion products.

Qualitative Observations

For Al wires 20 mils in dia or less and at least 1 in. long, changes in the wire metal such as melting, stretching, or boiling, or its surface such as metal vapor diffusion through the oxide or melting of the oxide (rather than mechanical breaking of the wire) appear to be the precursers of ignition. For the 35-mil wire, ignition could be obtained reproducibly only if the wire was heavily anodized. Since this anodization precluded study of other surface effects, no further tests were conducted. In observations of hundreds of wire ignition tests, most of which were recorded by high-speed cinematography and examined frame by frame through the ignition transient, not a single case has been seen where a wire broke mechanically with subsequent ignition of the broken ends. In each case of ignition, the wire remained intact (without falling) for a measurable time after ignition. In some cases, especially at low pressures, the intact wire (relatively cool) could be observed through the flame for a finite period before heat from the flame melted the oxide coating and destroyed the mechanical integrity of the wire. These observations support the validity of the use of wire ignition temperatures as representative of particle ignition temperatures, since in particle ignition, changes in surface (oxide melting) or metal (vapor pressure increases) rather than mechanical stresses will precede ignition.

Quantitative Results

Effect of Pressure and Oxygen Concentration

The ignition temperature of pure (99.99 percent) aluminum wire (20-mil dia) was measured over a range of pressures from 0.25 to 1000 psia. The power to achieve ignition was also determined, and was found to increase with pressure at a constant ignition temperature (above about 10 psia), but decreased rapidly with decreasing pressure in the region below 10 psia where low ignition temperatures were observed. Experimentally measured power requirements and ignition temperatures typical of aluminum are shown in Fig. 14 for Al in 100 percent oxygen, and are shown in Ref. 14 for all Al tests.

As is indicated in Fig. 14, above a critical ignition pressure (ca. 2 to 10 psia), the ignition temperature is essentially constant, and for the case of aluminum burning in pure oxygen it is approximately equal to the melting point of aluminum oxide (2318 K). The apparently low ignition temperatures at high

pressure are presumed inaccurate, since the power required to ignite was not correspondingly low. The ignition temperature at pressures above the critical ignition pressure appears to vary slightly with oxygen concentration as is more clearly demonstrated in Fig. 15. In addition to this slight decrease in the ignition temperature with decreased oxygen concentrations (at pressures above the critical ignition pressure), there is correspondingly a narrowing of the pressure range in which ignition occurs as oxygen concentration decreases. For example, the lower pressure limit of aluminum ignition observed was 0.25 psia at 100 percent oxygen, 0.5 psia at 70 and 50 percent oxygen, 5 psia at 30 and 20 percent oxygen, and 16 psia at 10 percent oxygen. The upper pressure limit of ignition was less distinct, since wires would occasionally break without ignition below the maximum pressure at which ignition occurred. No upper pressure limit was observed at 100 and 70 percent oxygen, since ignition occurred at 1000 psia, the design pressure limit of the apparatus. However, no ignition was observed above 250 psia at 50 and 10 percent oxygen, or above 125 psia in 30 and 20 percent oxygen, although tests were conducted up to 1000 psia in each case. Tests results for 10 to 30 percent oxygen show generally less effect of oxygen concentration than the results for 50 to 100 percent oxygen.

To indicate one of the observed differences between ignition and nonignition, some of the power requirements recorded for cases of nonignition and ignition are plotted in Fig. 16. It can be noted that, contrary to power requirements for ignition in pure oxygen, the power to break the wire in pure argon is low and essentially independent of the pressure. This is undoubtedly due to the almost complete absence of an oxide coating for these conditions with the result that temperatures only slightly above the melting point of pure aluminum are required to break the wire. In atmospheres containing oxygen, where an oxide coating can build up before the wire breaks but ignition does not occur, the power required to reach the breaking temperature is higher and generally increases with both pressure and oxygen concentration. Similarly, when ignition occurs, power required to reach the ignition temperature increases with pressure.

Effect of Inert Species with Oxygen

In order to evaluate the effect of inert gas type on aluminum ignition temperature, experiments were conducted in mixtures containing 50 percent oxygen and 50 percent argon, nitrogen, or helium. Pressures employed for these tests were selected on the basis of ignition behavior of aluminum as reported above. For a 50 percent oxygen-50 percent argon mixture, it had been observed that the aluminum ignition temperature was essentially constant between pressures of 8 and 250 psia, with progressively lower ignition temperatures being observed at pressures less than 8 psia and no ignition being found above 250 psia. Tests with helium and nitrogen as inerts and repeat tests with argon as the inert at 50 percent oxygen concentration were conducted at 4, 64, and 500 psia (one pressure in each of the three regions described above). Two or more samples were tested at each pressure for each inert using different heating rates in order to establish the reproducibility of the

ignition behavior. There was no significant difference in ignition behavior observed with argon and nitrogen as the inert. Use of helium required slightly higher power levels, on the average, to attain the same wire temperature achieved with nitrogen or argon as inert. At 500 psia no ignition was observed with any of the samples tested at 50 percent oxygen, regardless of inert gas. At 64 psia, even though ignition was achieved with each gas as diluent, there were additional tests which did not result in ignition; these tests were generally run at too high a rate of voltage increase, resulting in melting and breaking of the wire below the ignition temperature before a thick mechanically supporting oxide film could form.

Other Oxidizers

Tests were performed on aluminum wire in pure nitrogen at pressures from 64 psia to 500 psia. Ignition occurred only at pressures of 400 psia and above. The Pilling and Bedworth ratio of aluminum nitride, AlN, is 1.26, and thus it should be protective at room temperature. However, the measured ignition temperatures were considerably below both the melting point of AlN (2473 K), and the sublimation temperature of AlN (2273 K at 1 atm), indicating that the coating becomes non-protective at higher temperatures. Aluminum wire was observed to ignite below its melting point (933 K) when heated in 1/2 atm of pure CTF. The observed flame was violet-tinted but not brightly luminous and appeared to result from surface reactions.

Pulse Ignition

The pulse ignition apparatus was tested with 20-mil and 2-mil aluminum wire and 20-mil aluminum-5 percent magnesium wire in air at 1 atm pressure. After the circuit parameters were properly adjusted, tests were run on 20-mil Al wires in 100 percent O_2 at 32 and 64 psia pressure. In all tests it was found that there was a certain threshold energy (characteristic of the metal, wire diameter, and oxidizer pressure) below which the wire did not even break, and above which it always ignited. The minimum voltage for ignition was 220 volts, equivalent to a temperature of about 2300 K. It is believed that the short period of delay before ignition (0.2 to 10 msec) was insufficient to affect the surface grossly by additional oxidation, and therefore this technique was advantageous in studying surface effects on a time scale matching closely that existing in rocket motor combustion.

Aluminum Combustion

Qualitative Results

Flame Description

The combustion of aluminum can be characterized as a function of the total pressure and oxygen concentration as being: (1) typically gas phase with a

11

voluminous flame at low pressures; (2) relatively slow with the flame zone on or near the surface at high pressures and low oxygen concentrations; or (3) rapid and vigorous with some fragmentation at high pressures in high concentrations of oxygen. In the low pressure region (below 5 to 10 psia), ignition always occurred in the vapor phase, initially producing a diffuse, voluminous flame through which the aluminum wire extended intact. The flame spread slowly along the wire, until the heat from this flame caused the wire to break. In the region of 5 to 10 psia, combustion was typified by ignition at one or more points followed by a flame on each end of the wire burning back from the point of ignition. This flame was typically spherical and rather opaque (in comparison with transparent or translucent flames at lower pressures). Figure 17 shows a typical aluminum ignition and combustion sequence at 32 psia, where the spherical flames are slightly smaller than at lower pressures.

At the very high pressure (e.g., 1000 psia), and for oxygen concentrations of 50 percent or less, the first indication of ignition was the appearance of a hot bright spot under, on, or very close to, the surface. This surface ignition at low oxygen concentrations ($\leq$ 50 percent O_2 by volume) caused a discontinuity in the wire, with both ends of the ruptured wire continuing to burn on or near the surface. At higher oxygen concentrations ($\geq$ 50 percent O_2 by volume), the spread of the hot surface ignition along the wire from the initial point of ignition was extremely rapid, usually occurring before the wire had a chance to drop due to gravity. The ignited wire, heated far above the melting point of even aluminum oxide, was then drawn by surface tension into a series of droplets. Each droplet then burned independently. At low pressures (10 to 100 psia), the droplets then burned while falling under the influence of gravity, while at higher pressures ($\geq$ 100 psia) the droplets were more likely to explode or fragment before falling into the tray. The duration of combustion in these cases was in the order of hundreds of milliseconds (for 250 to 500 micron particles which did not fragment), as predicted theoretically, using the technique described in the Analytical Studies section. Aluminum flames typical of different pressures and oxygen concentrations are shown in Fig. 18.

Products of Combustion
=========

The products of combustion, observed both during the actual burning and subsequent examination of residues, were different depending on the type of combustion. Vapor-phase combustion at low pressures produced a smoke-like product which deposited loosely on cold surfaces in the test chamber, such as on the brass electrodes. This "smoke" could be seen streaming from the burning wire during the relatively long combustion period (up to 10 sec). Generally, the flame front was comparatively widely separated from the end of the wire. In the region of surface combustion, a relatively dense globule of oxide formed on the end of the wire (Fig. 19), with combustion usually quenched when the flame regressed close to the heat sink of the electrodes. In contrast, the exploding type of combustion produced large numbers of small solid and hollow spheres of aluminum oxide (Fig. 20).

12

Flame Size

The flame-to-wire radius ratio was determined for a number of aluminum flames from the photographic records. The experimentally determined values are shown in Fig. 21. For small flames at high pressures, this value is less precisely determined since the actual diameter of the wire under the flame was in some cases increased through accumulation of oxide. At low pressures the wire could sometimes be seen through the flame, allowing corrections for such deposits of oxide.

Pulse Ignited Tests

Aluminum wire ignited by a pulse invariably fragmented as is shown typically in Fig. 22 (discussion will be made below of the beryllium results shown also in Fig. 22). The products of this type of combustion were almost always very small oxide spheres (or smoke).

Beryllium Ignition

Qualitative Observations

Tests in Oxygen

The first general conclusion which may be drawn from past and present experimental studies is that beryllium wire is considerably more difficult to ignite than aluminum. Ignition of beryllium does not necessarily occur at average surface temperatures higher than those observed for ignition of aluminum (as is predicted from consideration of the relative melting points of the two metal oxides, i.e., 2318 K for Al_2O_3 and 2820 K for BeO). Rather the beryllium ignition temperature is affected more substantially by the condition of the metal surface and ignition is often promoted at a "hot spot." There also appears to be considerable preignition reaction in the case of beryllium wire, indicating that, at least at higher temperatures, BeO as formed is less protective than Al_2O_3.

The preignition reactions of beryllium in oxygen experimentally observed in this study were generally localized at the junction between molten and solid beryllium during slow heating and progressed towards the electrodes as power was increased. As a probable result of the uneven heating produced in this manner, the molten beryllium wire encased in BeO sagged in a very uneven and nonreproducible shape typified by Fig. 23. Beryllium wire heated in inert gases (e.g., Ar) was observed to sag and then become taut before eventually breaking. (Believed due to surface tension effects as the oxide softens or melts.) When pulse-heated in oxygen, beryllium wires commonly ignited at one spot followed by fragmentation (Fig. 24). Occasionally a second ignition spot was observed. At voltage settings below 240 volts, no ignition occurred, an indication that the fragmentation was not due to significant excesses of electrical input power. From Fig. 25, it is evident that ignition of beryllium may be preceded by "preignition reactions."

Frames 11 through 17 of Fig. 25 have been underexposed in printing to show details of the preignition reaction and the rapid transition to combustion.

Comparison of the qualitative ignition characteristics of aluminum and beryllium show significant differences. Figure 22 displayed the results of comparable tests with 20-mil Al and 20-mil Be wires, both in pure O_2 at a pressure of 125 psia, and both with 250 volt charges on the same condenser systems. This voltage produced a temperature in the order of 2500-3000 K on both wires, and was above the minimum voltage for ignition to both metals. Whereas the beryllium (shown in Fig. 22 in a sequence continuing from that reproduced in Fig. 25) ignited only after about 1.5 msec and then apparently at only two locations on the wire, the aluminum ignited more rapidly, and as many as 12 separate points of ignition are identified in the first 0.4 msec of reaction. The aluminum wire was completely consumed in a very short period while the beryllium combustion apparently did not spread from the points of ignition but did continue for several tens of msec. Although the beryllium fragmented, fragment velocities were relatively low compared with the velocities of the aluminum fragments formed under similar conditions.

Tests in Simulated Combustion Products
=======================================

In many cases of attempted pulse ignition of beryllium wire in 39.9 HCl/39.7 CO_2/20.4 N_2 mixtures (simulating solid propellant combustion products), the major portion of the wire remained after the test, although a flash appeared which might have been interpreted as ignition. This would indicate that at some point along the wire the temperature increased sufficiently to cause a self-luminous reaction which did not produce sufficient energy to sustain the reaction when the electrical heating ceased (complete discharge of the condensers). The flash of light produced under these circumstances was sufficiently bright to be recorded on the photo cell as shown in Fig. 26. In this example, the voltage trace did not return to its initial position because the condensers were not completely discharged before the wire broke. When the heat was applied slowly, an obvious reaction was produced as recorded on the hot portion of the beryllium wire shown in Fig. 27. This wire did not ignite in the sense of progressing to self-sustaining combustion, but did produce a tangible product (thick fluffy white porous coating), and eventually the wire broke and cooled down. The continuing nature of the reaction while the wire was resistively heated (and well below the BeO melting point) indicates very strongly the nonprotective character of the product at least in the presence of the oxidizers utilized (HCl, CO_2 and N_2). The effects observed in cool simulated combustion product gases were independent of surface treatments of the beryllium wire.

Attempts were made to burn beryllium wire in gaseous mixtures of HCl/CO_2/N_2/H_2O. These attempts were unsuccessful because the beryllium wire reacted completely during the time required to introduce all the gases into the reaction chamber. It is believed that the observed rapid reaction was essentially dissolution of the

beryllium in concentrated hydrochloric acid which condensed upon it. Solution of HCl (gas) in the water supply being heated also caused etching and eventual failure of resistance heating elements immersed in the water. Similar tests were conducted without using HCl in order to prevent both preignition reaction of the wire and failure of the water heater. Several test runs were made using the slow heating technique in mixtures of $CO_2/N_2/H_2O$ containing a CO_2/N_2 ratio of approximately 1:1.5 and water vapor in equilibrium with water at 201 C at a total pressure of 500 psia. Reaction continued after internal heating ceased, indicating that ignition had occurred. There was no sagging of the wire before ignition indicating that temperatures preceding reaction were below the melting point of beryllium.

Pulse ignition tests conducted with beryllium wire in $CO_2/N_2/H_2O$ mixtures produced a flash but no apparent subsequent combustion. No white product was seen on the wire, but the wire appeared either to fragment (into approximately 1/4-in. pieces) or to melt back from the point of rupture. This result is consistent with a slow reaction easily quenched by the large excess of water present.

Pickled 20-mil Be wire heated in pure CTF at approximately 1/2 atm glowed a dull red without sagging before igniting. The wire did not appear to melt before ignition. Similar tests in pure H_2O vapor also produced ignition below the melting point of beryllium.

Quantitative Results

Ignition tests have been conducted on all of the Be wire samples listed in Table I, in pure oxygen, with the results tabulated in Table III. These results illustrate that ignition of beryllium is not predictable or reproducible, that there is a wide range of apparent temperatures in which ignition may occur, and that the ignition behavior is significantly affected by the processing, purity, and surface condition of the beryllium. Many of the recorded temperatures in Table III are not the actual ignition temperature, but were brightness temperatures optically averaged over the length of the wire sample just before ignition. Subsequent tests in which local "hot spots" were identified and characterized preceding ignition have indicated that in almost all cases of ignition in oxygen or oxygen/ inert mixtures, the real ignition temperature was just below the melting point of beryllium oxide, but generally higher than the ignition temperature of Al. This fact is illustrated qualitatively in Figs. 28, 29, and 30, where the hottest segment of the temperature reference wire is just above the ignition temperature of aluminum (Fig. 28), but the same segment is below the temperature of Be breaking in Argon (Fig. 29) or igniting in oxygen (Fig. 30).

In general, it has not been possible to measure ignition temperatures by comparison with a reference wire when using pulse ignition. This is due to the extreme gradient of temperature with time which results in the wire usually being invisible in the frame prior to ignition, even at 10,000 pps, and therefore gives no opportunity for comparison. However, the temperature can be estimated as follows.

The minimum voltage on the condensers required to achieve pulse ignition in 39.9 HCl/39.7 CO_2/20.4 N_2 at 500 psia was determined (210 v on a capacitor bank of 10,320 μf). This voltage represents a stored energy of 228 joules, of which 110 joules were delivered to the wire. The temperature corresponding to this energy input has been estimated (after subtracting all known circuit losses) to be approximately 1640 K. This temperature is in approximate agreement with independent estimates from the electrical resistance of the wire and from integration of the power vs time curve (both calculated from current and voltage oscilloscope traces). Corresponding results for Be in 100 percent O_2 at 125 psia were a minimum ignition voltage of 240 v and an ignition temperature of about 2400 K.

Tests in Oxygen

Wire Type A, as-drawn wire received from Brush Beryllium, could not be ignited by slow heating in oxygen. This was probably due to the heavy coating of die lubricant (MoS_2) which was so thick that special treatment with a liquid metal contacting material (Viking 232) was necessary to achieve electrical contact with the electrodes.

Wire Type B, which was similar to A but annealed by the manufacturer, did not ignite below 16 psia, but at pressures from 16 to 1000 psia a significant number of tests resulted in ignition. A second sample of this same wire (B-2) with similar chemical properties could not be ignited at any pressure tried but invariably broke at low temperatures. On the sample of Wire B which ignited, the apparent ignition temperature varied from about 1550 K to 2500 K. The low temperatures estimated from photocell output were due in part to the nonuniform temperature of the wire. Since the photocell is exposed to the entire wire, and gives an output based on the weighted average temperature, the actual maximum temperature must be above that recorded. An example of a typical beryllium wire just prior to ignition was shown in Fig. 23. The next frame in this photographic sequence identified as ignition, is shown in Fig. 31. Samples of wire (B-1) were tested in argon over the range 0.25 to 1000 psia. Above about 2 psia, the recorded breaking temperature was 2300 to 2500 K, while the breaking temperature was somewhat lower at pressures below 2 psia (Fig. 32).

Tests conducted on Wire C (pickled by the manufacturer) produced no ignition in oxygen at 25 and 64 psia. One sample tested at 500 psia in pure oxygen ignited but only after application of maximum voltage for a relatively long period (normally ignition occurs as voltage is increasing in the slow heating technique).

Since only small samples of Wires D and E were available, tests were limited to one pressure (100 psia). Wire D (coated with chromium) could not be ignited, presumably because the coating prevented the formation of oxide at lower temperatures, and the wire then broke on reaching its melting point. Wire E behaved similarly to Wire B-1, breaking in oxygen in the range of 1600-1800 K.

16

Two samples of nickel coated wire (Type G) were tested at 64 psia in pure oxygen. These ignited in the range 2150-2350 K but differed by 50 percent in resistance at the moment of ignition. The uniformity of the nickel coating is unknown, and variations in coating thickness could be expected to produce such changes in resistance.

Berylco as-drawn wire (Type F) was tested in pure oxygen at pressures of from 1.0 to 500 psia. Ignition occurred only at pressures of 64 psia and above at apparent temperatures of 1700 to 2000 K. Wire breakage (without ignition) occurred at pressures of 125 psia and lower and at temperatures from about the Be melting point to over 2200 K. Four additional types of wire were tested, all of which were derivatives of Wire F (as-drawn wire from Berylco) for which analysis is given in Table I. Type H wire (Type F pickled in H_2SO_4) shows an improvement in purity compared to Wire F, as follows: Be content increased from 97.0 percent to 99.4 percent, insoluble BeO decreased from 0.3 percent to 0.1 percent, calcium (from the die lubricant) decreased from 1.0 percent to 0.07 percent, sodium decreased from 0.3 percent to 0.05 percent and magnesium decreased from 0.3 percent to "not detected." All other changes in ingredients were measured in hundredths of a percent. Type I wire (Type H, gold plated) was not analyzed, but was plated to produce only a thin gold coating. Type J wire (Type H, treated with alcoholic $HgCl_2$) was surface coated with amalgam, but not analyzed for mercury content. Type K wire was prepared from Type F by first pickling and then anodizing in a chromate-nitric acid bath for 20 sec at a current density of approximately 10 milliamperes per sq cm of wire surface. It is estimated that an oxide coating of 300 Angstroms was applied in this process.

Of these wires, the number igniting and the average ignition temperature (based on the numerical average of the observed integrated brightness temperature for the igniting wires) are shown in the following table:

Wire	Number Tested in 100% O_2	Ignited	Average Ignition Temperature
F	26	7	1856 K
H	8	2	1625 K
I	2	0	-
J	15	5	1865 K
K	13	8	1919 K

It should be noted that a wide range of apparent ignition temperatures was observed. For Type J wire (amalgamated) apparent ignition temperatures varied from 1450 to 2500 K. For Type K wire (anodized) the apparent ignition temperature was 1650 to 2460 K. Since these tests were conducted utilizing integrated brightness as an indication of temperature, and without facilities for estimating "hot spot" temperatures, it is assumed that the real "ignition temperature" was probably above 2400 K in each case.

In pure oxygen at 500 psia, Type H wire (Type F wire pickled in H_2SO_4, see Table I) was found to ignite, whereas it did not ignite at 125 psia. At 32 psia, Type K wire (Type F wire pickled in H_2SO_4 and then anodized) did not ignite when heated at the same rate. However, when the rate of voltage rise was reduced, Type K wire also ignited.

Type H beryllium wire was found to ignite in pure N_2 at 500 psia. The measured ignition temperatures did not deviate widely from their average of 2347 K. This is very near the melting point of Be_3N_2 (2473 $\pm$ 100 K) and the decomposition temperature of Be_3N_2 (2513 K). The Pilling and Bedworth ratio (defined as the volume of surface film formed to the volume of metal required for its formation) for Be_3N_2 cannot be calculated accurately since values of the density of Be_3N_2 are unknown. However, the experimental results are consistent with the presence of a protective coating.

Ignition tests were performed in pure oxygen on samples of beryllium wire (Type M, General Astrometals Corp., SR grade, annealed and pickled) over the range of pressure from 1 psia to 500 psia. Ignition was obtained on all runs at pressures of 32 psia or higher but not at pressures below 32 psia. This high frequency of ignition is in contrast to the ignition frequency of only about 25 percent for beryllium from other sources. The samples were of smaller diameter than those used on previous runs (0.0140- to 0.0145-in. dia compared with 0.020-in. dia) and the reproducibility of ignition may be the effect of the smaller diameter. This conclusion is based on previous work on aluminum wire of a wide range of diameters (0.0005 to 0.0800 in.).

Tests in Gases other than Pure Oxygen

Tests were conducted to determine ignition characteristics of beryllium in mixtures of oxygen and argon. Ignition under these conditions (70, 80, and 90 percent O_2 in Ar) was difficult and nonreproducible with only 2 ignitions in 12 tests. This is contrary to the experience obtained with aluminum, where ignition was obtained down to and including 10 percent oxygen, with only a narrowing of the pressure range of ignition as oxygen concentration decreased below 50 percent O_2.

In order to check results obtained in a previous UAC study (not published), several wires (Type F) were ignited in mixtures at 500 psia total pressure containing 30 to 60 percent water vapor with most of the remainder nitrogen (small quantities of Ar, O_2, or H_2 were present but did not affect the results). In almost every case, ignition occurred close to the melting point of beryllium, which was partially confirmed by undeflected wire residues recovered after combustion was quenched. It is estimated that ignition occurred between 1500 and 1600 K, based on the resistance of the samples at the instant of ignition.

During ignition tests in pure CTF, the maximum ignition temperature was about 1100 K (well below the melting point of Be:ca 1550 K). Tests in simulated solid

18

propellant gases containing CTF as an additive gave evidence of reaction at an equally low temperature, but the reaction stopped after electrical continuity had been broken. It is probable that reaction would have continued in hot gases such as actually occur in a rocket motor, but the relatively cold gases in this case quenched the reaction.

A summary of the ignition temperature observations made during all of the tests of beryllium with the various different oxidizing gases is presented in Table IV.

Beryllium Combustion

Qualitative Observations

Tests in Oxygen

The combustion characteristics of beryllium wire also contrast strongly with those of aluminum wire. Where aluminum burned smoothly but slowly at low pressures, beryllium wire did not burn at all. At higher pressures in pure oxygen, where aluminum combustion was rapid and sometimes resulted in fragmentation, beryllium combustion was always erratic, always produced fragmentation, and was considerably slower overall. The typical beryllium wire combustion sequence, after slow heating, following ignition at a local hot spot, consisted of an initial shower of particles from the point of ignition, a rapid regression rate of the burning surface for a distance of 0.25 to 2.0 in. followed by another fragmentation. This sequence was usually repeated until the entire wire was consumed. Figure 33 illustrates a typical ignition-combustion sequence filmed at 128 frames per sec. Note that the first pulse of fragmentation occurred about 0.1 sec after ignition. Subsequent pulses (not shown in Fig. 33) were erratically spaced. Figure 34 is an enlargement of frame No. 13 of the sequence in Fig. 33 and illustrates the trajectories of individual fragments. Although the framing rate was 128 fps, each frame was exposed for only about 165 microseconds, which accounts for the stopped motion. Bright fragments trailing smoke are believed still burning, while circular images without smoke trails, or separated from their apparent smoke trails, are thought to be oxide particles remaining luminous after combustion was completed. The unburned wire is still clearly visible, but was subsequently completely consumed. Because of this pulsating type of combustion it was difficult or impossible to estimate accurately flame radii for any type of comparison with predicted quasi-steady-state conditions.

It is obvious from the size of the oxide sphere residues seen in flight in Fig. 34, and also collected after the tests (Fig. 35), that significant amounts of beryllium oxide must have deposited on the burning Be particles during combustion.

Above the critical voltage required for ignition of beryllium by pulse discharge in oxygen, the nature of the combustion appeared similar: ignition at one

or two points with subsequent fragmentation. A typical example of this type of combustion is shown in Fig. 36.

Tests in Simulated Combustion Products

The reaction of beryllium in 39.9 HCl/39.7 CO_2/20.4 N_2 mixtures generally occurred only while the wire was being electrically heated. At slow heating rates, significant surface reaction occurs when the Be wire is still below the melting point of the metal. This initiation temperature is believed to lie below 1273 K (below the range of the Therm-O-Scope currently being used to monitor temperature). On continued heating, a thick luminous region appears around the wire (Fig. 27), and on cooling there remains a thick crust of porous BeO. Figure 37 shows a photograph of the product of a typical run under these conditions. The maximum "flame" temperature recorded (measured at the hottest part of the reaction zone) was in each case below the melting point of BeO. A typical temperature history of the reaction zone as measured by the Therm-O-Scope and recorded electronically is shown in Fig. 38. The product has been analyzed both chemically and by X-ray and found to consist only of BeO. Since the "flame" temperature is well above the boiling temperature of $BeCl_2$ (the only other stable beryllium compound possibly produced), it is not surprising that only BeO was found.

A number of attempts were made to induce unassisted reaction of beryllium in $HCl/CO_2/N_2$ mixtures by interrupting the electrical heating after heating the wire above the initiation temperature. When the wire was heated continuously until it broke, the temperature increased slowly up to a point (< 1273 K, estimated), at which time the temperature rose rapidly to about 1550 K (the melting point of Be). After a pause of up to 1 sec at this temperature, presumably to melt all or most of the Be metal, the temperature rose rapidly again to its maximum (estimated at 2400 to 2800 K), and held at this level until the wire broke. At this point the temperature dropped rapidly to room temperature and all apparent reaction ceased. When the temperature was allowed to reach the maximum and then the electric power was stopped abruptly while the wire was intact, reaction ceased, the temperature dropped and the wire did not break. When, however, at a lower temperature (e.g., 1800 K), the electric power control was reversed by reversing the direction of drive on the motor driven variac, the temperature continued to rise, even though the voltage applied was decreasing (Fig. 39). It has not been possible to maintain a stable reaction at less than the maximum temperature. In one test, for which a modified chamber-filling procedure was used (the chamber was filled with CO_2 then evacuated and refilled with the dry $CO_2/HCl/N_2$ mixture), a more compact, adherent BeO coating was produced instead of the fluffy, porous coating observed in other tests.

Beryllium ignited by pulse in $HCl/CO_2/N_2$ mixtures generally showed much less fragmentation than in oxygen, and the reaction stopped (was quenched) in a few milliseconds leaving the major portion of the wire unburned. A typical record of this type of reaction is shown in Fig. 40.

The initial tests with water added to the $HCl/CO_2/N_2$ mixture were conducted with less than 0.1 percent H_2O. Under these conditions no significant differences were observed. No runs were completed at higher concentrations of H_2O in mixtures containing HCl because of the corrosive action of the condensate ($HCl \cdot H_2O$) on the wire and the dissolved HCl on the heater in the water bath.

A number of runs were made in $H_2O/CO_2/N_2$ at 500 psia, a mixture which should theoretically simulate $HCl/H_2O/CO_2/N_2$ since Be will react preferentially in the order $CO_2/H_2O/HCl/N_2$ (See Appendix I). During the initial runs, the actual reaction was obscured by condensation on the windows of the reaction chamber, but the residue reclaimed at the completion of the run (Fig. 41) was similar in appearance to that recovered after $CO_2/N_2/HCl$ runs previously made. This residue consisted of a white deposit on the ends of the beryllium wire. In subsequent tests under the same conditions, the viewing windows were heated to prevent condensation. This heating resulted in improved visibility and movies were taken which showed the progressive heating to ignition with subsequent combustion. A single frame taken at 500 pictures per second at this reaction of Be in $H_2O/N_2/CO_2$ (during the combustion stage) is shown in Fig. 42. The residue recovered from this run is shown in Fig. 43, indicating the balls of oxide which remained attached to the wire. The reaction zone itself was above the melting point of beryllium, as evidenced by slight drooping of the ends of the wire within the reaction zone. In the $H_2O/CO_2/N_2$ mixture, beryllium continued to burn after the electrical current stopped (after slow heating) as shown in Fig. 44. However, pulse ignition in the same mixture did not produce continuing combustion but caused reaction mainly on the ends of the wire where ignition first occurred. The residue from a typical run is shown in Fig. 45.

Tests in Gases Containing CTF

Beryllium was burned in ClF_3 (CTF) and mixtures of ClF_3/Ar as well as in $HCl/CO_2/N_2/ClF_3$ mixtures. In pure CTF at 7.5 psia, the beryllium burned with no visible flame. The wire warmed to ignition at about 1073 K and then the wire ends regressed to the electrodes without any major change in temperature (maximum 1200 K), but with generation of gaseous beryllium halides, as evidenced by the deposit which condensed on the electrodes (Fig. 46). The ball of molten beryllium on the end of each wire was about 4-5 times the original diameter of the wire (Fig. 47). Although no flame was visible during combustion in CTF, Fig. 48 shows a flame visible to the film used (which probably recorded the ultraviolet emission from BeF_2 or BeF), when testing at 17.5 psia. As seen, the unburned wire did not sag, indicating ignition below the melting point of Be. At lower concentrations of CTF (11.7% and 4.5%), but higher pressures (150 and 165 psia), a flame such as shown in Fig. 48 was not visible, but combustion did proceed at the same relatively low temperatures as in pure CTF. Figures 49 and 50 show typical ignition and combustion sequences in CTF/Ar mixtures.

Combustion of beryllium in $ClF_3/CO_2/HCl/N_2$ mixtures was evidenced not only by low-temperature ignition and combustion, but by the lack of any visible

combustion product or flame. As shown in Figs. 51 and 52, the wire decreased in diameter within the reaction zone (the crusted length was in the electrodes), and at several locations formed into balls which have been analyzed as essentially pure beryllium. This behavior is similar to that encountered in heating Be in argon, where balls on the wire were formed as sections melted (see Fig. 29). This behavior is postulated to result from the formation of beryllium halide but not oxide, with all of the products vaporized and a gradual thinning of the wire until the wire temperature locally reached the melting point, forming balls, and eventually breaking. At higher mole fractions of ClF, reaction continued to completion.

Other Metals

Selected tests were made during the course of the program on metals other than Al and Be. Mg and Al/Mg alloy wire were used to check out the effectiveness of the Kerr Cell intensity control circuit, because of the ease with which they ignited, shown typically in Fig. 12. Several runs were made with 10 mil Zr wire in N_2, O_2, and air for comparison of the wire technique with flash ignition techniques. These tests were recorded at 10,000 pps after pulse ignition at 1 atm (Figs. 53, 54, and 55). Several runs were made in air, N_2, and O_2 using 4 mil Boron deposited on 1/2 mil tungsten. The B wire burned in air and O_2 but showed only minor localized surface reaction in N_2 even at 500 psia. Typical of reaction in air was a dense uniform deposit of oxide on the electrode (Fig. 56). Quenched drops which fell to the glass slides on the tray showed a spherical black drop in the center (probably tungsten) surrounded by a white deposit in concentric layers. Similar results were obtained in oxygen except that oxide deposits were less uniform.

Spectrographic Tests

Flame spectra were obtained, using an F/4 Hilger-Watts prism spectrograph, from aluminum and beryllium wires ignited in pure oxygen by the pulse technique. Figure 57 shows a spectrum of beryllium, heated slowly (10^2 deg K/sec) to the ignition temperature, burning in 100 percent O_2 at 64 psia. Three band systems of BeO have been identified in this spectrum, but no atomic Be lines are seen. Figures 58 and 59 show spectra of beryllium ignited by the pulse technique (with a heating rate of $\sim 5 \times 10^5$ deg K/sec) and burning under the same conditions as above. A 1 percent transmission neutral density filter was used to prevent over-exposure in Fig. 58. In addition to the band systems seen in Fig. 57 a multitude of atomic emission lines are seen. Two intense lines in the near ultraviolet have been identified as trace impurities. The remaining lines have been read and identified as Be or BeO plus other impurities. Figure 59 also contains a spectrum of aluminum (pulse-ignited) burning in 100 percent O_2 at 64 psia. All three figures also show reference Hg arc spectra. The atomic lines appearing in the pulse-ignited spectra are possibly due to high voltage electrical excitation of beryllium vapor as the wire breaks.

Tests were conducted using pickled 20-mil Be wire received in the annealed condition from Brush Beryllium. These tests were performed in pure oxygen at 125 psia, using the pulsed ignition apparatus at a number of different condenser voltages. These voltages ranged from a low of 240 volts (the lowest value to result in ignition consistently under these conditions) to 300 volts. Spectra were taken of each run in the initial series of tests, to determine the effect on the complexity of the emitted light of voltages above the minimum required for ignition. Selected spectra are shown in Fig. 60. The intensity of the spectral image is a function of the alignment of the spectrograph with the region of maximum reaction, but not of voltage, whereas the number of lines and general complexity of the spectra are related to the voltage. Optimum simulation of ignition in rocket motors was achieved by using condenser voltages near the lower limit for ignition. This facilitated identification of species present in the flame.

General Comparisons

The dissimilarities between aluminum and beryllium in their ignition and combustion behavior have been demonstrated. Where aluminum ignites reliably and reproducibly, beryllium is much more difficult to ignite and does so only under the most favorable conditions, namely at high oxygen concentrations and pressures. Beryllium ignition and combustion behavior in turn is strongly affected by the oxidizing gas reacting readily at low temperature with water and chlorine trifluoride, and mixtures containing significant portions of these gases (20 percent or more), but reacting slowly with cold mixtures containing only $HCl/CO_2/N_2$ mixtures. Reaction in the latter mixture of gases apparently produces essentially solid BeO formed on the metal surface, at least while the gases are cold. Addition of CTF to this mixture results in no oxide being produced in the surface, although reaction occurs. Therefore, it must be presumed that the reaction with CTF generates only volatile halides. Hence, it is concluded that reliable, low temperature (hence short delay) ignition of beryllium will occur only in the presence of significant fractions of H_2O or ClF_3 in the oxidizing gases.

ANALYTICAL STUDIES

Procedure

Analytical studies were performed, based on the method discussed in Refs. 11 and 12 which considers the vapor phase combustion of spherical metal particles. The steady-state analytical model (Fig. 61) includes radiative, convective and conductive heat transfer, nonequilibrium evaporation rates, and degree of combustion product dissociation. Included as independent variables are the metal species, particle diameter, oxidizer species, inert species, environmental gas temperature, effective radiant temperature of the surrounds, and total system pressure. The solution to the equations which describe the mathematical model (Refs. 11-14) is based on the iterative calculation of flame and particle temperatures, with associated transport properties, until oxidizer and fuel flows match stoichiometrically at the flame front. The rate of heat release, the evaporation rate, and the burning rate are calculated, as well as the location of the flame front and the degree of dissociation of the products. In this model, the reaction kinetic rates are assumed infinite, and the rate limiting steps are the mass and energy transport to and from the reaction zone.

Based on selected input of thermodynamic and transport property values suitable to the system under study, values of flame temperature (T_B), particle temperature (T_A), fraction of oxide dissociated or vaporized (α), dimensionless burning rate (W), ratio of flame front radius to particle radius (R_B/R_A), diffusion rates (D_O and D_f), burning rate in gm-moles/sec per particle (W_f), and other parameters are obtained as output for each particle diameter as functions of the oxidizer concentration in the ambient atmosphere. The first five of these values are also plotted graphically as program output. Typical plots are shown in Figs. 62 and 63 for 50-micron particles of beryllium burning in oxygen-argon at 300 K and 1 atm. At the lowest value of oxygen concentration ($X_{O_{min}}$) for which combustion can be calculated, it can be observed that (1) the flame temperature (T_B) and particle temperature (T_A) are the same and (2) the flame to particle radius ratio (R_B/R_A) is unity. This is the predicted flammability limit, below which self-sustained combustion cannot take place. The lowest value of oxygen concentration for which α is greater than zero has been designated X_O* and, in general, will represent a lower limit for true vapor phase flames. Below the value of X_O*, only condensed phase products will form in the flame, and although this does not interfere with the theoretical calculations, it will mean in the practical case that over a finite but short period of time a complete sheath of condensed products may surround the particle, reducing oxidizer diffusion and generally reducing the combustion rate.

As reported previously (Ref. 14), and as will be discussed below, experimentally measured flame/particle radius ratios for burning aluminum wires did not

agree with similar ratios previously calculated for burning aluminum particles of similar dimensions. It was postulated that one factor which contributed to this discrepancy was the presence of additional heat feedback to the metal by back diffusion and condensation of the metal oxide which was not accounted for in the original theoretical model. An attempt to predict analytically the effect of this feedback of heat through oxide diffusion appears in the appendix to Ref. 14. This analytical treatment has been programmed for inclusion in the metal droplet combustion program at UARL, and a number of calculations were performed to determine the general effect of including back diffusion of the burning rate and flame radius as functions of pressure, oxygen concentration, and particle diameter. To facilitate these calculations, a number of simplifying assumptions were made. These assumptions could be eliminated if a treatment of back diffusion were incorporated in the heat transfer equations in the basic computer program. It was assumed that the ratio of flame to particle radii (R_B/R_A) is proportional to the burning rate, and therefore to the rate of evaporation of metal. It was also assumed that oxide would diffuse back to the metal only if α, the fraction of oxide vaporized, is greater than zero, and that this back diffusion would alter only the flame radius, evaporation rate, and burning rate, but not the transport properties, or the fraction of product vaporized (dissociated).

The computer program for burning rates of metal droplets has been utilized to predict burning times of beryllium particles both with and without back diffusion of oxide from the flame to the particle. Following the technique described in the appendix to Ref. 14, the fraction, λ, of vaporized or dissociated oxide which diffuses back to the particle has been calculated by the revised program in addition to the standard output previously discussed. The product ($\alpha\lambda$) describes the fraction of oxide produced which eventually reaches and remains on the metal particle. If M is the mass of the metal in the particle at any time in gm-mole, and M_0 is the original mass of metal, the radius of the particle at any time, τ, can be calculated from the expression:

$$r = \left[(A - B\alpha\lambda)M + B\alpha\lambda M_0\right]^{1/3} \tag{1}$$

where $A = \frac{3}{4}\pi\rho_m$ and $B = \dfrac{3\,MW_{ox}k_{st}}{4\pi MW_m n_{st}\rho_{ox}}$

Since

$$dt = \frac{dM}{W_f} \tag{2}$$

can be written

$$dt = \frac{dM}{r(w_f/r)} \qquad (3)$$

substitution of Eq. (1) into Eq. (3) and integration give the burning time τ, as

$$\tau = \int_{M_0}^{0} \frac{dM}{\left[(A-B\alpha\lambda)M + B\alpha\lambda M_0\right]^{1/2} (w_f/r)} \qquad (4)$$

This equation can be solved explicitly if W_f/r is constant and the product $\alpha\lambda$ is constant. These two factors are not truly constant but are not strongly dependent on particle diameter over a range of conditions, as will be shown in the following section.

Calculated Results

Results of the metal droplet combustion computer program have been obtained for both aluminum and beryllium in room temperature oxygen/argon mixtures for pressures from 0.01 to 100 atm and for particle diameters from 10^{-4} to 10^{-1} cm (1 to 1000 microns). The values of X_0^* (representing the lowest oxygen concentration of oxygen for which the flame temperature is equal to the boiling point of the metal oxide) are plotted in Figs. 64 through 66 as functions of the particle diameter and at five different pressures. The values for aluminum are shown in Fig. 64 and for beryllium in Fig. 65 with a comparison of selected results being shown in Fig. 66. For both aluminum and beryllium, the value of $X_{0_{min}}$ is essentially independent of pressure and almost independent of particle size except for the larger diameter droplets. The value of X_0^* for both metals is strongly dependent on pressure and particle size. The implication of this relationship is that vapor phase flames are most probable at low pressures and for smaller particles and, as shown in Fig. 66, are more probable for aluminum than for beryllium.

Qualitatively, combustion of smaller particles at higher oxygen concentration is more likely to result in vapor phase flames. Decreasing the pressure broadens the range of oxygen concentration and diameter which will accommodate vapor phase flames (rapid combustion). For large particles at very high pressures, vapor phase flames are not predicted ($X_0^* > 1$). When the value of oxygen concentration is below X_0^*, it is predicted that all of the oxide product formed will be in the condensed phase and will accumulate in the flame zone until it becomes a continuous layer which retards combustion. Since $\alpha = 0$ (no vaporized oxide) for $X_{0_2} < X_0^*$, back diffusion of vaporized oxide need not be considered in calculating X_0^* and $X_{0_{min}}$.

The calculated burning rates of aluminum and beryllium, without back-diffusion, in gm-moles/sec, are shown in Figs. 67 and 68 as a function of particle diameter for two oxygen concentrations at each of five pressures. Although the predicted burning rate (in gm-moles/sec) is higher for Be than for Al, correction for molecular weight and density provides a better comparison in terms of volumetric burning rate. For example, at 10 atm pressure in pure oxygen, the volumetric burning rate of a 100-micron (10^{-2} cm) aluminum particle is calculated as 24.6×10^{-12} cc/microsecond, whereas for the same size beryllium particle, it is 24.1×10^{-12} cc/microsecond.

The effects of back diffusion of oxide upon burning rate is shown in Figs. 69, 70, and 71. These figures display W_f/r, the ratio of burning rate to particle radius, with and without back-diffusion, as a function of particle diameter, for a series of oxygen concentrations. Figures 69 and 70 are for pressures of 1 and 10 atmospheres, respectively, and an ambient temperature of 300 K. Figure 71 is for a pressure of 1 atm and an ambient temperature of 3000 K. The horizontal portions of the curves in Figs. 69, 70, and 71 indicate the regions in which the "d^2 burning law," observed experimentally by many investigators, is followed. In fact, the "d^2 law" may be simply derived from the relation W_f/r = constant. The calculated results with and without back-diffusion of oxide are both seen to be consistent with the "d^2 law," over a range of particle sizes.

Calculations of predicted particle burning times were made using Eq. (4). It is apparent from these calculations, which are based on the integration of Eq. (2) - i.e.,

$$dt = \frac{dM}{W_f}$$

that for the region where W_f/r is constant and the product of ($\alpha\lambda$) is constant (the net flux of oxide back to the particle), the "d^2 law" still holds. Both W_f/r and $\alpha\lambda$ are approximately constant for a wide range of oxidizer concentrations and for particles up to about 100 microns (10^{-2} cm) in diameter.

It should be noted that for all cases shown, the range of particle diameters for which W_f/r remains approximately constant increases with increased ambient temperature (extending to larger diameters) but W_f/r does not change significantly in value. A typical plot of the product $\alpha\lambda$ is shown in Fig. 72, again indicating the region of validity of Eq. (4) for the case of back diffusion.

For a condition with no back diffusion, characteristic of low oxidizer concentration or very large diameter, Eq. (4) takes the simpler form:

$$\tau = \int_{M_0}^{0} \frac{dM}{(AM)^{1/3} \, (W_f/r)} \tag{5}$$

27

It is obvious that with back diffusion of oxide, the particle does not disappear at the completion of combustion (M = 0). The size of the final oxide residue (if assumed a compact solid sphere--not hollow) has been estimated from the calculated values of α and λ and is shown for typical conditions in Fig. 73.

Typical values of the predicted burning times are shown for 1 atm and 300 K in Figs. 74 and 75. In Fig. 74, the burning times without back diffusion appear as essentially straight lines obeying the "d^2 law." In Fig. 75, the effect of back diffusion is seen as a decrease in burning time, with the overall effect obeying the "d^2 law," but with changes in the curves representing transition from no back diffusion to back diffusion with decreasing particle size. In the transition regions, a wide divergence of burning time might be observed experimentally for only slight changes in initial diameter, giving the appearance of gross experimental scatter. Any test of these predictions in the transition region should therefore be made with an extremely narrow cut of particle sizes.

Calculations including the effects of back diffusion have shown that the ratio R_B/R_A is increased significantly for all conditions where α is not zero. As shown in Fig. 76, where R_B/R_A is shown as a function of oxidizer concentration for a 50-micron (5×10^{-3} cm) aluminum particle burning at 0.1 atm, back diffusion increases the theoretical flame diameter by a factor of 5 to 10. Extrapolation of experimental values of R_B/R_A based on wire combustion (Fig. 21) to a pressure of 0.1 atm permits estimates of R_B/R_A of from 8 to 10 at oxygen concentrations of 0.4 to 0.5, which is indeed closer to the theoretical prediction for back diffusion than to the case for no back diffusion (Fig. 77).

As shown in Fig. 78, the value of R_B/R_A with back diffusion is significantly larger than for the case of no back diffusion, with the values approaching each other only when α approaches zero. In the actual case, it is postulated that even when the overall thermodynamics predicts no product dissociation, such dissociation may occur with concurrent back diffusion to the metal and recondensation. This process is compatible with the thermodynamics involved but does predict a larger R_B/R_A through back diffusion when α is zero even though not shown in the present calculations. The data of Fig. 78 have been replotted in Fig. 79 in terms of the flame radius (R_B) and the flame-particle separation distance (R_B-R_A). Up to a particle diameter of about 5×10^{-2} cm (500 microns), back diffusion effects lead to the prediction of a flame-particle separation distance that is an order of magnitude greater than for no back diffusion. The curves indicate that as the particle diameter decreases from 10^{-1} to 2×10^{-2} cm (1000 to 200 microns) diameter, there should be a significant decrease in flame diameter if no back diffusion occurs, but only a slight change in the presence of back diffusion. It has been observed that once a flame is formed on a large particle (that does not fragment), the flame size does not vary significantly until just before the particle extinguishes. Since the burning time is proportional to the square of the diameter, 96 percent of the total burning time of a 10^{-1} cm (1000-micron) particle will be consumed by the time the particle has decreased to the size of 2×10^{-2} cm (200 microns).

The effects of the back diffusion of oxide from the flame to the particle have been calculated for beryllium particles under a number of conditions. These calculations are similar to those reported above for aluminum. As shown in Fig. 80, significant increases in the ratio R_B/R_A (flame radius to particle radius) are predicted if back diffusion is considered, at least for oxygen concentrations above X_0^*, below which α (dissociation fraction) is zero. In Fig. 81, the effect of particle size is shown. For all except large particles where $\alpha = 0$, the flame is predicted to be 3 to 4 times the diameter of the particle. The results of Fig. 81 have been replotted in Fig. 82 in terms of flame radius (R_B) and the flame-particle radius difference (R_B-R_A). Note that as the particle size decreases from 500 microns (5×10^{-2} cm) to 100 microns (10^{-2} cm) diameter, there will be only a slight change in flame diameter if back diffusion occurs. Below 100 microns diameter the change in diameter as the particle burns is reduced if back diffusion occurs. As shown in Fig. 83 for a 20-micron (2×10^{-3} cm) Be particle, the diameter decreases to zero with no back diffusion, while with back diffusion the final diameter is 60 percent of the original diameter. The effects of pressure on R_B/R_A for Be are shown in Fig. 84 both with and without back diffusion assumed.

A significant difference in the behavior of aluminum and beryllium in the presence of back diffusion of oxide is predicted for combustion at 1 atm total pressure. The calculated particle temperature for aluminum during combustion at 1 atm is sufficiently above the melting point of Al_2O_3 to postulate, at least initially, that all oxide diffusing to the surface will condense as liquid, and will probably not significantly change the shape, size, or rate of reaction until close to the completion of combustion when the oxide layer may be thick or non-symmetrical. In the case of beryllium, the predicted metal temperature during combustion at 1 atm is below the melting point of the oxide, so that BeO diffusing back to the particle must condense as the solid. Complete coating by a thick solid layer of oxide during combustion could quench the entire reaction. In this case, reignition would occur only if the ambient gases were above the oxide melting point, and combustion would proceed sporadically with alternate melting and freezing of the oxide coating. At higher pressures (i.e., above 10 atm), a burning beryllium particle would be above the oxide melting point, and combustion could go more easily to completion. The pressure effects described in Ref. 1 can be accounted for by this mechanism. As noted previously both in this program and in similar studies elsewhere, the oxide of beryllium is not completely protective at high temperatures, and the predicted sporadic nature of beryllium combustion would not go through a condition of complete quenching. This predicted restriction on the combustion of beryllium would not hold if the combustion product had a low melting point, as for example, the beryllium halides. This is one basis for predicting improved ignition and combustion characteristics for beryllium in the presence of halogens and/or halogen acids.

An analysis was made of certain calculated results for the combustion of aluminum particles in oxygen-argon mixtures which showed that the quasi-steady-state temperature of the particle would be above the boiling point of the metal.

This condition is predicted under the conditions of low pressure, small particle size, and high oxygen concentration. In the combustion of an aluminum particle burning in O_2 at room temperature and 0.01 atm, it is predicted that any particle below about 250 microns (2.5×10^{-2} cm) dia will have a temperature above the metal boiling point and therefore will be thermally unstable, resulting in fragmentation. At higher pressures, this predicted maximum diameter will be decreased. Heating rates for cool spherical metal particles injected into a flowing hot gas at temperatures comparable to those in a rocket combustion chamber have been calculated. For a 20-micron Al particle, the predicted temperature-rise rate is about 5×10^4 deg K/sec. Under these conditions it has been calculated that temperature nonuniformities within the particle will be less than 1 deg K, confirming one of the basic assumptions upon which the theoretical model is based.

Calculations were performed, using the metal droplet combustion computer program, for aluminum burning in mixtures O_2 with He and O_2 with N_2 for comparison with previously completed results for O_2-Ar mixtures to determine the effect on combustion characteristics of variation in the thermal conductivity of the inert gases. The variations in the calculated flame to particle radius ratio (R_B/R_A) with particle size for each of the three inert gases are shown in Fig. 85 for an oxidizer concentration of 20 percent. The differences between the three curves are due to the differences in the thermal conductivity of the inert. In addition, the decrease in radius ratio for small particles is a result of a shift in the peak value of R_B/R_A to lower values of X_O as R_A decreases (see Fig. 85).

<div align="center">Comparison of Analytical and Experimental Results</div>

Aluminum

A comparison was made between experimentally measured aluminum flame diameters (from motion picture frames) and theoretically predicted values of R_B/R_A. As was shown in Fig. 17, although the initial flame on an aluminum wire may be roughly cylindrical, it rapidly resolves itself into two spherical flames concentric with the wire ends. This behavior demonstrates the validity of the comparison of experimental results with the calculated values based on a spherical droplet flame model in the computer program. In determining the experimental values of R_B/R_A, the diameter of the small molten metal sphere (pseudo-particle) at the end of the wire was used for calculating R_A in those cases where it was visible. Where this was not the case, the wire diameter as measured from the motion picture frame was used, and the earliest frame with a spherical flame was selected, assuming that the metal sphere diameter on the end of the wire had not had time to grow much beyond the diameter of the wire. The flame radius was taken as that of the visible luminous envelope.

The results indicating the effect of pressure on the flame to pseudo-particle radius ratio were previously shown in Fig. 21 where a comparison was made of the

measured values of R_B/R_A for aluminum wires at various oxygen concentrations and for various inert gases. A distinct dependence on pressure is seen in the experimental results, while variations due to oxidizer concentration and inert species seem small. In fact, except for the points at 100 percent O_2, a single curve might well be drawn through the data. Anomolous behavior at 100 percent O_2 might well be expected as here the flow of oxidizer inward to the flame changes from diffusion through stagnant inert to simple radial flow. The measured values differ considerably from the theoretical values without back diffusion shown in Fig. 76. For a particle diameter of 5×10^{-2} cm (approximately that of the wire used), even for the case of He as the inert species at 0.01 atm, the theoretical R_B/R_A is less than 1.5 whereas the extrapolated value of measured R_B/R_A is greater than 8. The following factors are thought to contribute to this discrepancy.

    a. Additional heat feedback to the droplet by back diffusion and condensation of the metal oxide formed in the combustion zone.

    b. Flame emissivity, EM2, smaller than the value of 1.0 used in the calculations.

    c. A luminous envelope visible in photographs which represents a region of oxide condensation outside the flame zone predicted by the theory.

    d. Uncertainty in input values of transport properties and stoichiometric coefficients used in the computer program.

In the following paragraphs these factors are considered in more detail.

In cases where α , the fraction of oxide vaporized, is greater than zero, the possibility exists that such vaporized oxide will diffuse inward as well as outward, and condense on the relatively cooler droplet surface. Experimental evidence of such accumulations of oxide on a droplet surface have been obtained at the Naval Ordnance Test Station at China Lake (Ref. 13). Such diffusion is quite reasonable since oxide vapor concentration is appreciable in the flame zone and essentially zero at the cooler droplet surface, but was not considered by Brzustowski in his model (Ref. 12) from which the present computer program evolved. If such back diffusion of oxide were considered, it would constitute an additional heat input to the droplet with resultant increase in burning rate, W_f, and R_B/R_A. An approximate theory has been derived using an enthalpy balance and an oxide vapor diffusion equation to determine the effect on the ratio of R_B/R_A caused by oxide back diffusion and to estimate the fraction of vaporized oxide which diffuses inward. A sample calculation for a 2×10^{-2} cm dia aluminum particle burning in 80 percent O_2-20 percent Ar at 0.1 atm predicts that approximately 40 percent of the vaporized oxide will diffuse inward and that R_B/R_A will be approximately 4.6 instead of the value of 1.2 predicted without back diffusion of oxide. This increase of nearly a factor of 4 seems to be a possible major contributing factor in the discrepancy between experimental and theoretical values of R_B/R_A. The detailed theoretical analysis appears in Appendix I of Ref. 14.

The detailed effects of pressure on R_B/R_A were shown in Fig. 77 for both back diffusion and no back diffusion. The case for considering back diffusion of oxide is reinforced by comparing the results shown in Fig. 77 with those shown in Fig. 21, where experimental values of R_B/R_A were plotted. In the experimental case, pressure had a much stronger effect than oxygen concentration in fixing R_B/R_A. In the experimental case, the value varied from about 8 at 0.1 atm to about 4 at 1 atm and 2 at 10 atm, which is a much closer correlation with the curve representing back diffusion than with the curve for no back diffusion.

Since the oxide particles in the flame scatter as well as absorb light, the emissivity of the flame, EM2, will be less than unity, even for an optically thick (opaque) flame. Considering the optical properties of Al_2O_3 and a simple single-scattering approximation, a value of EM2 = 0.1 seems more realistic than the value of 1.0 previously used, especially in view of the fact that many of the flames do not appear opaque. The effect of EM2 on calculated R_B/R_A is shown in Fig. 86. A value of EM2 = 0.1 results in an increase of about 30 percent in R_B/R_A over that predicted for EM2 = 1.0.

Since vaporized oxide diffuses outward from the flame zone (for $\alpha > 0$), and the temperature drops with distance from the flame zone, it is evident that condensation of oxide outside the flame zone is possible. As long as the rate of condensation is high enough to overcome heat losses, these condensing oxide particles should remain near the oxide boiling point and hence be luminous. Thus, the luminous envelope seen in photographs probably includes this condensation zone, and is hence larger than the true flame (reaction) zone whose diameter is given by the computer program.

Computer calculations in which the thermal conductivity of aluminum vapor was varied by a factor of 2 showed negligible effect upon the results largely because of the relatively low concentration of aluminum vapor relative to inert in region AB (between particle and flame--see Fig. 61). The possibility of error exists in the average thermal conductivity in regions AB and BC (between flame and ambient) due to uncertainty in the variation of gas composition with position. This uncertainty is certainly no greater than a factor of 2 in thermal conductivity and should result in only a small change in R_B/R_A. Some uncertainty exists in m_{st}, the maximum number of moles of dissociated products from each mole of oxidizer, but this uncertainty is also another factor of 2 as a maximum.

As discussed earlier, aluminum was found to ignite below its melting point (933 deg K) in CTF, and far below the melting point of Al_2O_3. This is in accordance with the theoretical prediction that in halogenated oxidizers, no protective oxide coating would exist. Experimental burning rates were calculated from the observed regression rate and wire diameter. For aluminum burning in 20% O_2 - 80% Ar at 32 psia (Fig. 17), the experimental values are a linear burning rate of 6.25 cm/sec and a molar burning rate of 1.23 x 10^{-3} g-moles/sec, based on a pseudo-particle diameter equal to the wire diameter. The theoretical value (without back

diffusion) for this situation is 2.5×10^{-6} g-moles/sec. Back diffusion can account for no more than about one order of magnitude of this difference. The remainder may be accounted for by a pseudo-particle diameter greater than the wire diameter, and by the observed regression being largely due to melting back of the wire, with most of the molten metal going to increase the droplet diameter rather than being burned immediately.

Beryllium

A comparison has been made between results of the metal droplet combustion computer program and measurements taken from motion picture frames of 20-mil beryllium wire combustion runs. Because of the violent and erratic nature of beryllium combustion, and frequent overexposure of film by the extremely bright beryllium flame, the data are not abundant and contain much scatter. The measured ratio of flame to wire radius (R_B/R_A) for beryllium in 100 percent O_2 was 2.4 at 64 psia and ranged from 1.6 to 2.7 at 125 psia. Part of this scatter is due to uncertainty in flame diameter caused by halation of the film image of the small, intense flames. The use of a new anti-halation film recently announced by Kodak (Type 7278) alleviated this problem on subsequent tests with simulated combustion gases. A linear burning velocity of 30 cm/sec and a molar burning rate of 1.2×10^{-2} gm-moles/sec were measured for 20-mil beryllium wire in 100 percent O_2 at 250 psia. At 125 psia, measured values of linear burning velocity ranged from 6 to 70 cm/sec (molar burning rates from 2.3×10^{-3} to 2.9×10^{-2} gm-moles/sec). The variation in burning rate corresponds to variability in preignition condition as well as in the diameter of the molten droplet at the end of the wire. For comparison purposes, R_B/R_A predicted by theory without back diffusion for 20-mil dia (500 micron) beryllium droplets in 100 percent O_2 ranges from 1.06 at 1 atm to 1.04 at 10 atm. The predicted molar burning rate without back diffusion for a 20-mil dia particle is 8×10^{-5} gm-mole/sec at 10 atm, and back diffusion raises burning rates by the same factor it raises R_B/R_A, less than an order of magnitude. The difference between observed and predicted flame radii is undoubtedly caused by the same factors as discussed for aluminum above. Although the measured linear regression rate is quite accurately determined, conversion to molar burning rates was based on assumptions which may not be valid, so the values calculated above from linear rates represent maximum values only. As was illustrated in Fig. 34, a significant fraction of the metal is ejected from the flame zone during fragmentation pulses, which reduces the amount of metal consumed in the flame zone at the end of the wire during linear regression. Measured burning times for Be particles (Ref. 15) show much closer agreement with the values predicted herein.

As would be expected theoretically, and as has been described above for aluminum, the ignition temperature of beryllium in CTF and CTF-Ar mixtures is lower than in oxygen-containing mixtures, because no protective oxide coating can be formed.

One would expect the combustion temperature of beryllium in CTF to be low, since the products of combustion, $BeCl_2$ and BeF_2, have low boiling points. Figures 46 and 47 showed the deposit formed by condensation of gaseous beryllium halides on the cold electrodes.

The theoretical flame temperatures for beryllium burning in mixtures of $HCl/CO_2/N_2$ and $HCl/CO_2/N_2/H_2O$ shown in Fig. 87 are supported by the experimental (Therm-O-Scope) readings shown in Figs. 38 and 44. These indicate that, as predicted, the experimental values all fall below the melting point of BeO, and that the measured temperature is higher in the H_2O-containing mixture. The white deposit formed on the wire during these runs (Fig. 36) has been shown (by X-ray diffraction and wet chemical analysis) to be BeO, which the theoretical product composition curves shown in Figs. 88 and 89 predict.

Summary of Analytical Studies

A mathematical model for calculating the properties of vapor phase flames of metal droplets, and including the effects of back diffusion of vaporized oxide to the droplet surface, has been evaluated. Previous models not including the effects of back diffusion do not predict flame-to-particle radius ratios differing significantly from unity. The present model yields predictions in good agreement with experimental results showing radius ratios as high as 8. The theoretical calculations also closely reproduce the experimental variation of flame to particle radius ratio with total pressure, as shown in Figs. 21 and 77.

The theoretical predictions for burning rates of particles the same diameter as the wire are approximately two orders of magnitude smaller than the values calculated from the observed regression rates of burning wires (both Al and Be). It seems likely that this discrepancy is due to one or a combination of the following effects. First, the wire may be equivalent to a pseudo-sphere having a diameter larger than the actual wire diameter, due to heat transfer, melting, and surface tension inefficiency. Second, the observed regression may represent melting back of the wire in addition to burning, with the molten metal increasing the droplet diameter rather than being burned immediately. Third, in the case of beryllium, the loss of metal during fragmentation gives a spuriously high burning rate. Similar discrepancies are not observed in comparing theoretically predicted Be particle burning times with the experimental results of Maček (Ref. 15). Agreement for a wide variety of oxygen concentrations was within a fraction of 2.

Another experimental result which supports the theoretical model including back diffusion of oxide is the observation that the burning metal particles do not change significantly in size during combustion.

In summary, it is concluded that the mathematical model presented, including the effects of oxide back diffusion, can reliably predict the properties of metal droplet vapor-phase flames, with respect to flame size, particle size and burning rate.

REFERENCES

1. Sehgal, R.: Low Pressure Combustion and Ignition of Solid Rocket Propellants Astronautica Acta, February 1967.

2. Markstein, G. H.: Combustion of Metals. AIAA Journal, March 1963.

3. Wolfhard, H. G., I. Glassman, and L. Green, Jr. (eds.): Heterogeneous Combustion. Academic Press, New York, 1964.

4. Brzustowski, T. A., and I. Glassman: Vapor-Phase Diffusion Flames in the Combustion of Magnesium and Aluminum: II. Experimental Observations in Oxygen Atmosphere, in Wolfhard, H. G. et al (eds.), Heterogeneous Combustion. Academic Press, New York, 1964.

5. Friedman, R., and A. Maček: Ignition and Combustion of Aluminum Particles in Hot Ambient Gases. Combustion and Flame 6, 9-19, 1962.

6. Friedman, R., and A. Maček: Combustion Studies of Single Aluminum Particles. Ninth Symposium (International) on Combustion. Academic Press, New York, 1963.

7. Blackman, A. W., and D. K. Kuehl: Use of Binary Light Metal Mixtures and Alloys as Additives for Solid Propellants. ARS Journal, September 1961.

8. Summerfield, M. (ed.): Solid Propellant Rocket Research. Academic Press, New York, 1960.

9. 2nd ICRPG Combustion Conference, El Segundo, California, November 1965. Proceedings to be published. Abstracts in CPIA Publication No. 95, September 1965.

10. 1966 Spring Meeting, Western States Section, Combustion Institute. Phipps Center, Denver Research Institute, Colorado, April 1966.

11. Kuehl, D. K.: Ignition and Combustion of Aluminum and Beryllium. AIAA Journal, December 1965.

12. Brzustowski, T., and I. Glassman: Vapor-Phase Diffusion Flames in the Combustion of Magnesium and Aluminum: I. Analytical Developments, in Wolfhard, H. G. et al (eds.), Heterogeneous Combustion. Academic Press, New York, 1964.

REFERENCES (Cont'd.)

13. Drew, C. M., R. H. Knipe, and A. S. Gordon: The Morphology of Aluminum Particle Combustion. Presented at the 1966 Spring Meeting, Western States Section/Combustion Institute, Preprint No. WSCI 66-33, April 1966.

14. Kuehl, D. K., M. L. Zwillenberg, and W. G. Burwell: First Annual Report. Investigation of the Ignition and Combustion of Metal Wires. UARL Report E910336-12, July 1966.

15. Maček, A.: Fundamentals of Combustion of Single Aluminum and Beryllium Particles, Eleventh Symposium (International) on Combustion. The Combustion Institute, Pittsburgh (1967).

LIST OF SYMBOLS

d	Diameter, cm
D	Binary diffusion coefficient, cm^2/sec
$EM2$	Flame emissivity, dimensionless
k_{st}	Number of moles of product (oxide) formed per mole of oxidizer
m_{st}	Number of moles of gaseous products formed per mole of oxidizer
M	Mass of metal, gm-mole
M_0	Original mass of metal, gm-mole
n_{st}	Number of moles of fuel which react with one mole of oxidizer
r	Radial distance from center of particle, cm
R_A, r_A	Particle radius, cm
R_B, r_B	Flame radius, cm
$R_B/R_A, r_B/r_A$	Ratio of flame to particle radius, dimensionless
t	Time, sec
T_A	Particle temperature, deg K
T_B	Flame temperature, deg K
T_{ig}	Ignition temperature, deg K
W_f	Fuel diffusive flux, gm-moles/sec
W	Dimensionless burning rate
X_0^*	Lowest oxygen mole fraction for which $\alpha > 0$, dimensionless
$X_{0\,MIN}$	Lowest oxygen mole fraction for which self-sustained combustion is computed, dimensionless
α	Fraction of products vaporized or dissociated, dimensionless

λ	Fraction of vaporized products which diffuse inwards, dimensionless
$(1-\lambda)$	Fraction of vaporized products which diffuse outwards, dimensionless
ρ	Density, gm/cm^3
τ	Burning time, sec

Subscripts

A	Particle surface
B	Flame zone
m	Metal
ox	Oxidizer
o	Initial value
f	Fuel

Table 1

ANALYSIS OF BERYLLIUM WIRE IMPURITIES
By Percent

Sample	A	B	B-1	B-2	C	D	E	F	G	H	H	M	N
Insoluble* Be?												***	***
Be (meta.)**												***	***
Soluble* BeO etc***												***	***
Al													0.2
B												1.1	1.1
Cr												<0.05	<0.05
Co												0.5	0.5
Cu	<0.001	0.001		0.02				0.04	0.002	0.01		<0.005	<0.005
Fe	<0.002	0.08		0.15				0.09	0.005	0.2	0.4	0.35	0.4
Pt									<0.001			<0.05	<0.05
Mg									0.005			2.0	2.5
Sr									<0.001	0.03		<0.02	<0.02
Mo	1.0								<0.005			<0.001	<0.001
Ni	<0.005	0.1		0.02				0.09	53.3	0.1		<0.02	<0.02
Si				0.05				0.05	<0.005	0.4	0.3	0.14	0.8
Ag								0.02		0.01	0.05	<0.01	<0.01
Sn									<0.001	0.01		<0.05	<0.05
Ti	0.002	0.002					0.2		<0.002	0.001		<0.01	0.10
Au	0.05											1.1	1.1
Ca												.10	.16
Na								0.3		0.3		<.2	<.2

Wire Identifications:

A   Brush Beryllium Wire - as drawn
B   Brush Beryllium Wire - annealed
B-1 Brush Beryllium Wire - annealed, Sample 1
B-2 Brush Beryllium Wire - annealed, Sample 2
C   Brush Beryllium Wire - annealed and pickled
D   Brush Beryllium Wire - annealed - activated by Berylco
E   Brush Beryllium Wire - annealed - passivated by Berylco
F   Berylco Wire - as drawn
G   General Astrometa Corp. - nickel-clad beryllium wire

H   Type F - pickled at UARL
     Type H - gold plated at UARL
     Type H - annealed at UARL
     Type H - anodized at UARL
M   Berylco Wire - pickled - heavily anodized
     General Astrometal Corp. - GH grade - annealed and pickled
     General Astrometal Corp. - GH grade - annealed
     General Astrometal Corp. - GH grade - annealed and pickled, repickled at UARL
     Type H-1 - pickled at UARL

* in Br-CH₃OH and HCl-CH₃OH

** = .. percent

*** Not measured

Table II

RAW MATERIALS SPECIFICATION

Material	Specification	Source
Nitrogen	99.995%, dry	Union Carbide
Argon	99.995%	Union Carbide
Oxygen	99.995%	Union Carbide
Carbon Dioxide	99.8% dry	J. F. Baker Chem. Co.
Hydrogen Chloride	99.0%	J. F. Baker Chem. Co.
Chlorine Trifluoride	99.0% min.	Allied Chem. Corp.
Water	tap water	
Oscillograph Paper	Lino-WRIT Spec #28	Dupont
Oscillograph Paper Developer	#49943-3	CEC
Movie Film	16 mm 136A Superior 2	Dupont
Movie Film	16 mm Tri-X 7278	Kodak
Film for Hilger-Watts Spectrograph	Polaroid Type 52 or Type 1-F Glass Plates	Polaroid Kodak
Film for ARL and Dietert Spectrograph	Plus-X or Tri-X 35 mm	Kodak
Reference Lamp for Temperature Calibration	GE 1926 18/T10/2P-6U with SR6A filament	General Electric General Electric
Viking 232	Tl-Hg-In alloy	Victor King Materials Lab

Table III

TEMPERATURES AT WHICH BERYLLIUM WIRES BROKE OR IGNITED

Wire Designation from Table I	Observed Reaction	0.75 – 15 psia	16 – 138 psia	139 – 460 psia	461 – 1380 psia
			100% O₂		
A	B		2140 ⟶ 3060	1884 ⟶ 2415	
B–	B	1858 ⟶ 2296	1961 ⟶ 2372	1438 ⟶ 1873	
	I	2132 (2932) 3375	2334 (2727) 3003	1773 (2107) 2636	1573 (2074) 2467
B–2	B			1438 ⟶ 1846	
C	B		1833 ⟶ 2303	2014 ⟶ 2642	
	I				(2129)
D	I		2443 (2559) 2635		
E	B		1192 ⟶ 1412		
F	B	1443 ⟶ 1928	1355 ⟶ 2124	1875 ⟶ 2414	
	I		1794 (1847) 2070	1752 (1866) 2127	(2291)
G	I		1704 (1934) 2430	(1934)	
H	B	1577 ⟶ 1732			
	I			1713 (1813) 2478	(2112)
I	B			1897 ⟶ 2443	
J	B				
	I			1633 (1944) 2345	
K	B		1422 ⟶ 1734		
	I		1435 (1712) 2413	1713 1747 2443	
	B		1877		
L	B	1777 ⟶ 2434	1733 ⟶ 1973		
	I		1714 (1947) 2403	1714 (1757) 2443	
			90% O₂ – 10% Ar		
B–	B		1873 ⟶ 2413		
	I		1943 ⟶ 2473		
C	I			(1934)	
			80% O₂ – 20% Ar		
C	B		1973 ⟶ 2343		
F	B			1	
			70% O₂ – 30% Ar		
B–	B	1773	1943 ⟶ 2443	1973 ⟶	
C	B		2073 ⟶ 2413		
F	B			1943	
			50% O₂ – 50% Ar		
H	B				1774
			100% Ar		
B–	B	1773 ⟶ 2434	2343 ⟶ 2473	1943	1943
	B		1457		
	B		2073		
H	B				1973
			100% N₂		
H	I				1934 (1943) 2473

Key

B indicates wire broke without ignition
I indicates wire ignited
⟶ indicates temperature range

All temperatures on Kelvin scale
Temperatures in parentheses are averages

Table IV

SUMMARY OF BERYLLIUM IGNITION BEHAVIOR WITH DIFFERENT OXIDIZERS
(Pickled Beryllium Wire)

Oxidizer	Pressure Range, psia	Ignition Temperature Range, Deg K	Remarks
O_2	0.25 to 1000	2400-2800	No ignition below 16 psia MP of BeO = 2820 K
O_2-inert	100 to 1000	-	No reproducible ignitions
N_2	500	2350	Reproducible
ClF_3	7.5 - 17.5	1073	Limited by CTF vapor pressure MP of Be = 1551 $\pm$ 5
ClF_3-inert	150-165	1100	Argon inert
H_2O	100	1000-1500	
H_2O-inert	100-500	1000-1500	
$CO_2/HCl/N_2$	500	Reacted between 2100-2500	Simulated combustion gases; no self-sustained combustion
$CO_2/H_2O/N_2$	500	1200-1500	Simulated combustion gases
$ClF_3/CO_2/HCl/N_2$	25	1550	

WIRE COMBUSTION APPARATUS

TEST CHAMBER
WINDOWS
TRAY
FAN
SAMPLE
VENTS
VENTS
VENT

FILTER
LIQUID N₂ TRAP
VACUUM PUMP

NaOH TRAP
N₂
ClF₃
HCl

X MANUAL VALVE
✳ RELIEF VALVE
⊗ BLOWOUT DIAPHRAGM
◔ PRESSURE GUAGE
▨ CHECK VALVE

HOOD WITH EXHAUST FILTER

CONTROL PANEL

PRESSURE REGULATOR
Ar
PRESSURE REGULATOR
CO₂
PRESSURE REGULATOR
N₂

FIG. 2
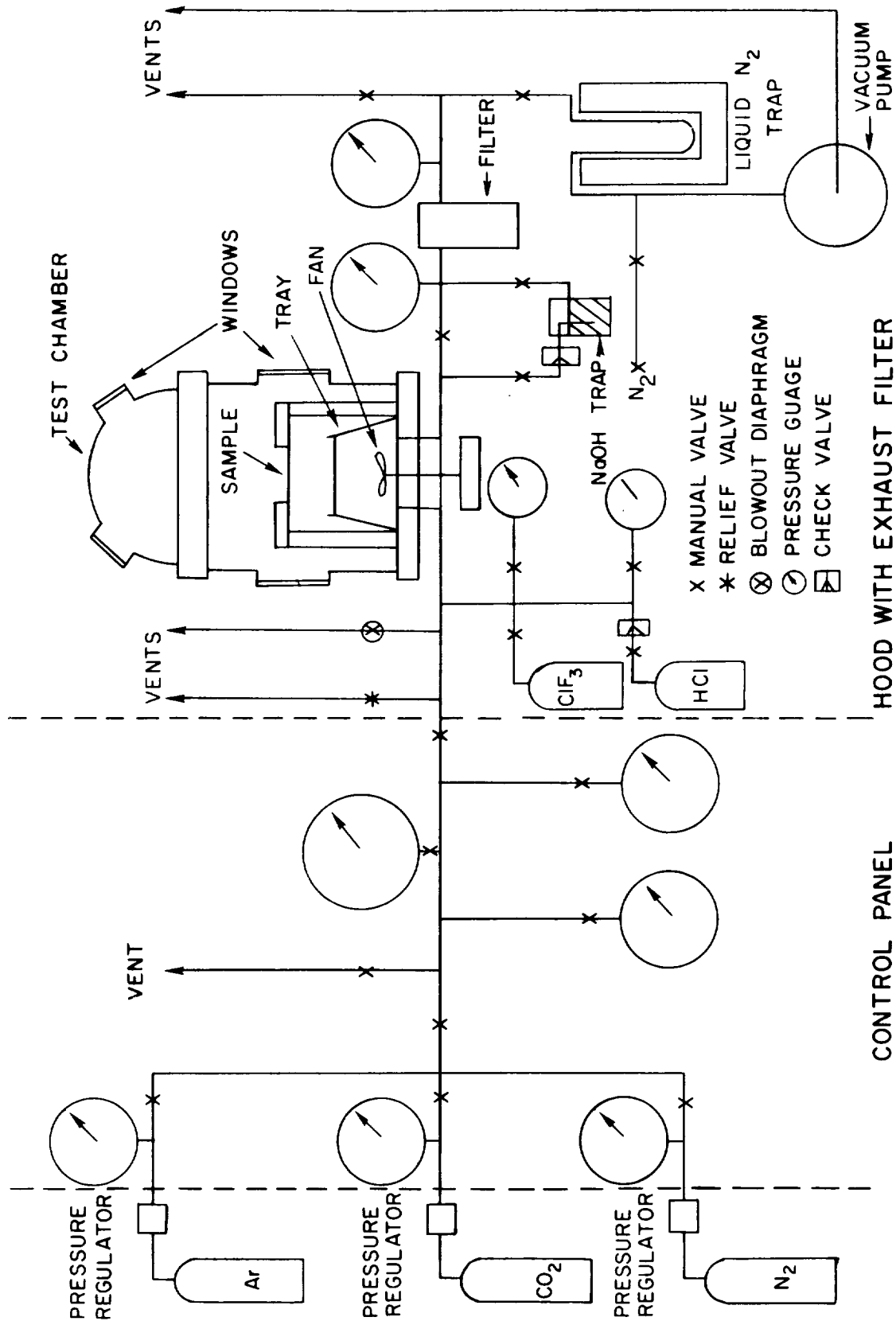
THERMOSTATICALLY CONTROLLED STEAM GENERATOR
DISASSEMBLED

WATER
RESERVOIR

OPTICAL CELL

THERMOSTAT

HEATER

THERMOMETER

FIG.3
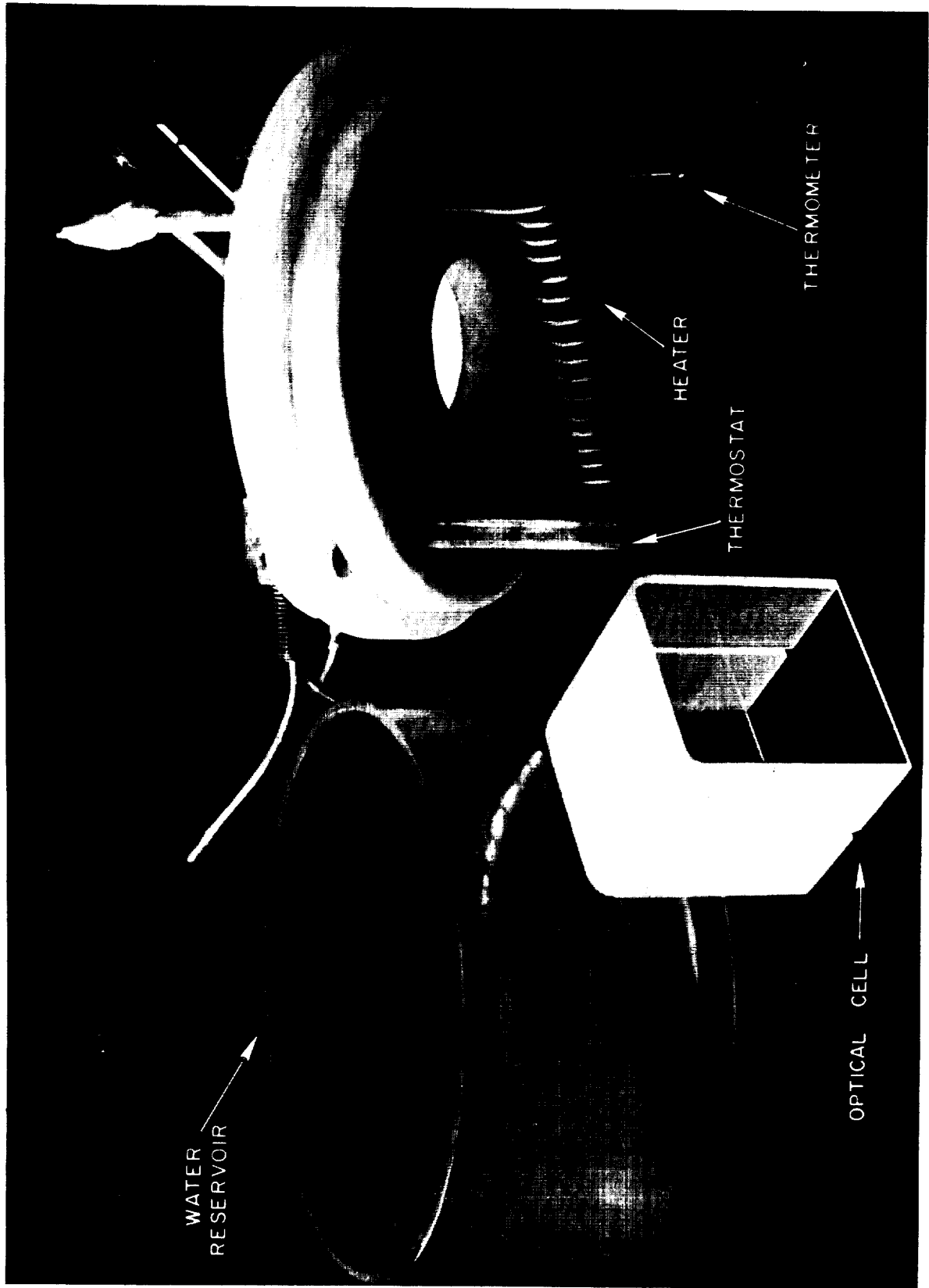
THERMOSTATICALLY CONTROLLED STEAM GENERATOR
ASSEMBLED

FIG. 4
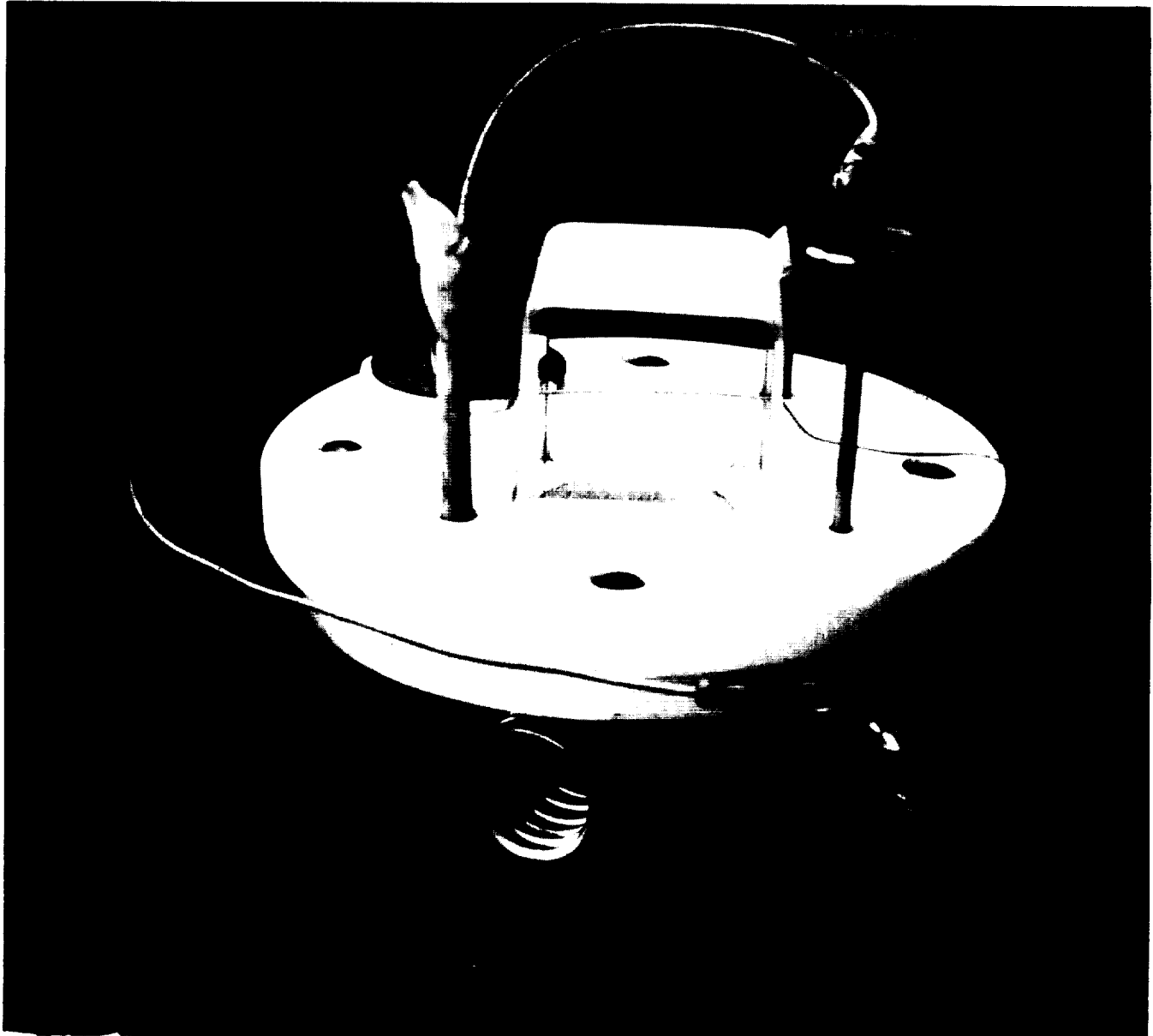
EXPERIMENTAL APPARATUS

CONTROL
PANEL

RECORDING
OSCILLOGRA

CAMERA

PHOTO CELL

TEST
CHAMBER

FIG. 5
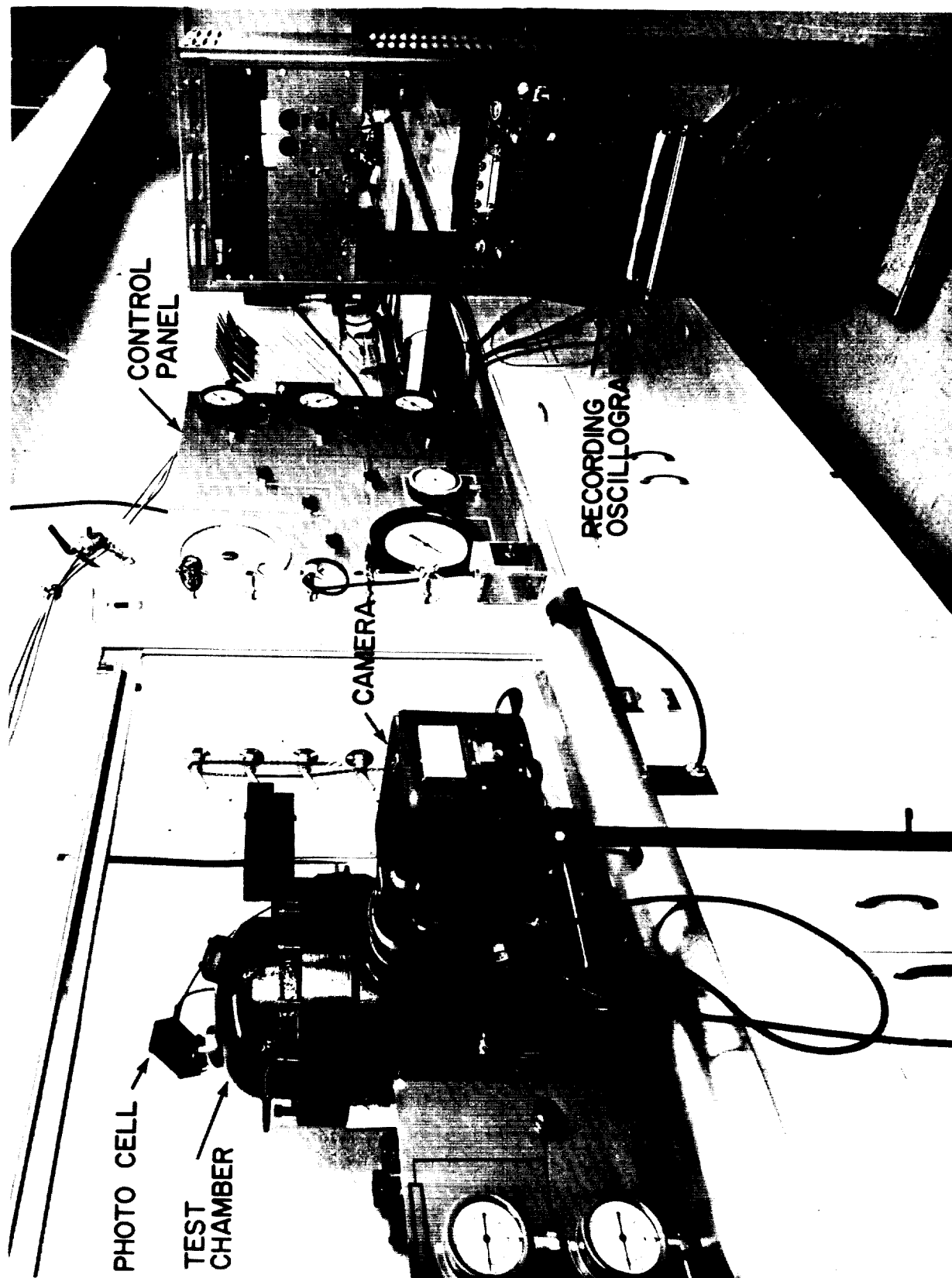
ELECTRICAL SCHEMATIC OF LOW HEATING RATE IGNITION SYSTEM

TEST CHAMBER

SAMPLE

OPTICAL FILTER

2 PHOTOCELLS, 1 WITH OPTICAL FILTER

DC AMP

AC AMP

RECORDING OSCILLOGRAPH

POWERSTAT

VARIAC

MOTOR

F

R

220 V

110 V

60 ~

FIG.6
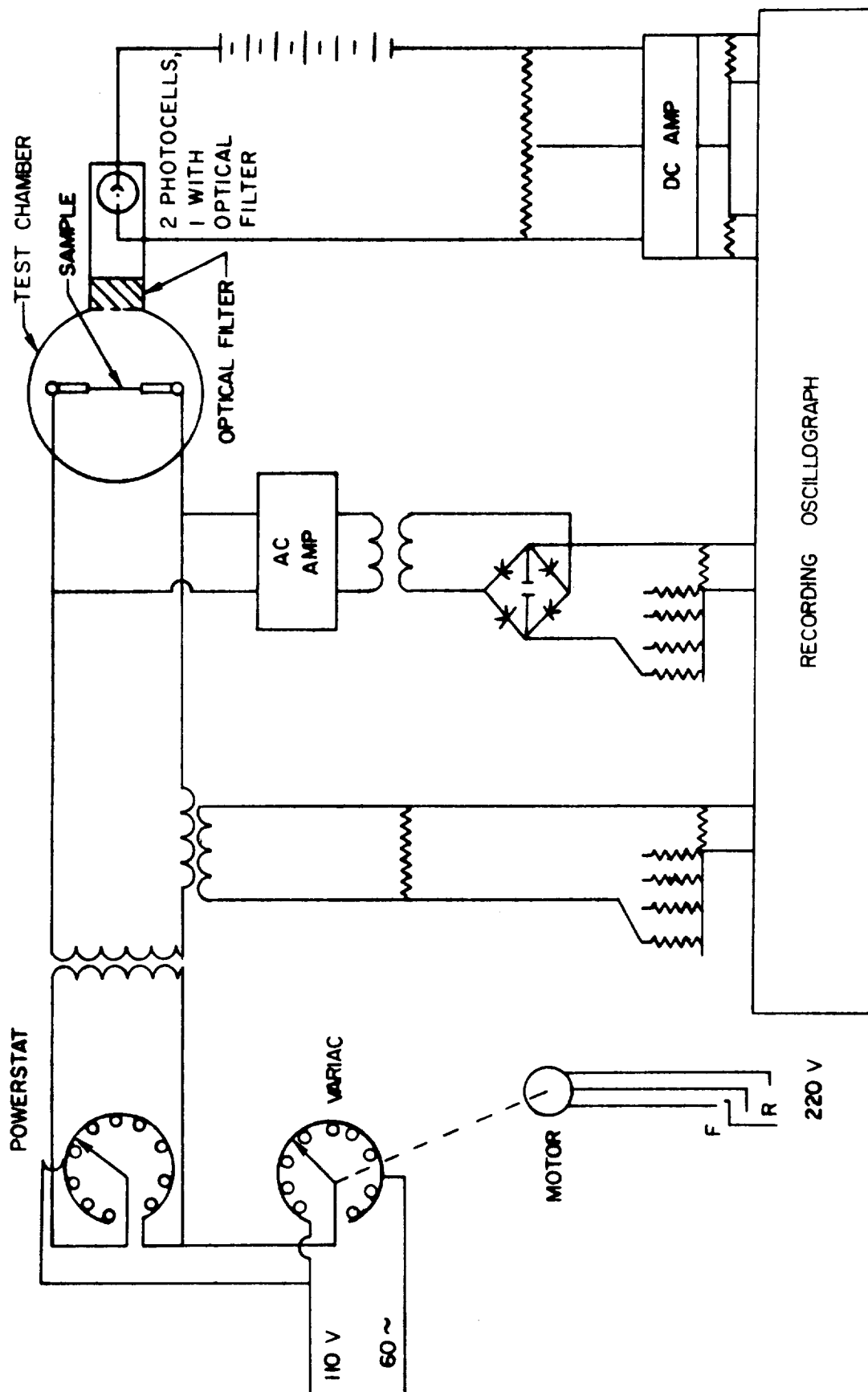
PULSE IGNITION CIRCUIT SCHEMATIC

TEST CHAMBER

SAMPLE

2 PHOTOCELLS
1 WITH OPTICAL
FILTER

TEMPERATURE

VOLTAGE

CURRENT

TRIGGER

V

I

T

FAST ACTING
SWITCH, JENNINGS MODEL FD49

.5mh

5K

SHUNT

9000 µf

0-300V

V

DC
POWER
SUPPLY

AC
115 V

TRIGGER
TO
SCOPE

SWEEP SAWTOOTH OUTPUT

+

−

DIODE

67.5 V

+

−

135 V

FAST
ACTING
SWITCH

NEON SYNCHRONIZING
LAMPS IN HIGH SPEED
MOVIE CAMERA

110V AC, 60 CPS
OR 1000 CPS SQUARE WAVE GENERATOR

FIG. 7

WIRE IGNITION CONTROLS

FAST ACTING
VACUUM SWITCH

PULSE IGNITION
CAPACITOR BANK
AND CONTROLS

MOTOR DRIVEN VARIAC

VARIAC MOTOR
CONTROL BOX

RL-67-143-B

FIG.8

VACUUM PHOTODIODES

MONITOR SIGNAL OUTPUT TO OSCILLOSCOPE

KERR CELL CIRCUIT DIAGRAM

D_1 D_2 D_3

R_1 R_2 R_3 R_D R_M

R_L

K   KERR CELL

DC POWER SUPPLY

+   —

V

FIG.9

KERR CELL OPTICAL DIAGRAM

POLARIZERS SET FOR
MAXIMUM TRANSMISSION
WITH FULL VOLTAGE ON
KERR CELL (NO LIGHT-
ON DIODES) AND MINIMUM
TRANSMISSION WITH MIN-
IMUM VOLTAGE ON KERR
CELL

FIG. 10
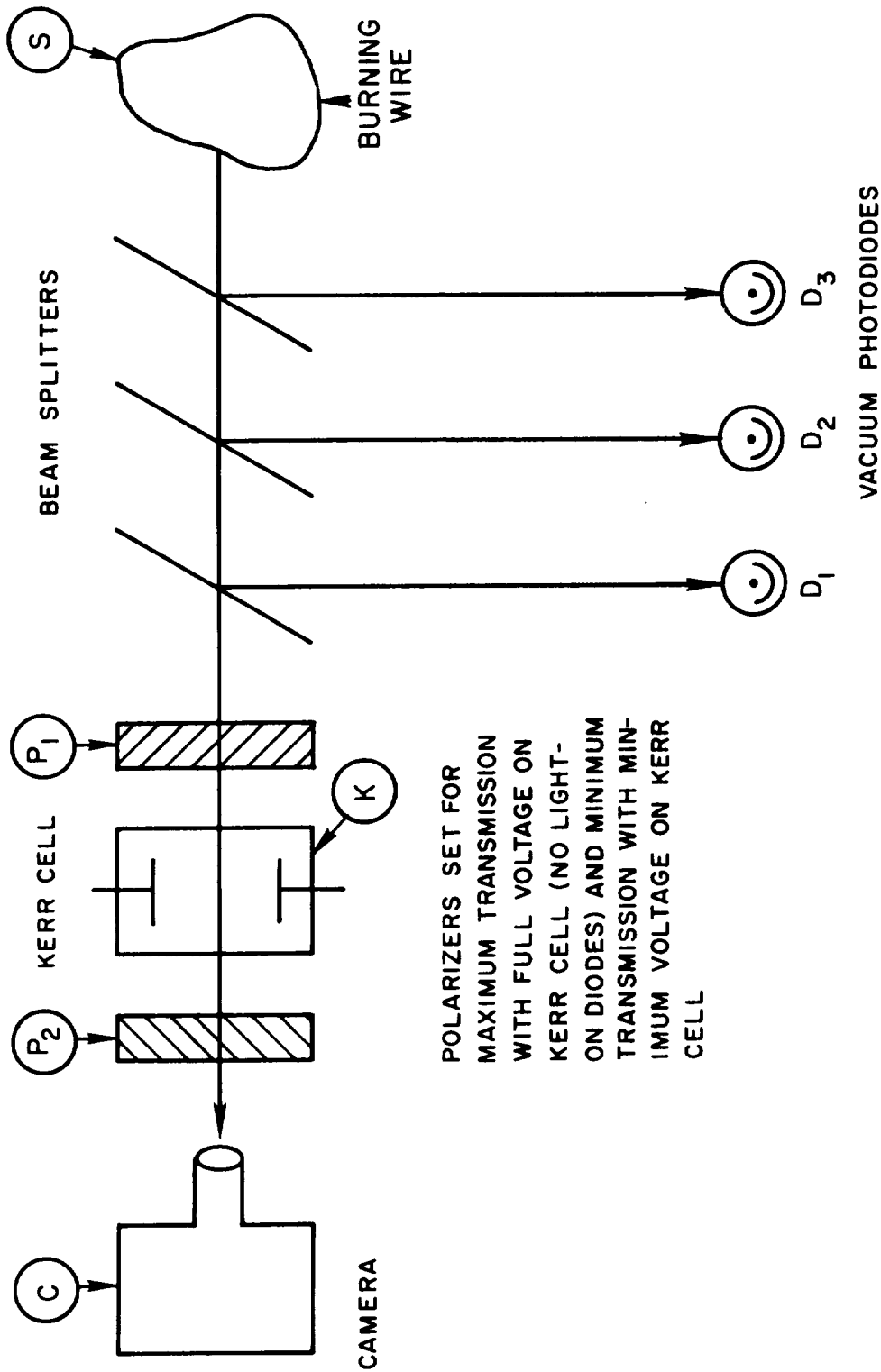
EFFECT OF APPLIED VOLTAGE ON OPTICAL DENSITY OF KERR CELL

FIG.11
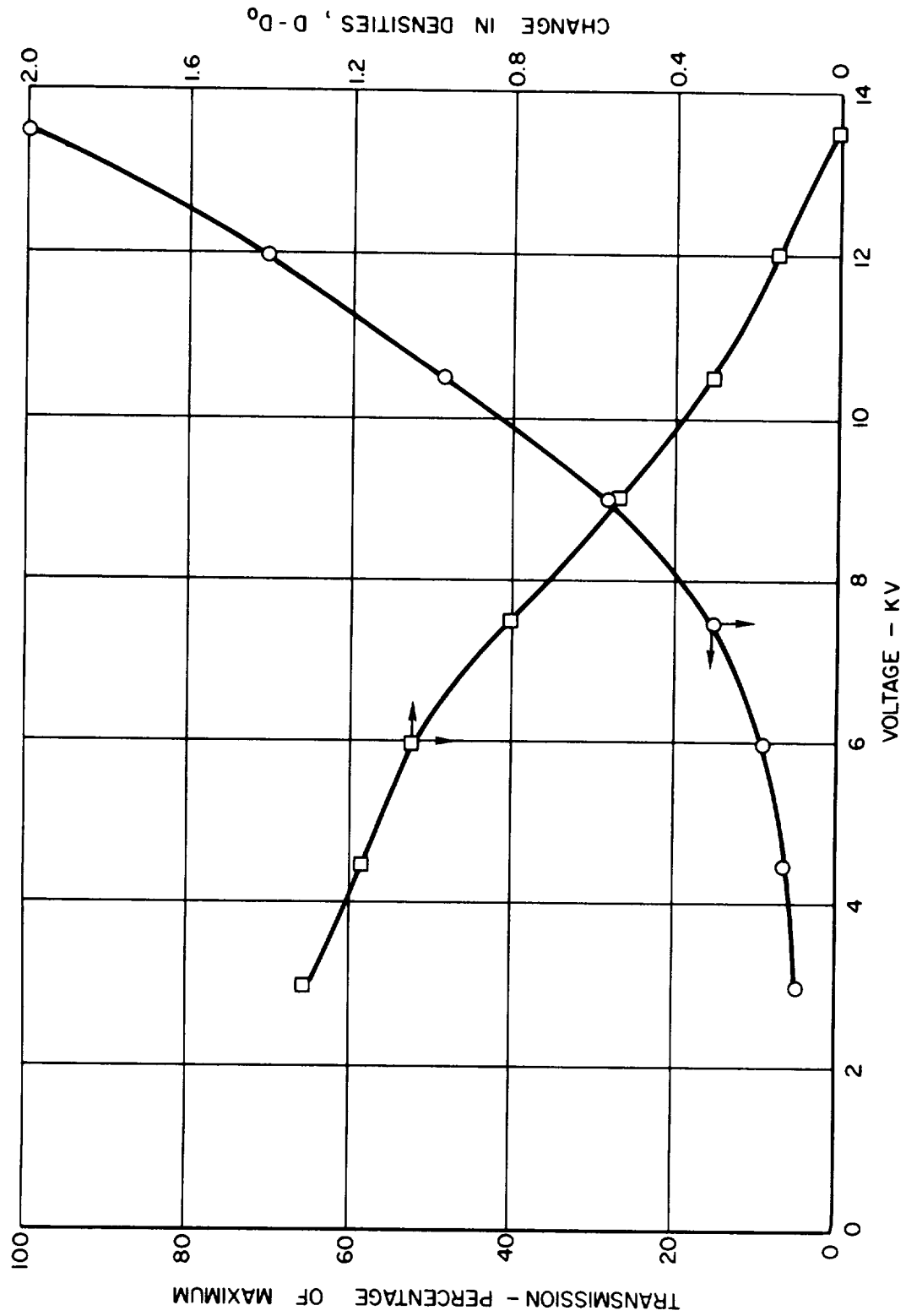
KERR CELL EXPOSURE CONTROL

FIG.12
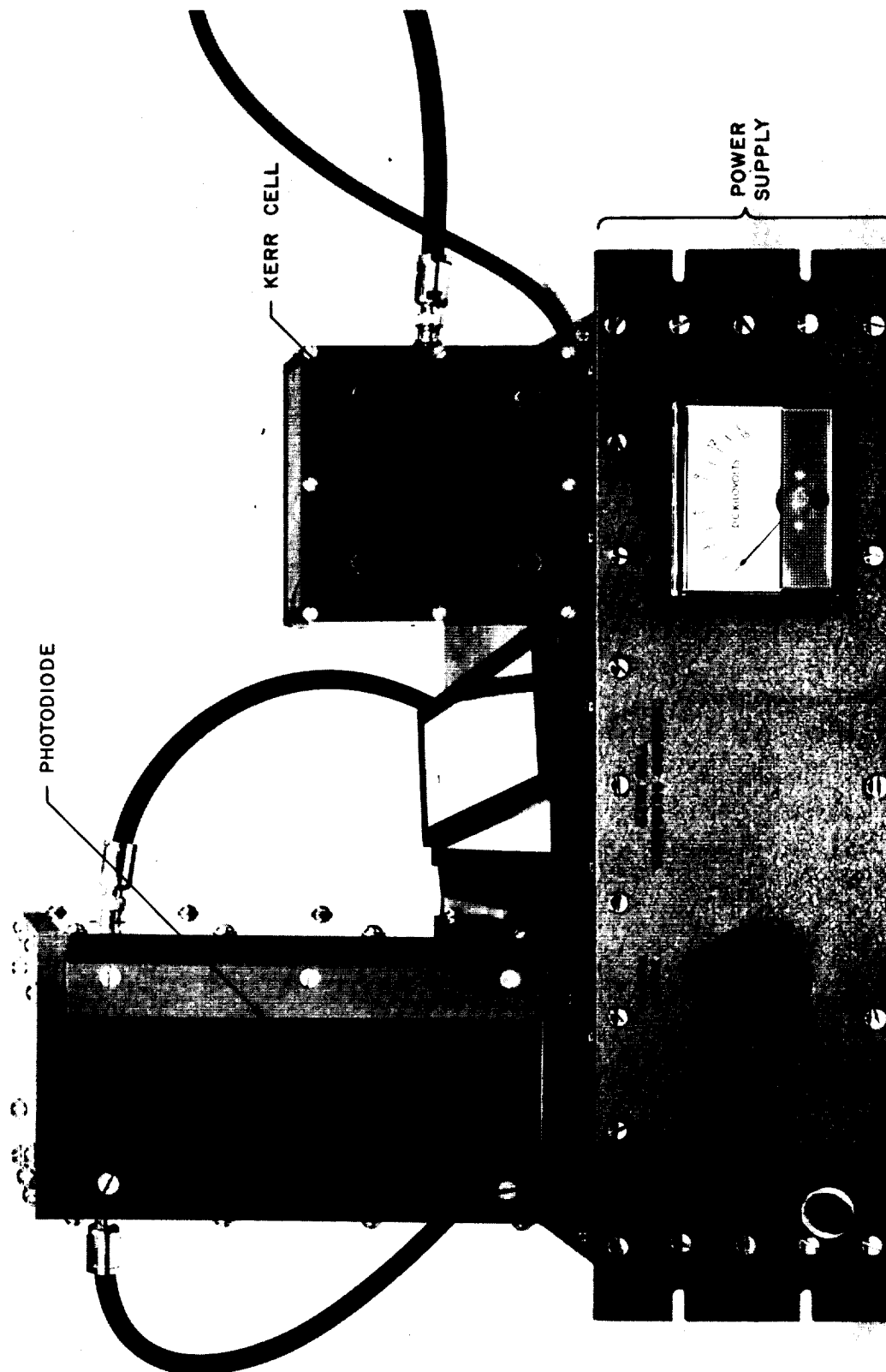
PHOTOGRAPHIC SEQUENCE AND OSCILLOSCOPE RECORD OF IGNITION AND COMBUSTION OF 20-MIL 95% Al 5% Mg WIRE AT 300 VOLTS

I ATM
AIR

~ 6000 PICTURES PER SECOND

FIG.13
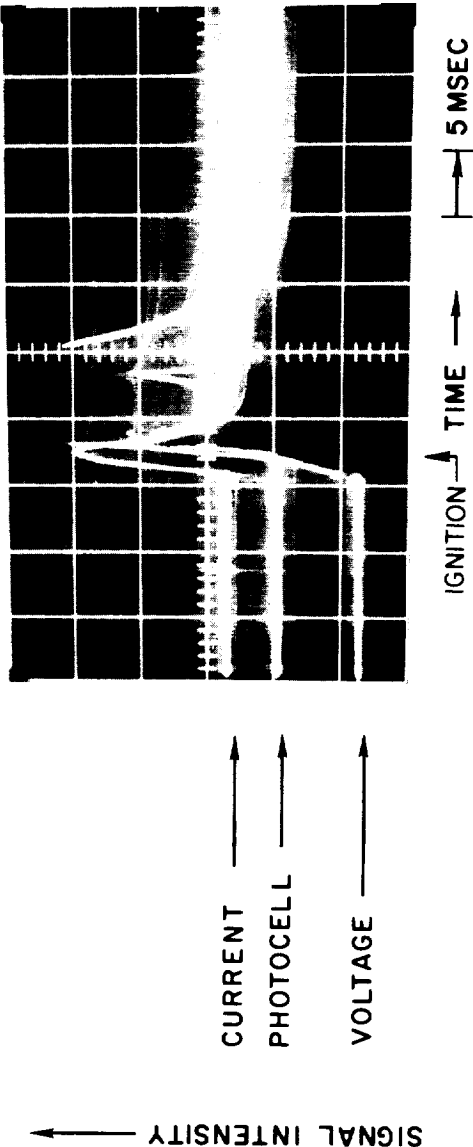
VAPOR PRESSURE CURVE OF ALUMINUM SHOWING POSSIBLE IGNITION TEMPERATURE – PRESSURE RELATIONSHIPS

FIG.14
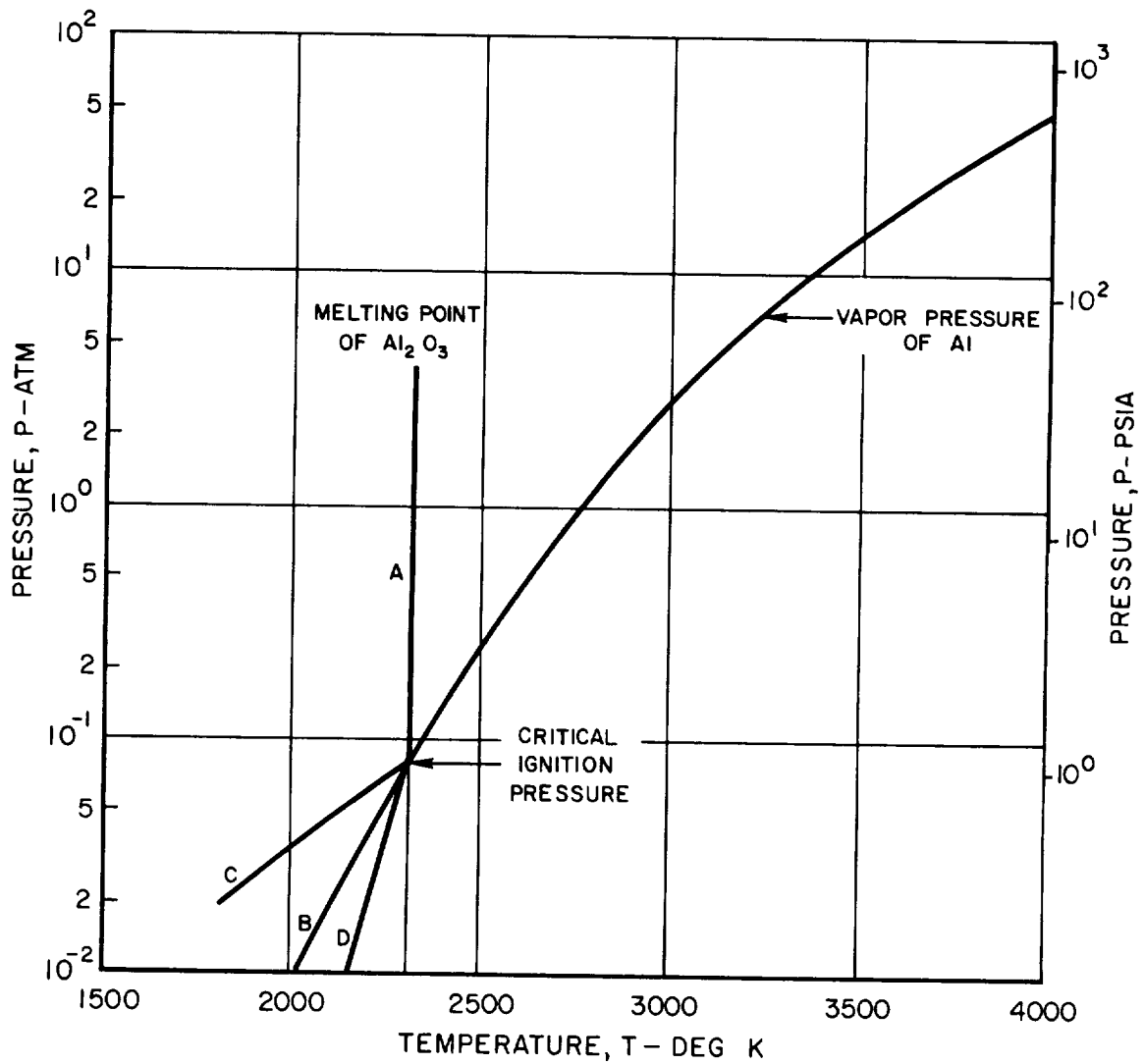
EFFECT OF PRESSURE ON IGNITION TEMPERATURE OF 20-MIL ALUMINUM WIRES IN 100 PERCENT OXYGEN
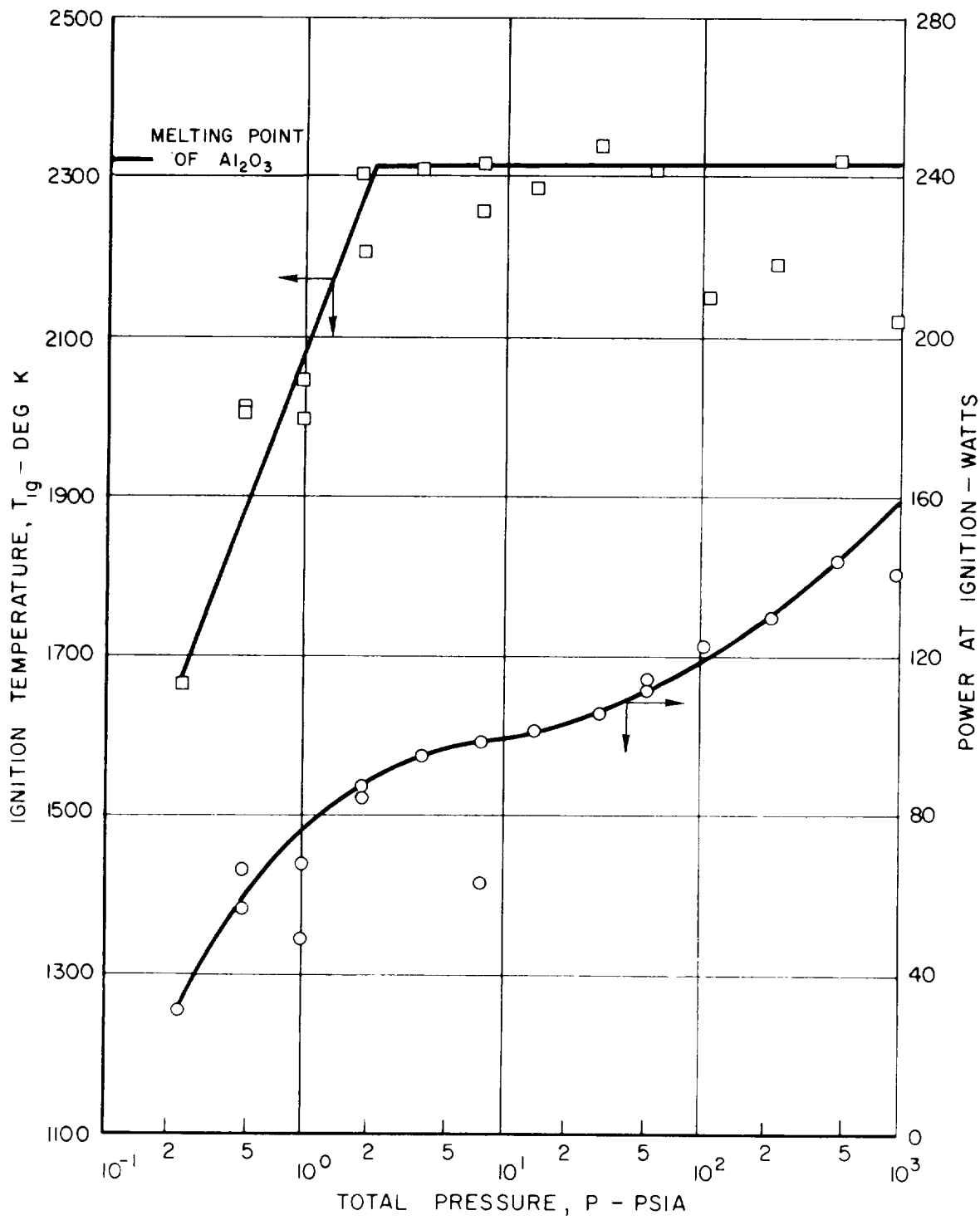
EFFECT OF OXYGEN CONCENTRATION ON IGNITION

TEMPERATURE OF 20-MIL ALUMINUM WIRES ABOVE

CRITICAL IGNITION PRESSURE
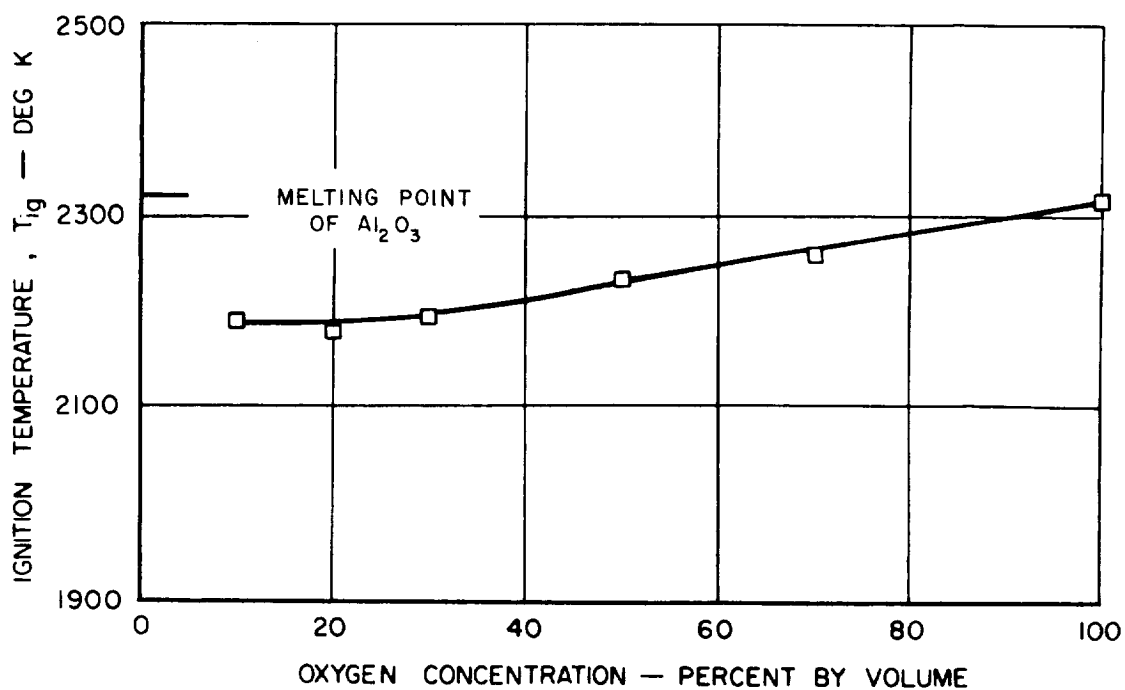
EFFECT OF PRESSURE ON POWER TO IGNITE OR
BREAK 20-MIL ALUMINUM WIRES IN ARGON AND
OXYGEN / ARGON MIXTURES

◇	100% ARGON
▽	100% OXYGEN
△	20% OXYGEN-80% ARGON

OPEN SYMBOLS - IGNITION

CLOSED SYMBOLS- NON IGNITION

FIG 17
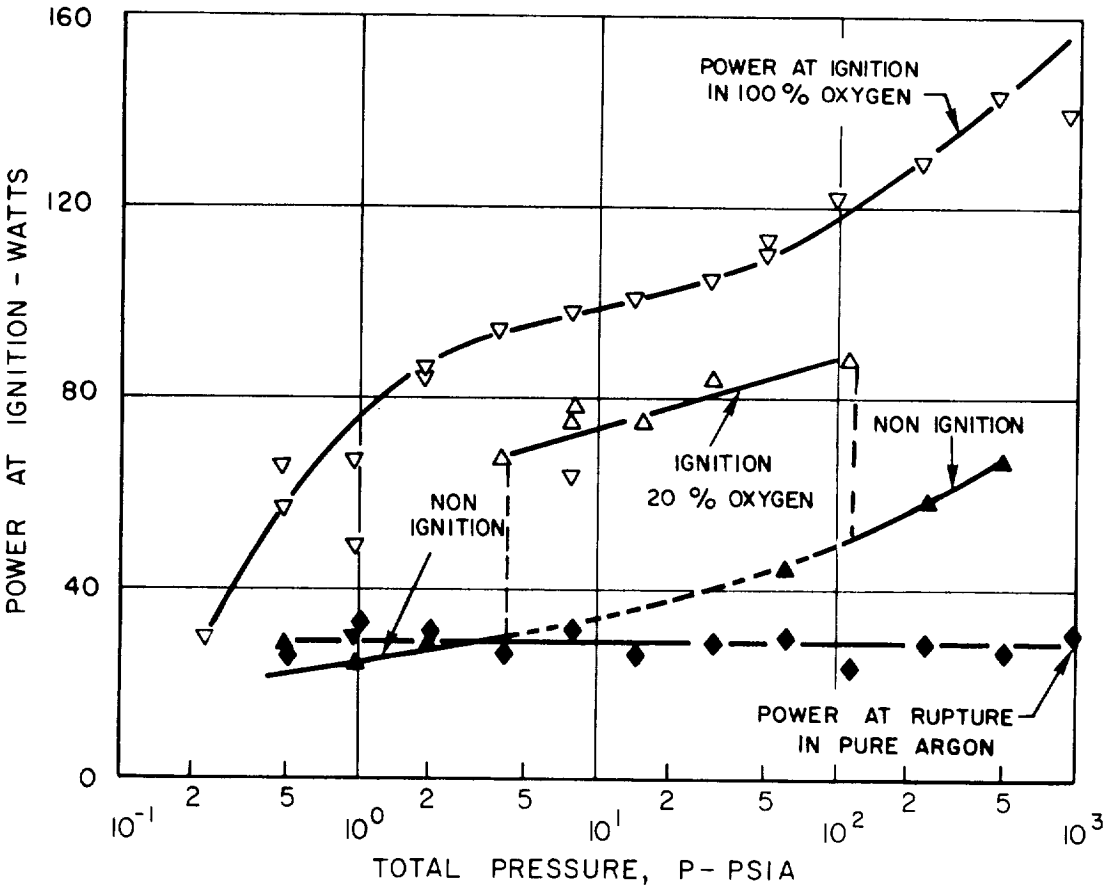
PHOTOGRAPHIC SEQUENCE ILLUSTRATING TYPICAL IGNITION AND COMBUSTION OF ALUMINUM WIRES AT MODERATE PRESSURES

TOTAL PRESSURE: 32 PSIA

OXIDIZER MIXTURE COMPOSITION: 20% O_2 – 80% Ar

WIRE DIAMETER: 20 MIL (500 MICRONS)

FRAMING RATE: 250 FPS

TIME ———⟶

TYPICAL ALUMINUM COMBUSTION CHARACTERISTICS

FIG. 19
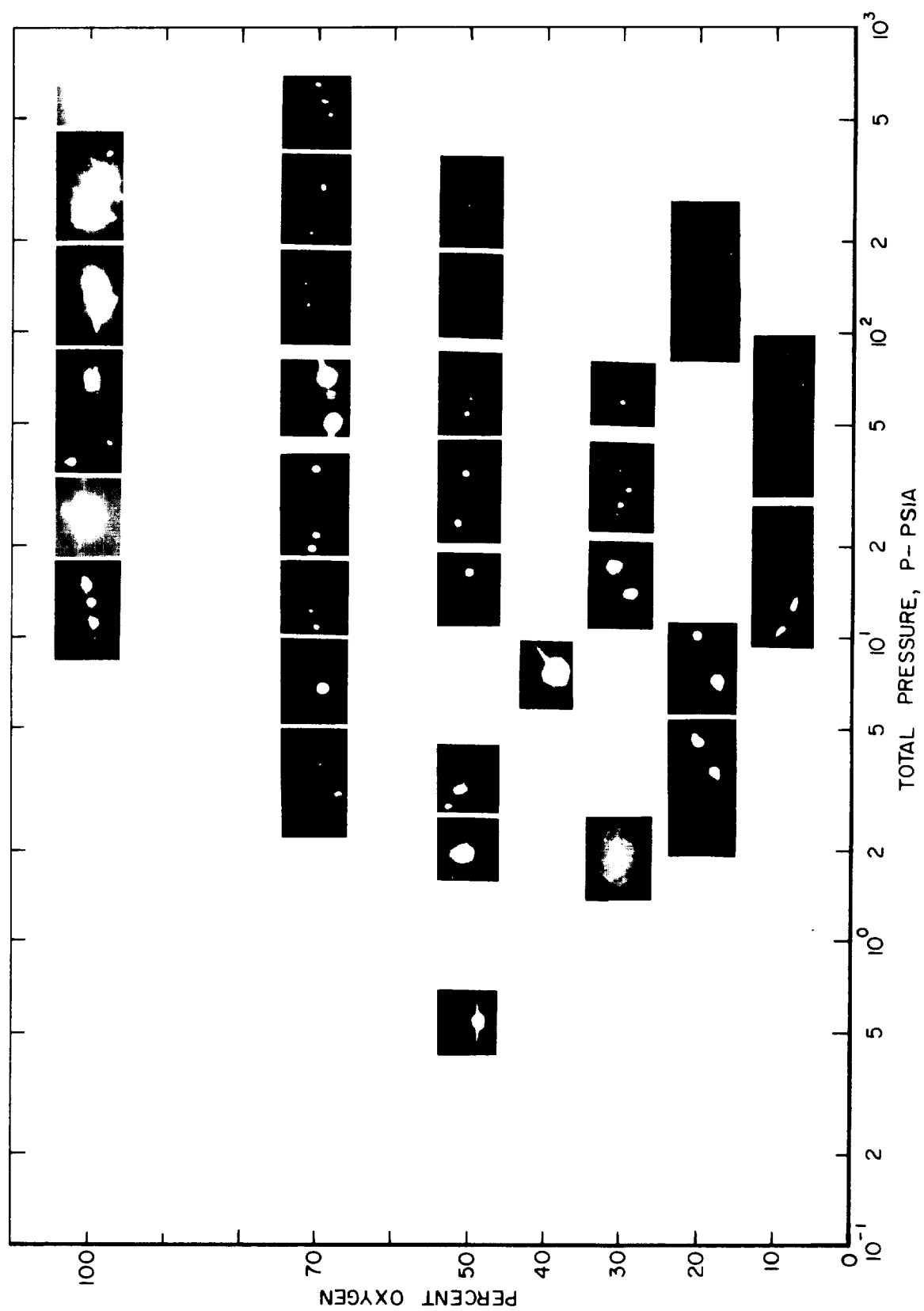
REACTION PRODUCTS, ALUMINUM IN 50% Ar, 50% O_2 AT 32 PSIA

RL-67-243-C
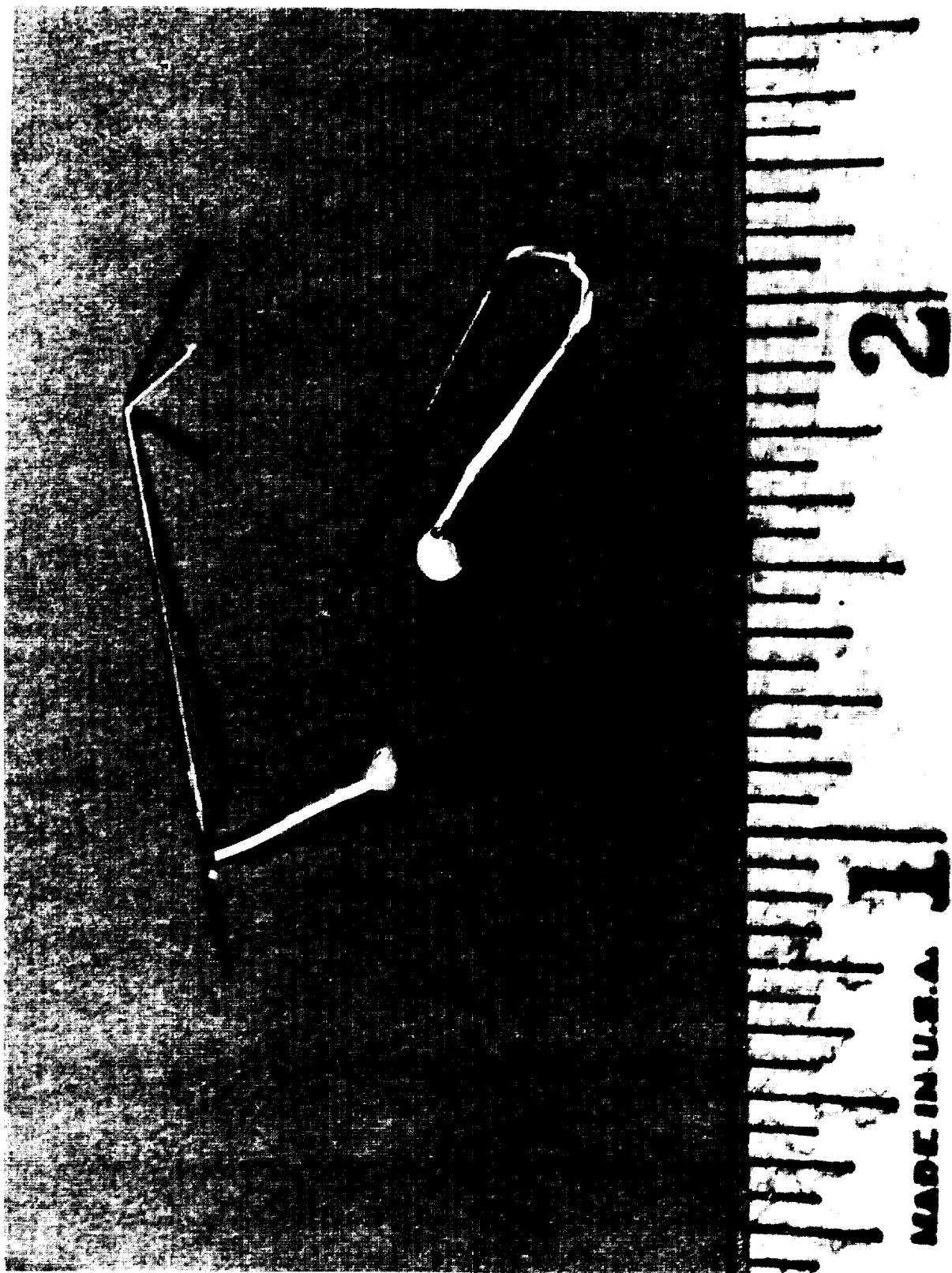
REACTION PRODUCTS, ALUMINUM IN 100% O₂ AT 500 PSIA

EFFECT OF PRESSURE ON MEASURED FLAME TO WIRE RADIUS RATIO (R_B/R_A) FOR 20-MIL (500-MICRON) ALUMINUM WIRES

□	100% OXYGEN
△	50% O_2 – 50% N_2
◇	50% O_2 – 50% He
●	50% O_2 – 50% Ar
▼	40% O_2 – 60% Ar
◆	30% O_2 – 70% Ar
■	20% O_2 – 80% Ar

NOTE: FLAME RADIUS DATA OBTAINED FROM
PHOTOGRAPHIC RECORDS OF WIRE COMBUSTION

FIG 22
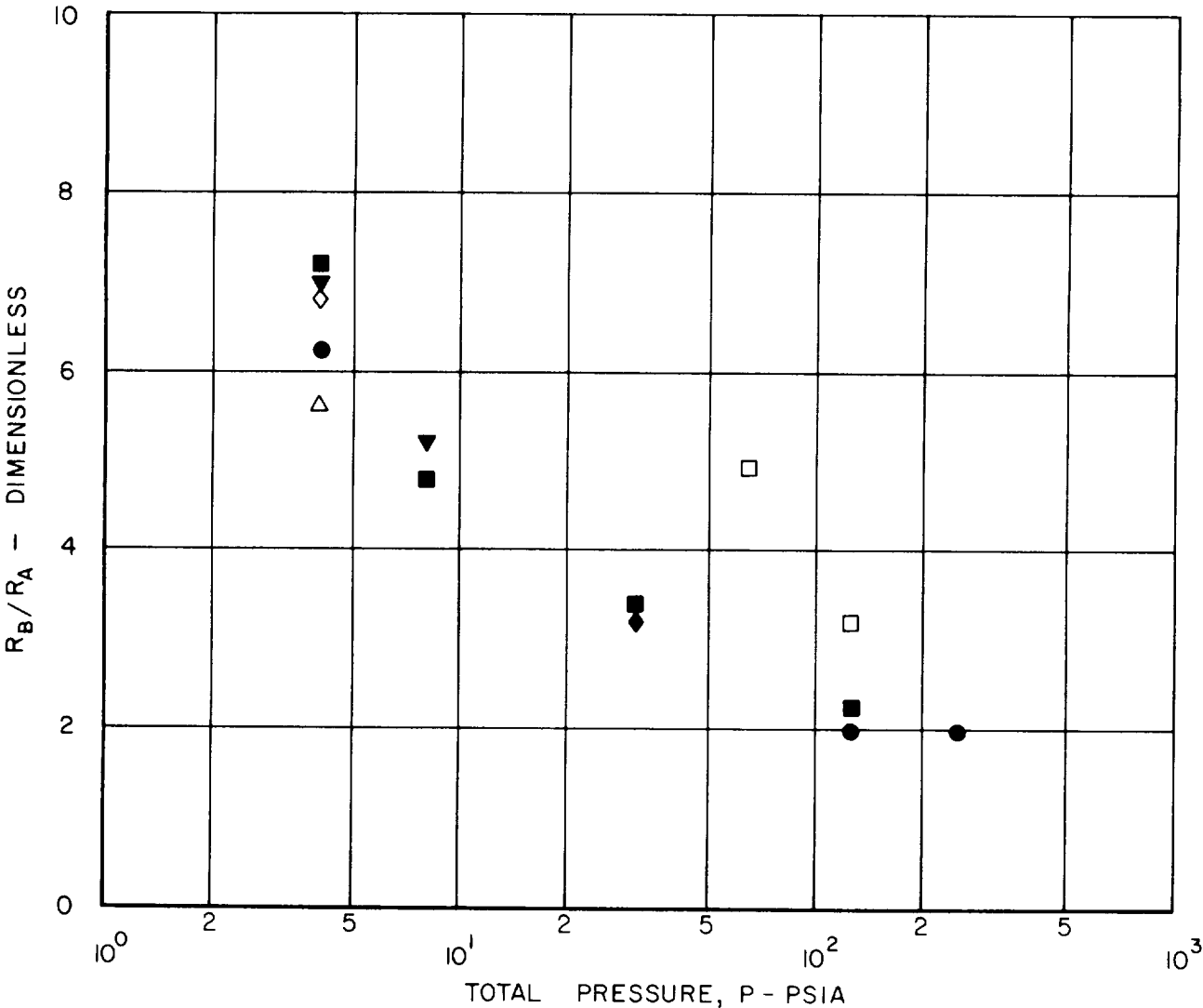
PHOTOGRAPHIC SEQUENCES FOR COMPARISON OF BERYLLIUM AND ALUMINUM IGNITION AND COMBUSTION

20-MIL WIRE   125 PSIA

100% OXYGEN   250 VOLTS

10,000 PICTURES PER SECOND

BERYLLIUM (SEE FIG. 24 FOR PRECEDING FRAMES - 1 THROUGH 10)

0.5 MSEC

IGNITION

ALUMINUM

IGNITION

FIG.23
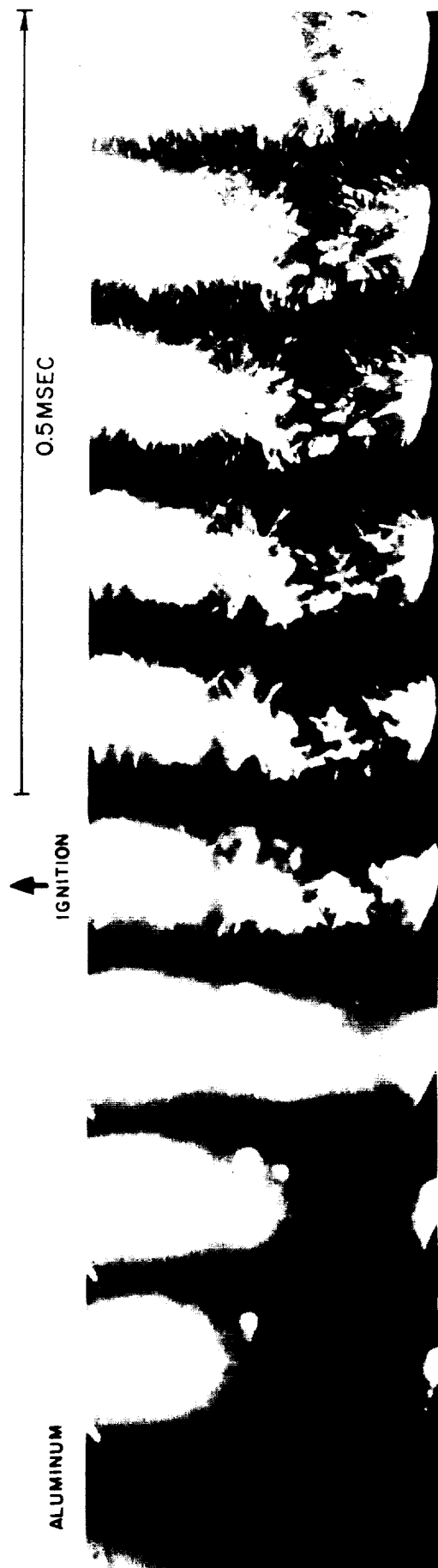
TYPICAL NONUNIFORMLY HEATED BERYLLIUM WIRE PRIOR TO IGNITION
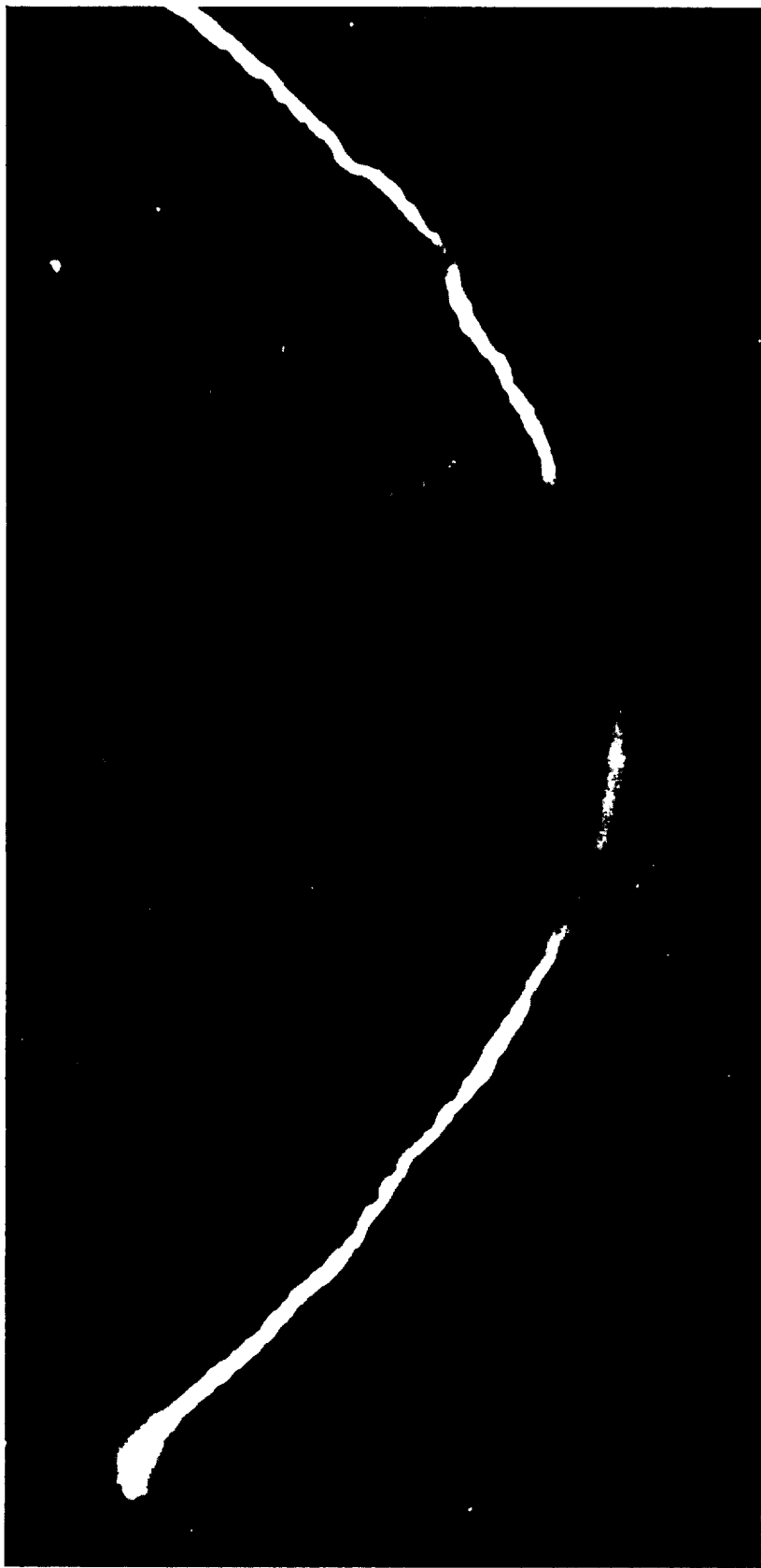
FIG. 24

PHOTOGRAPHIC SEQUENCE AND OSCILLOSCOPE RECORD OF IGNITION AND COMBUSTION OF 20-MIL BERYLLIUM WIRE AT 240 VOLTS

125 PSIA
100% OXYGEN

10,000 PICTURES PER SECOND

FIG.25

PHOTOGRAPHIC SEQUENCE AND OSCILLOSCOPE RECORD OF IGNITION AND
COMBUSTION OF 20-MIL BERYLLIUM WIRE AT 250 VOLTS

125 PSIA
100% OXYGEN

10,000 PICTURES PER SECOND
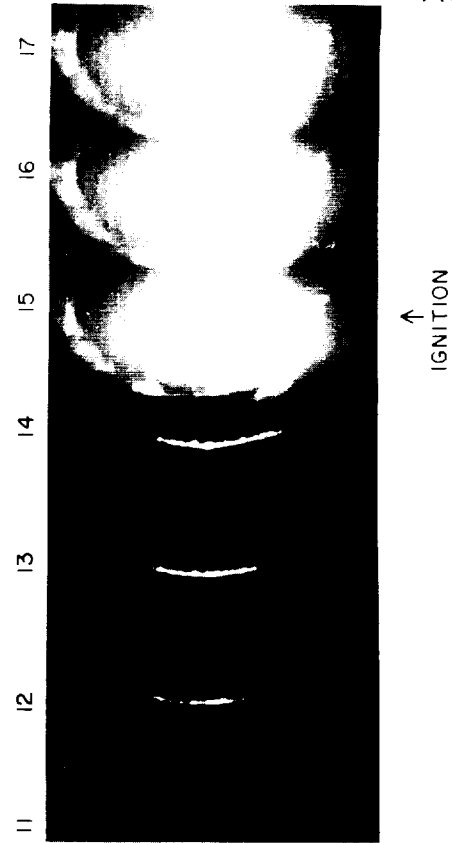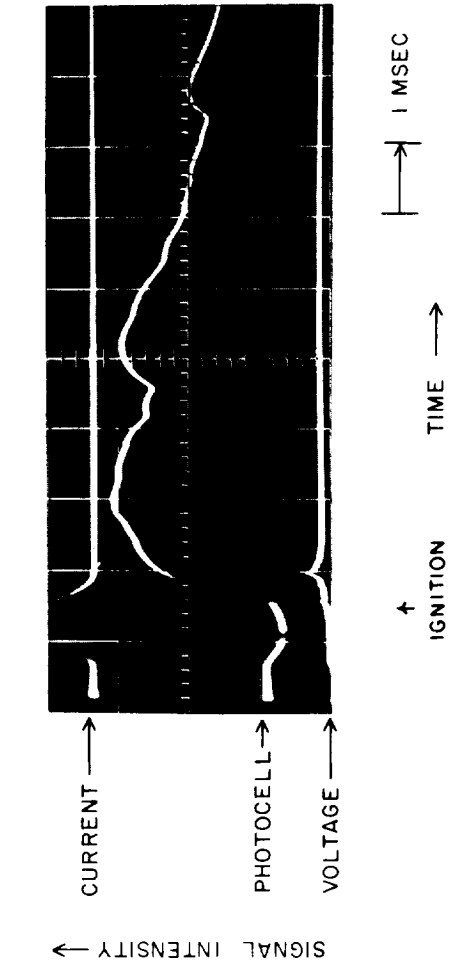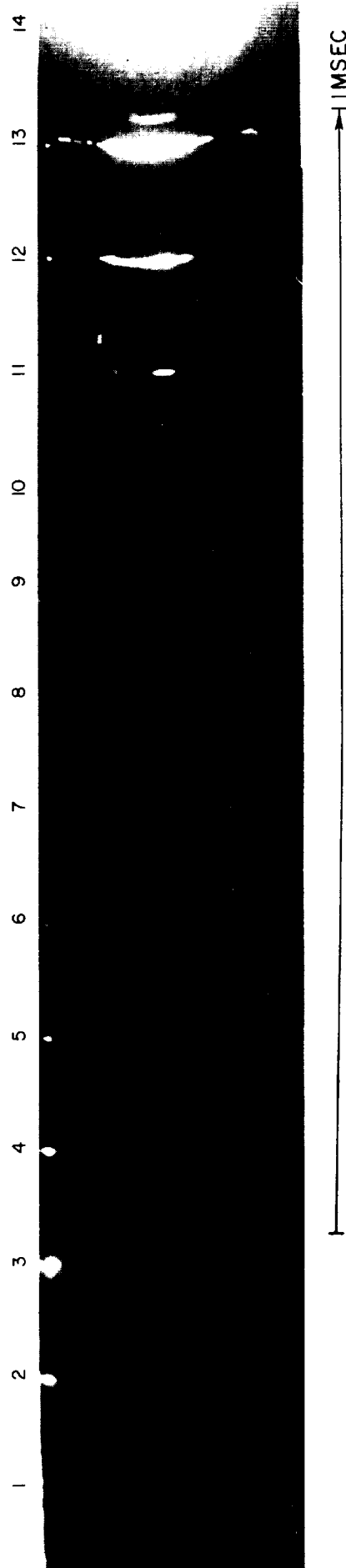
OSCILLOSCOPE RECORD OF 20-MIL BERYLLIUM WIRE PULSE HEATED

500 PSIA
CONDENSER VOLTAGE : 190 VOLTS
39.9% HCL , 39.7% CO_2 , 20.4% N_2

NOTE:PULSE DISCHARGE DID NOT RESULT IN IGNITION FOR THIS TEST

SIGNAL INTENSITY ⟶

CURRENT ⟶

PHOTOCELL ⟶

VOLTAGE ⟶

⊢⟶⊣ 2 MSEC

TIME ⟶

FIG. 27
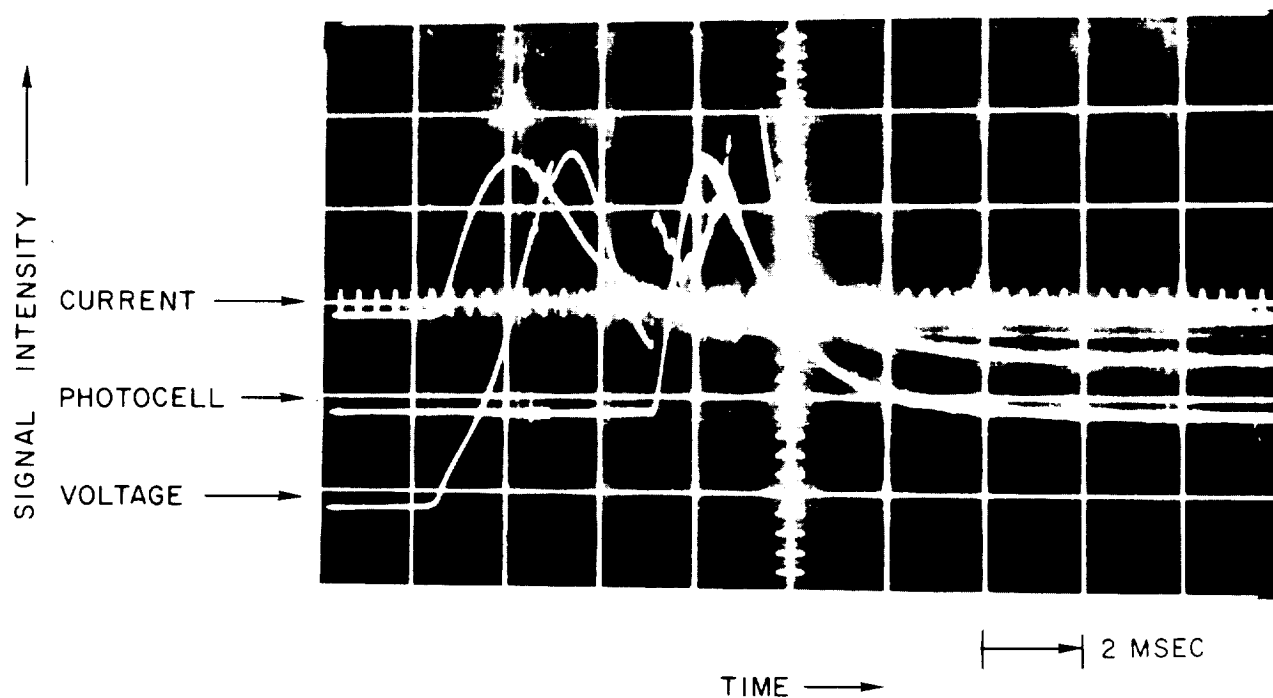
PHOTOGRAPH OF REACTION ZONE OF 20-MIL BERYLLIUM WIRE

500 PSIA
SLOW HEATING RATE
250 PICTURES PER SECOND
39.9% HCL, 39.7% CO_2, 20.4% N_2

FIG.28

ALUMINUM WIRE IN 100% O_2
125 PSIA
NO. 25 RED FILTER, 80 FPS, 7278 FILM

←REF WIRE

←AI WIRE

FIG.29

BERYLLIUM WIRE IN 100 % Ar
64 PSIA
NO. 24 RED FILTER, 80 FPS, 7278 FILM
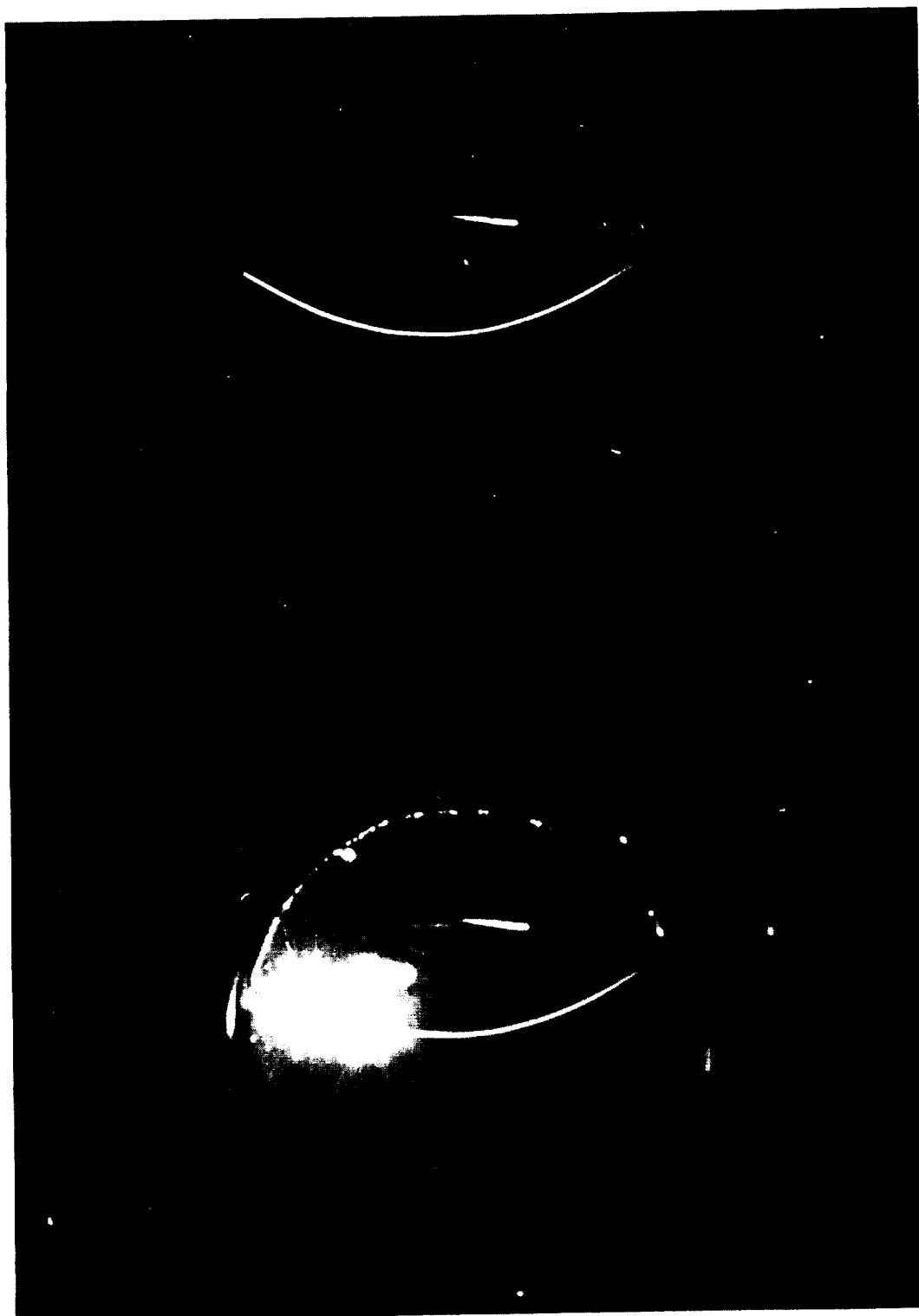
←REF WIRE
←Be WIRE

BERYLLIUM WIRE IN 100 % Ar
64 PSIA
NO. 24 RED FILTER, 80 FPS, 7278 FILM

FIG. 30

BERYLLIUM WIRE IN 100 % O₂
80 PSIA
NO. 24 RED FILTER, 80 FPS, 7278 FILM

←REF WIRE

←Be WIRE

FIG.31

BERYLLIUM WIRE IGNITING IN OXYGEN AT 125 PSIA
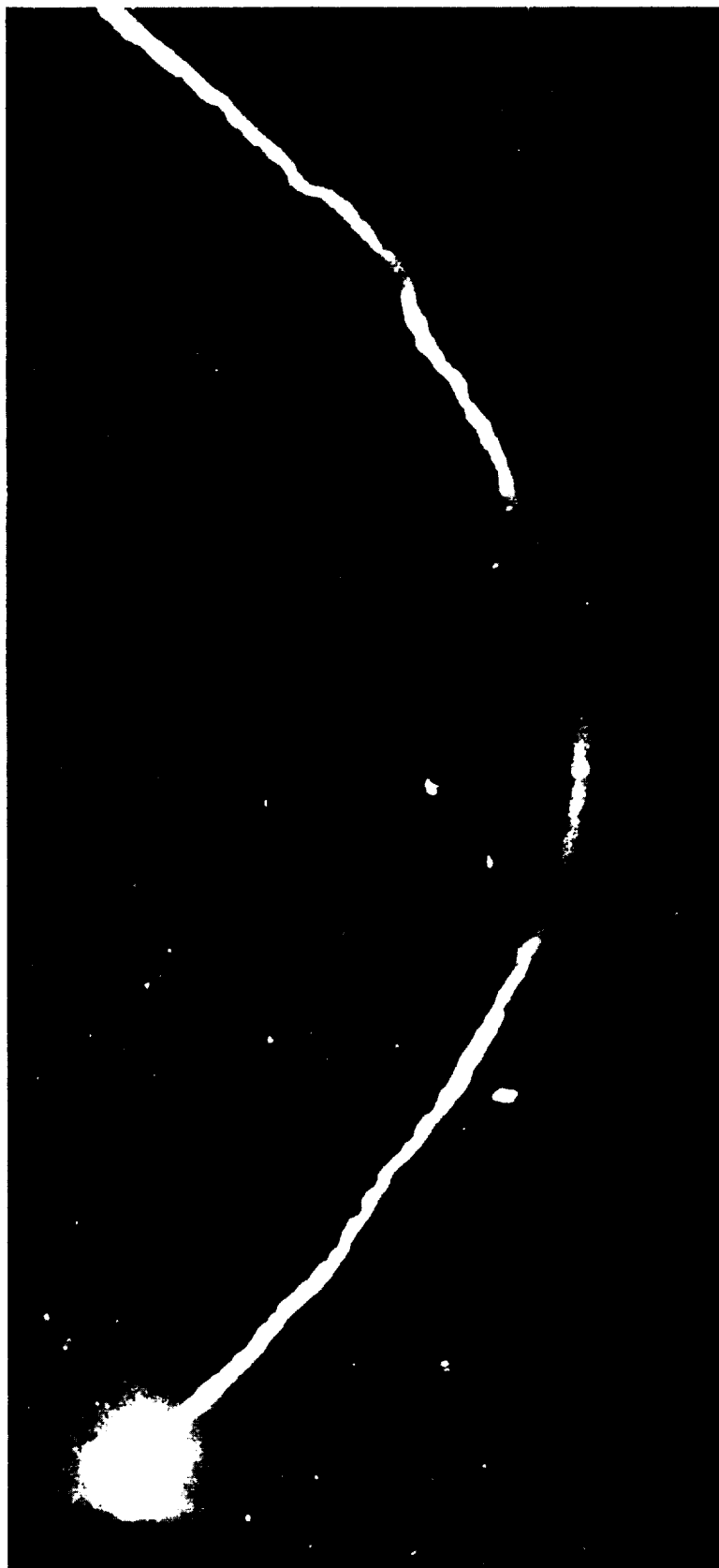
TEMPERATURE REQUIRED TO BREAK BERYLLIUM WIRE HEATED IN 100% ARGON AS A FUNCTION OF PRESSURE

20-MIL Be WIRE TYPE B-1

FIG 33
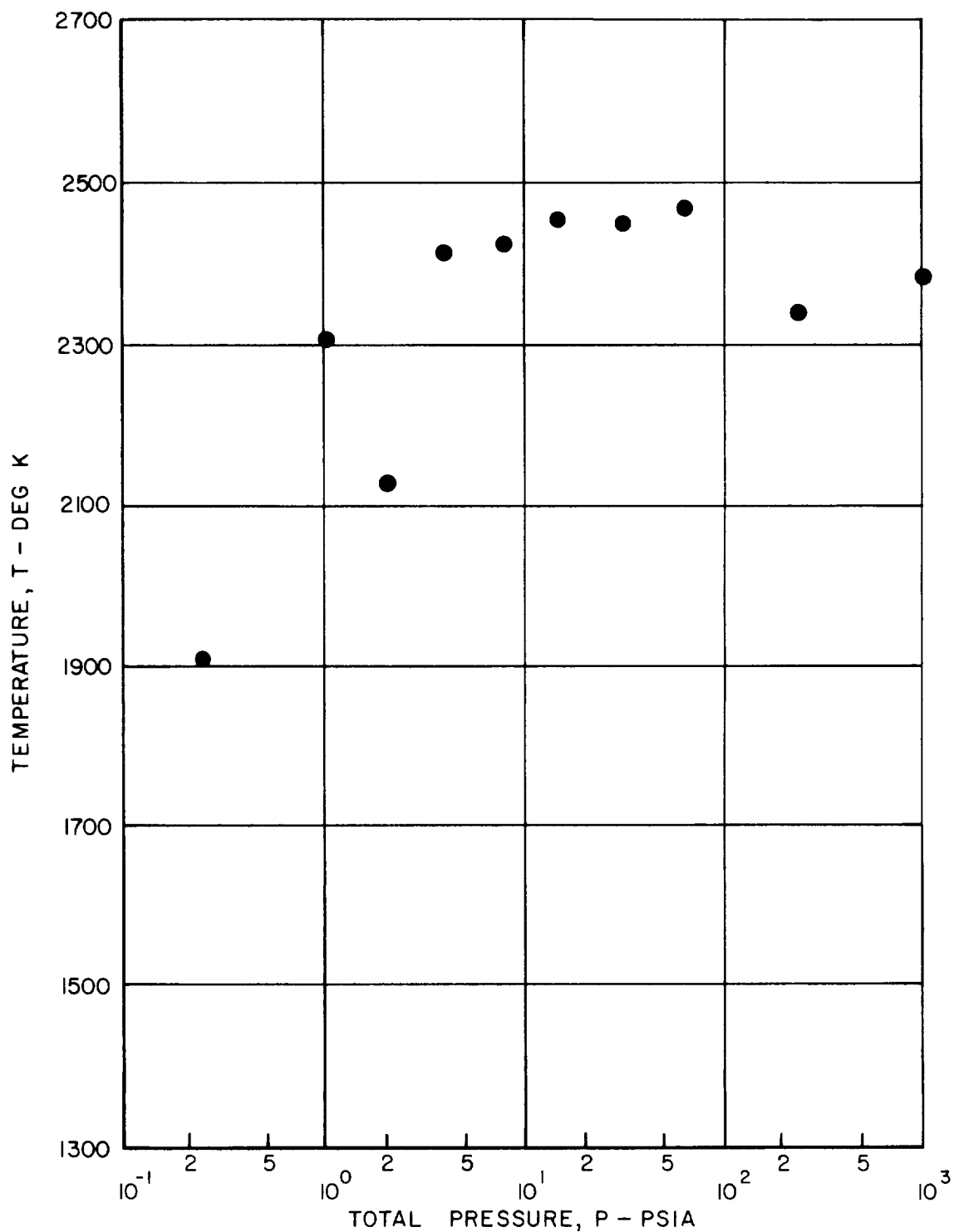
BERYLLIUM WIRE BURNING IN OXYGEN AT 125 PSIA

CAMERA FRAMING RATE: 128 FPS
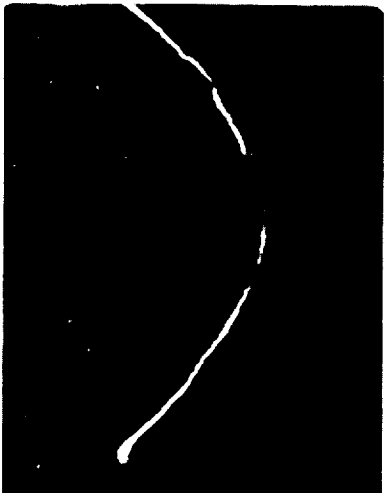
FRAME NO. 1
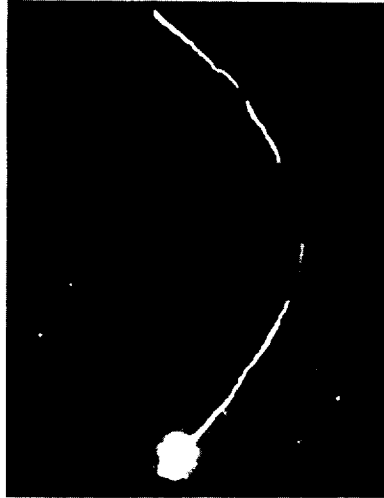
FIG 34

FRAGMENTATION OF BERYLLIUM IN OXYGEN AT 125 PSIA

FRAME NO. 13

FIG. 35

RESIDUE FROM BERYLLIUM COMBUSTION IN 100% O_2 AT 125 PSIA

FIG.36

PHOTOGRAPHIC SEQUENCE AND OSCILLOSCOPE RECORD OF IGNITION AND COMBUSTION OF 20-MIL BERYLLIUM WIRE AT 300 VOLTS

125 PSIA
100% OXYGEN
10,000 PICTURES PER SECOND
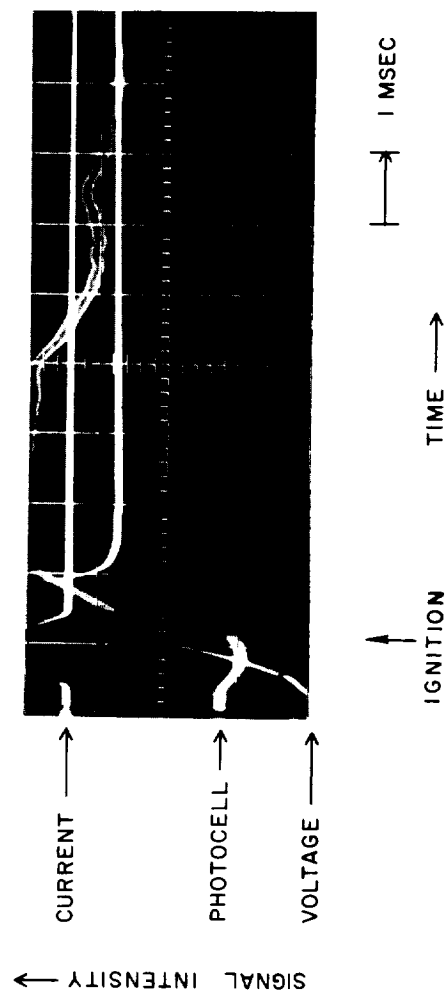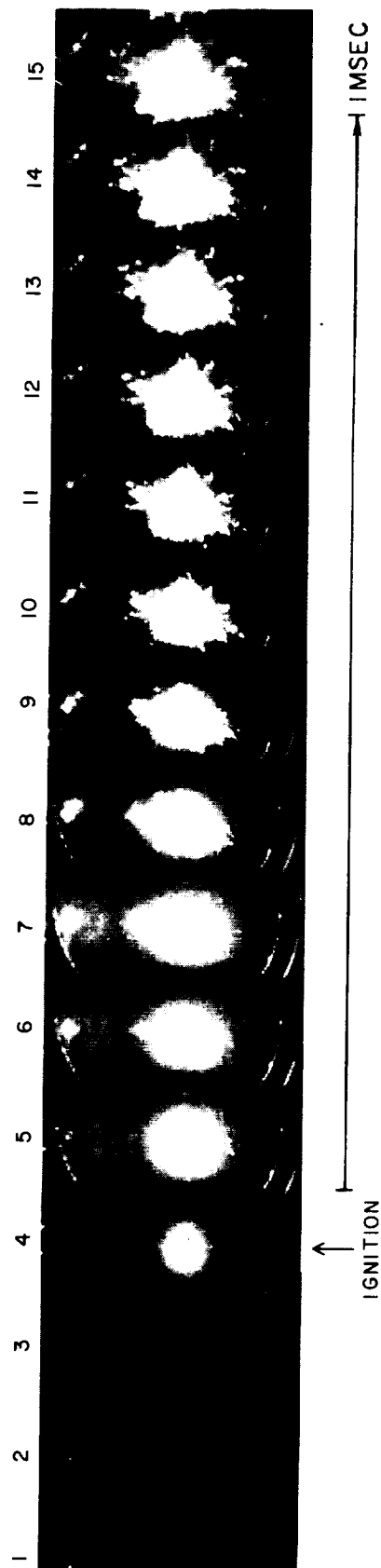
RESIDUE OF BeO ON 20-MIL BERYLLIUM WIRE HEATED
IN 39.9% HCL / 39.7% CO_2 / 20.4% N_2

P = 500 PSIA
SLOW HEATING RATE
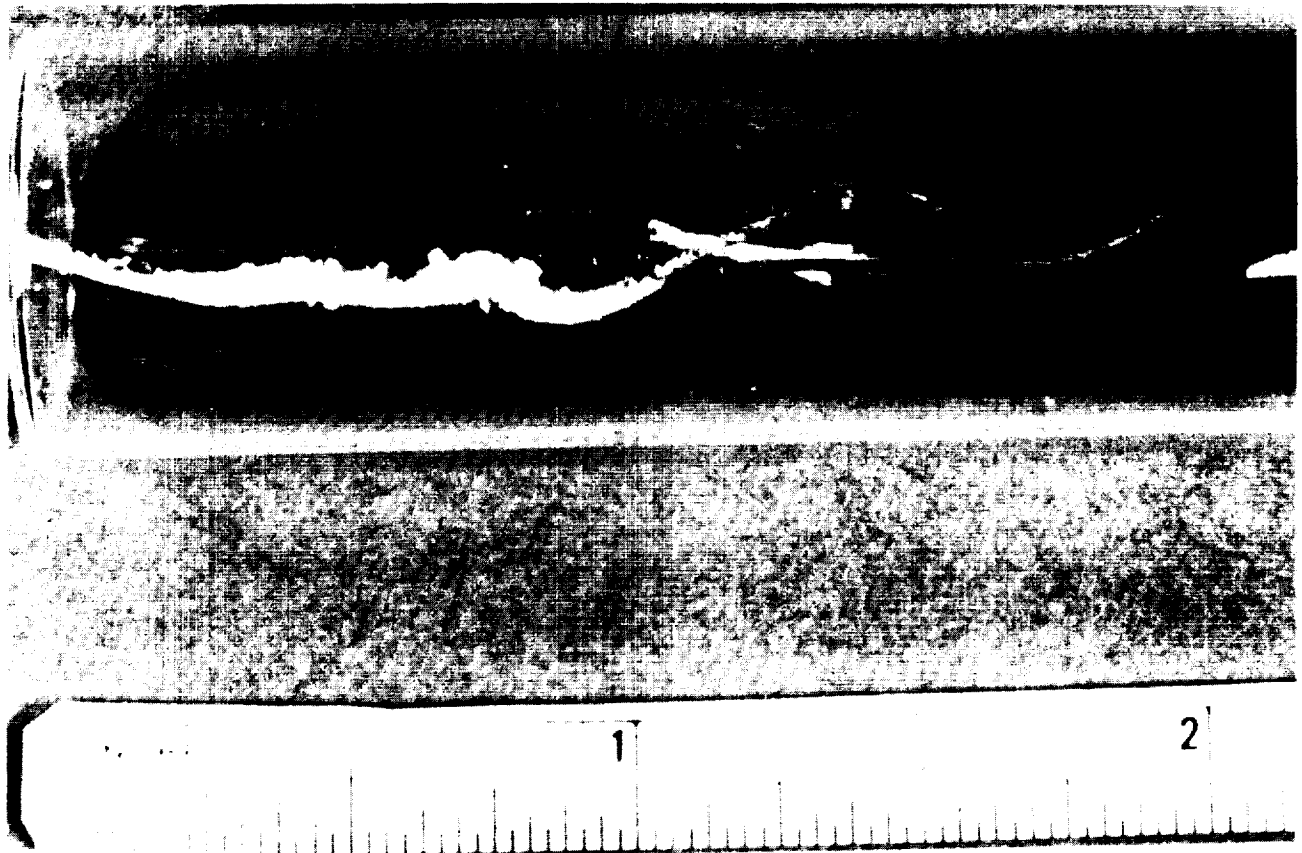
TIME –TEMPERATURE HISTORY OF 20-MIL Be WIRE REACTING IN 39.9 HCl / 39.7 CO₂ / 20.4 N₂ AT 500 PSIA

(VOLTAGE INCREASED CONTINUALLY DURING RUN)
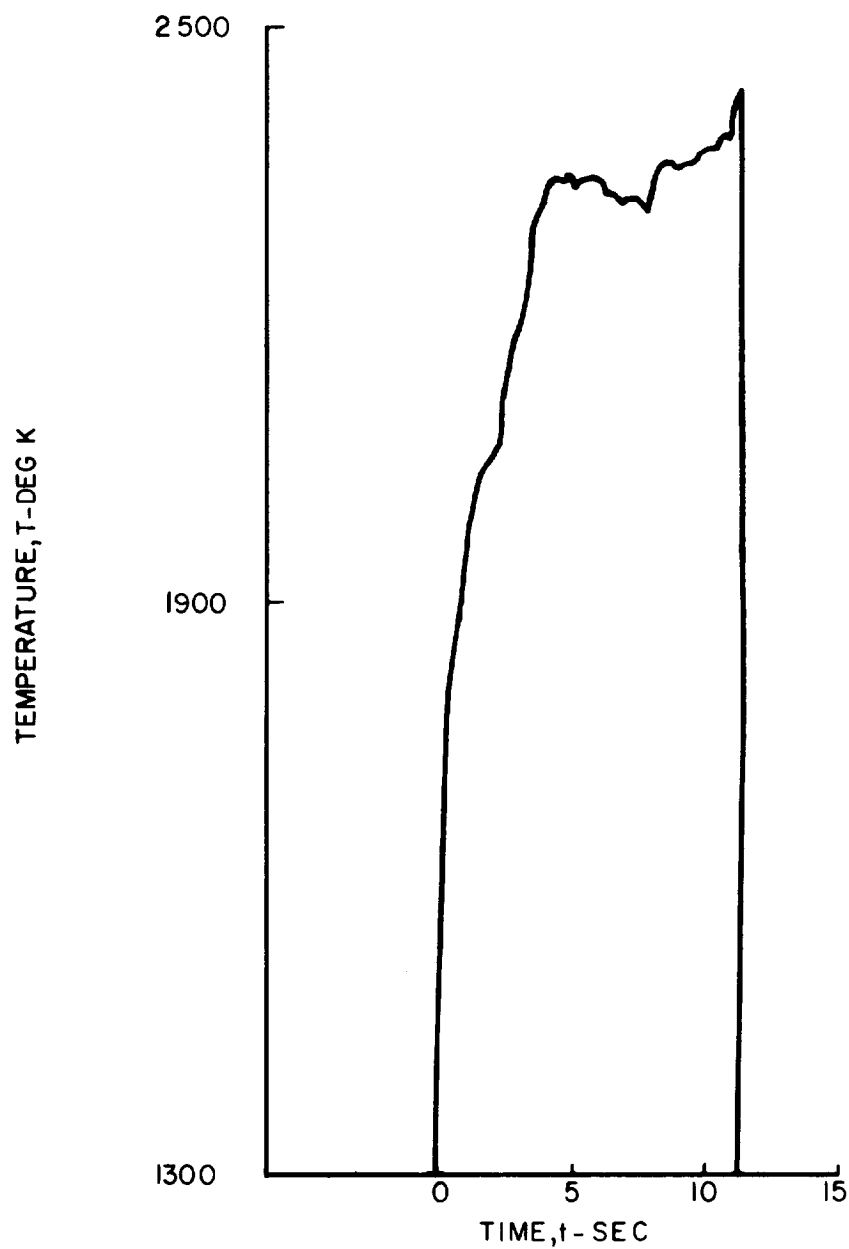
FIG. 39

TIME–TEMPERATURE HISTORY OF 20-MIL Be WIRE REACTING
IN 39.9 HCl / 39.7 CO_2 / 20.4 N_2 AT 500 PSIA
(VOLTAGE DECREASED AFTER TEMPERATURE = 1800 K)
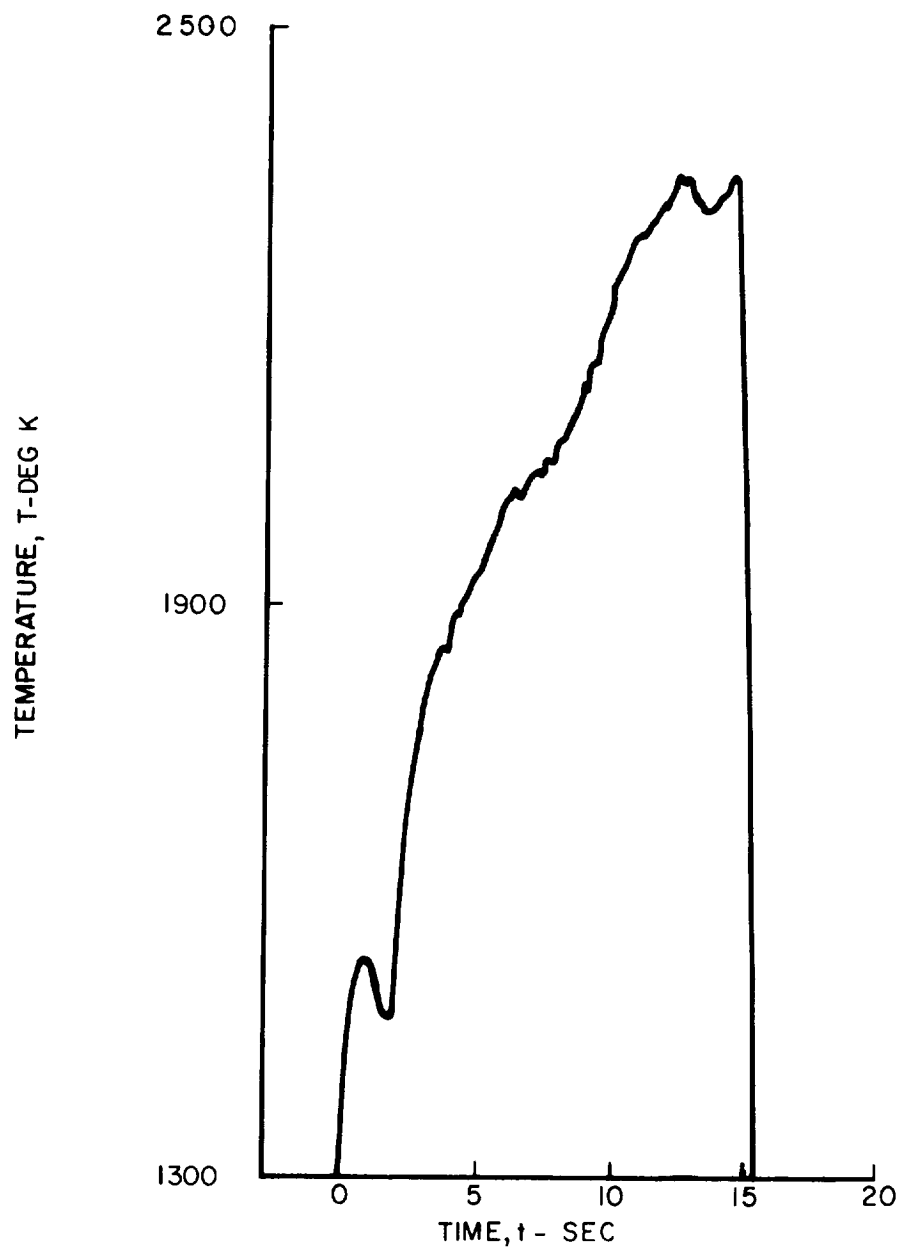
FIG.40

PHOTOGRAPHIC SEQUENCE AND OSCILLOSCOPE RECORD OF IGNITION AND COMBUSTION OF 20-MIL BERYLLIUM WIRE AT 312 VOLTS

500 PSIA
39.9% HCL
39.7% CO_2
20.4% N_2

~6000 PICTURES PER SECOND

FIG. 41
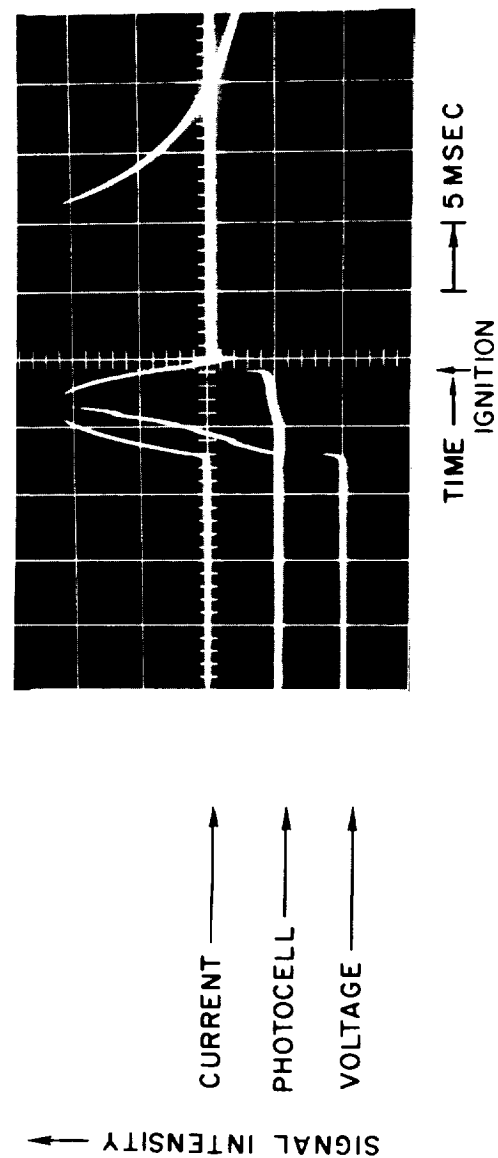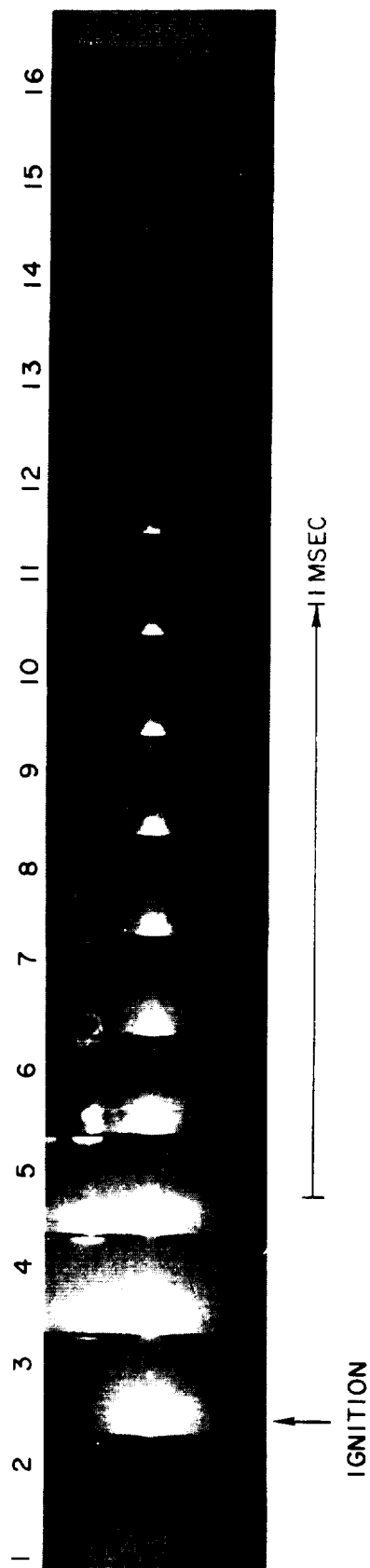
RESIDUE FROM BERYLLIUM COMBUSTION IN
$H_2O/N_2/CO_2$ AT 500 PSIA

SINGLE FRAME TAKEN AT 500 PICTURES PER SECOND
OF BERYLLIUM WIRE BURNING IN $H_2O/N_2/CO_2$ AT 500 PSIA

FIG.43

RESIDUE FROM RUN SHOWN IN FIGURE 42
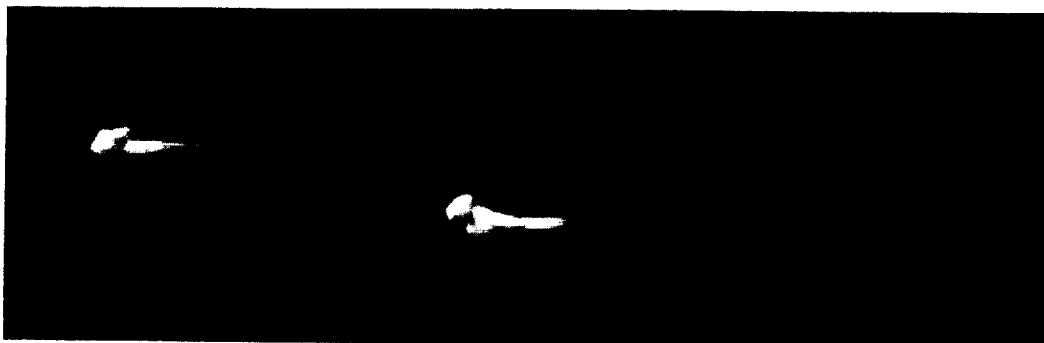
TIME –TEMPERATURE HISTORY OF 20-MIL Be WIRE REACTING
IN $H_2O/CO_2/N_2$ MIXTURE AT 500 PSIA

FIG.45
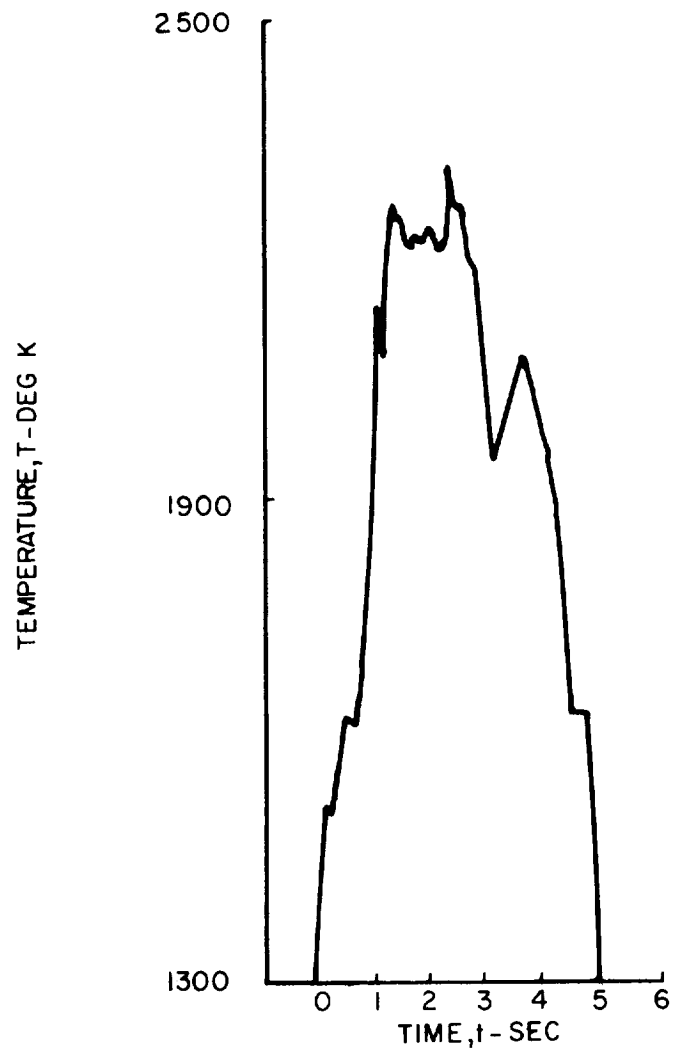
RESIDUE FROM BERYLLIUM REACTION AFTER PULSE
IGNITION IN $H_2O/N_2/CO_2$ AT 500 PSIA

DEPOSIT ON ELECTRODES AFTER COMBUSTION OF BERYLLIUM
WIRE IN 100% ClF_3
7.5 PSIA
SLOW HEATING
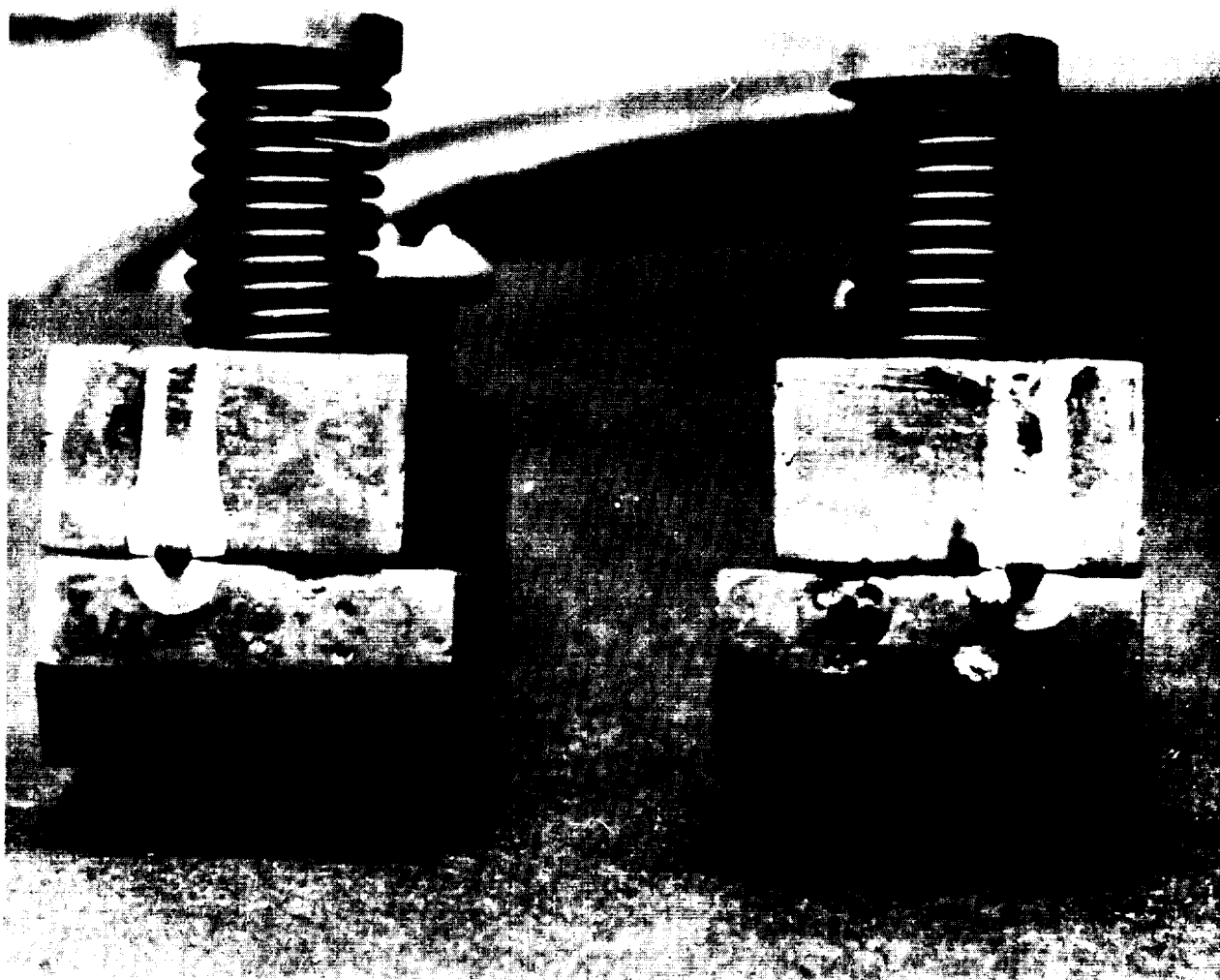
DEPOSIT ON ELECTRODES AFTER COMBUSTION OF BERYLLIUM
WIRE IN 100% ClF_3

7.5 PSIA
SLOW HEATING

FIG. 48
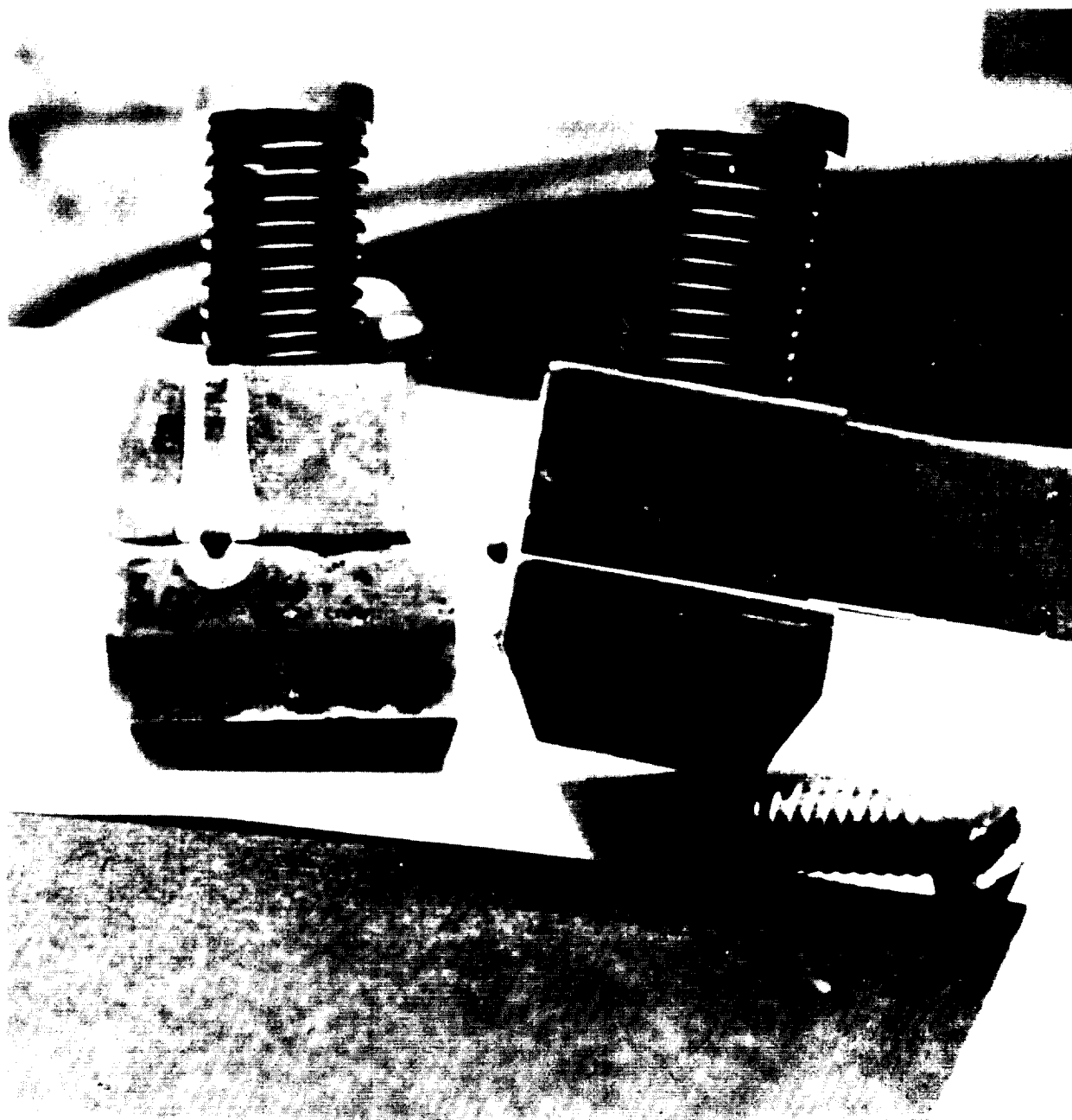
PHOTOGRAPHIC SEQUENCE OF THE COMBUSTION OF BERYLLIUM WIRE IN 100% ClF₃

17.5 PSIA , 24 FRAMES PER SECOND , SLOW IGNITION

0.25 MSEC

FIG.49
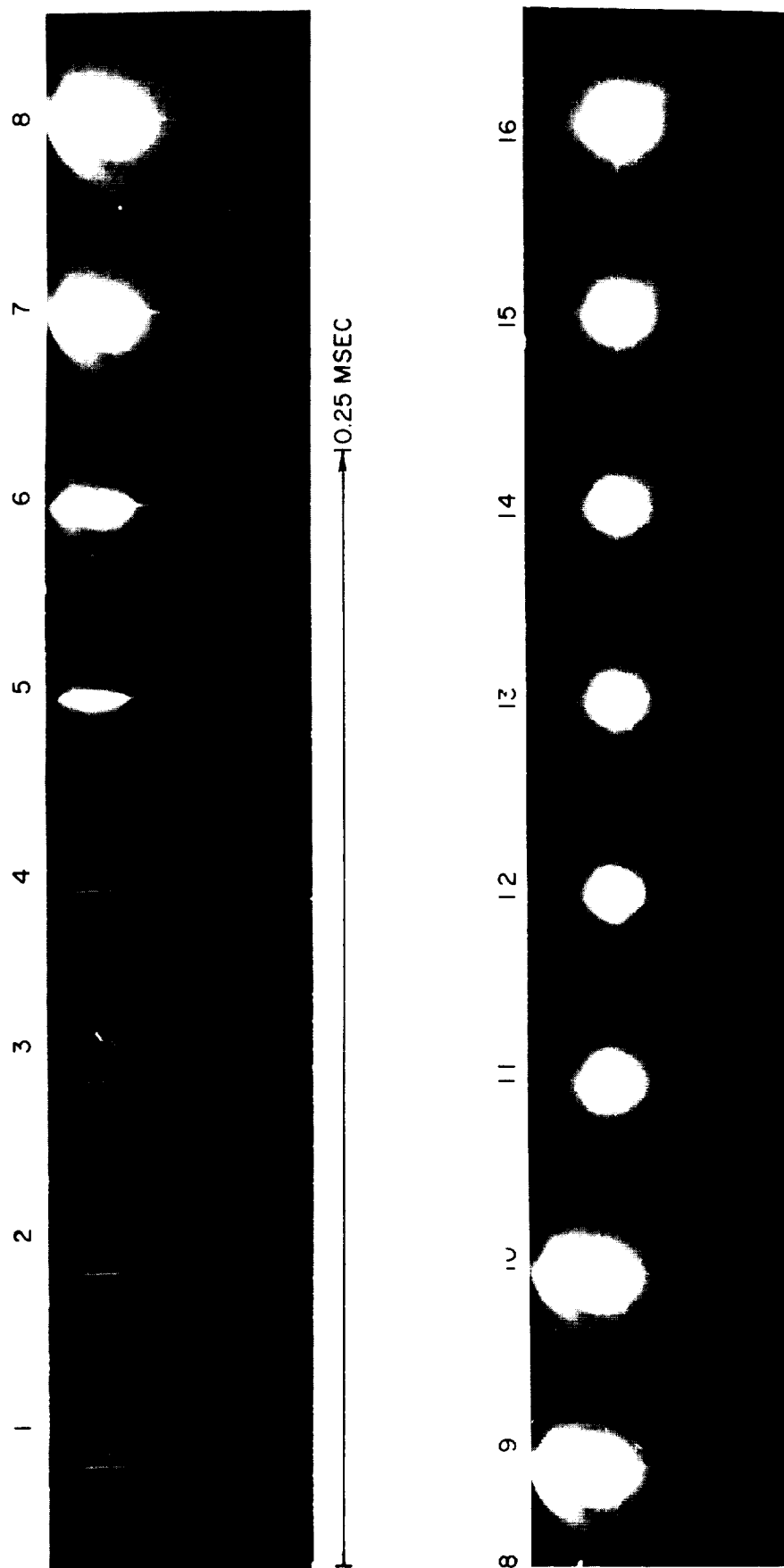
IGNITION AND COMBUSTION OF BERYLLIUM WIRE IN 11.7% ClF₃, 88.3% Ar

150 PSIA, 24 FRAMES PER SECOND, SLOW IGNITION
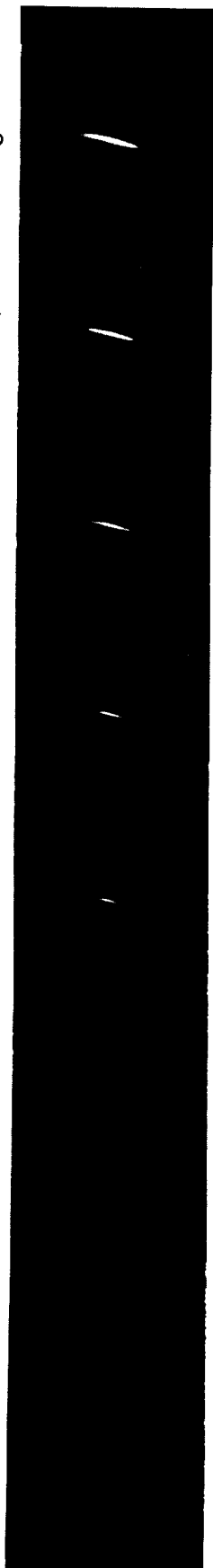
0.25 MSEC

FIG. 50
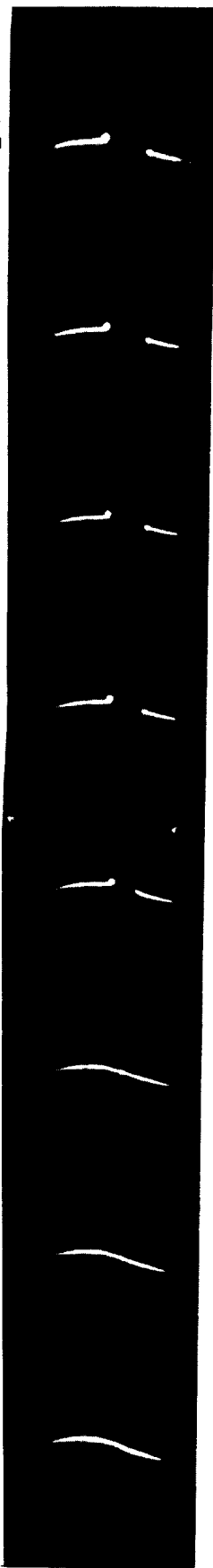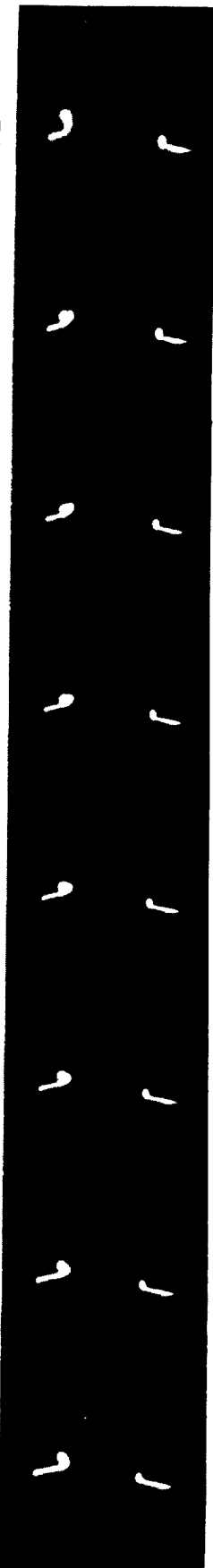
PHOTOGRAPHIC SEQUENCE OF COMBUSTION OF BERYLLIUM WIRE IN 4.5% ClF$_3$, 95.5% Ar
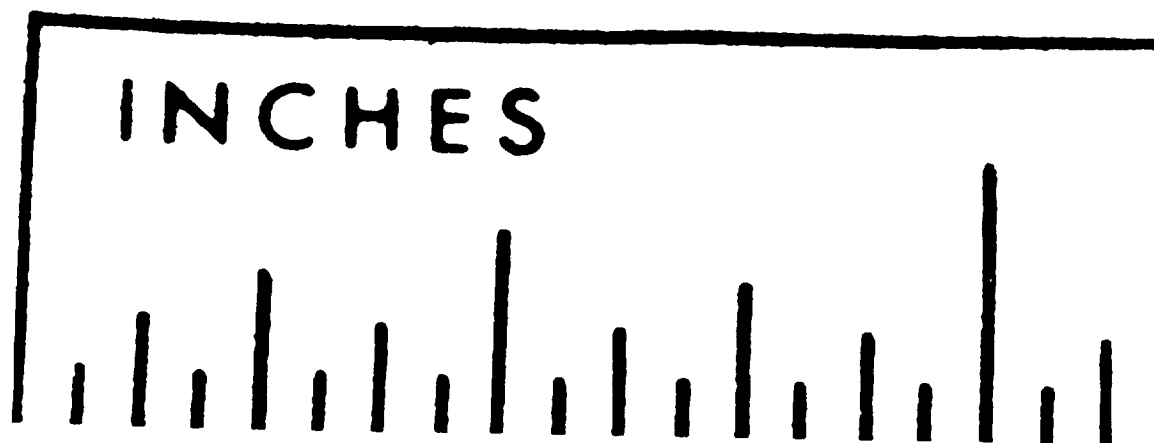
165 PSIA

24 FRAMES PER SECOND, SLOW IGNITION

0.25 MSEC

FIG.51
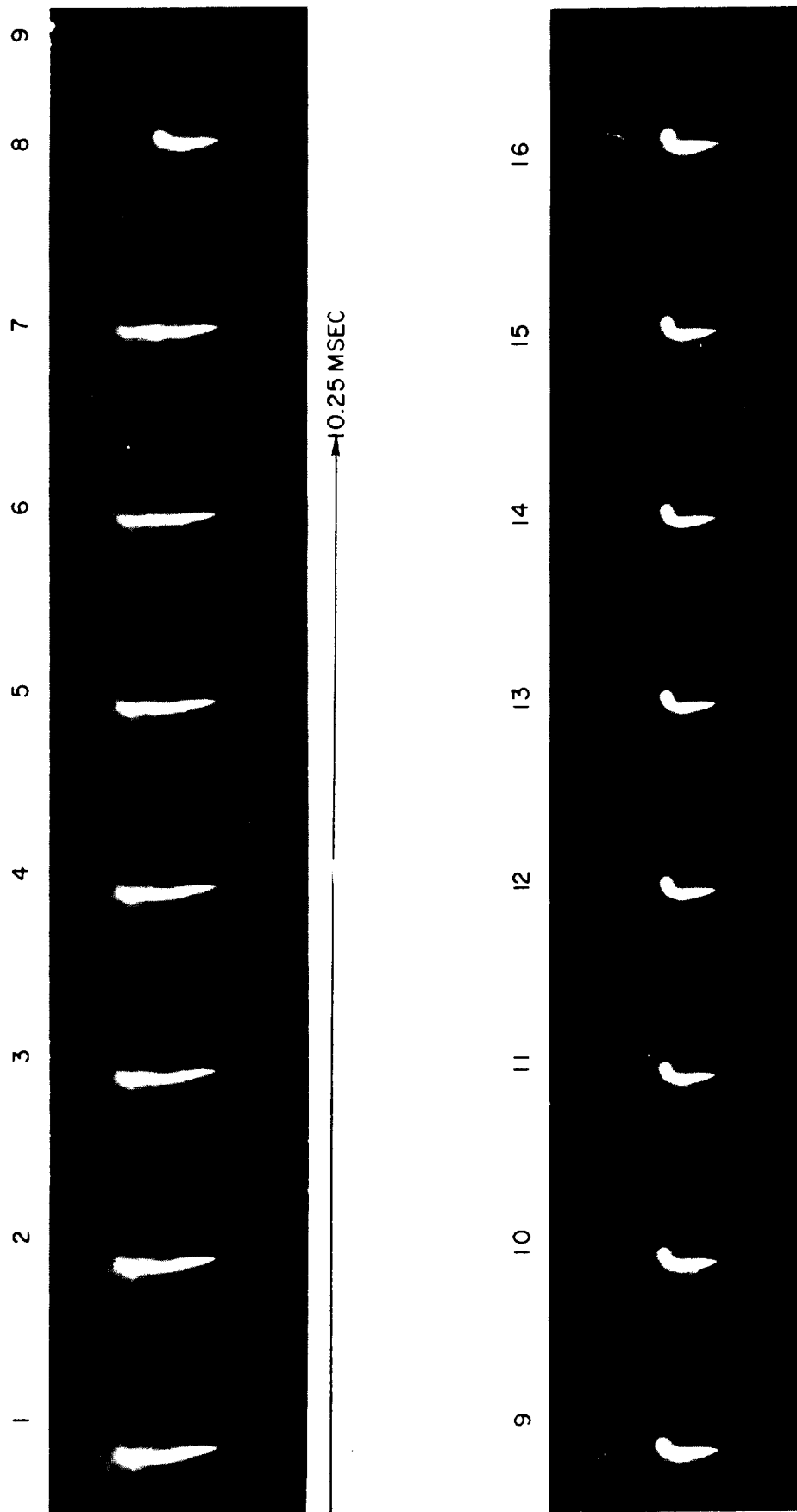
REACTION PRODUCTS, BERYLLIUM IN 20% ClF_3, 32% HCl, 16% N_2, 32% CO_2
25 PSIA
SLOW HEATING

REACTION PRODUCTS, BERYLLIUM IN 20% CIF$_3$, 32% HCl, 16% N$_2$,

FIG.52

25 PSIA

32% CO$_2$

SLOW HEATING

(ENLARGED)

INCHES

FIG.53

COMBUSTION OF 10-MIL Zr WIRE IN 1 ATM N₂

10,000 FRAMES PER SECOND, 150V, PULSE IGNITION
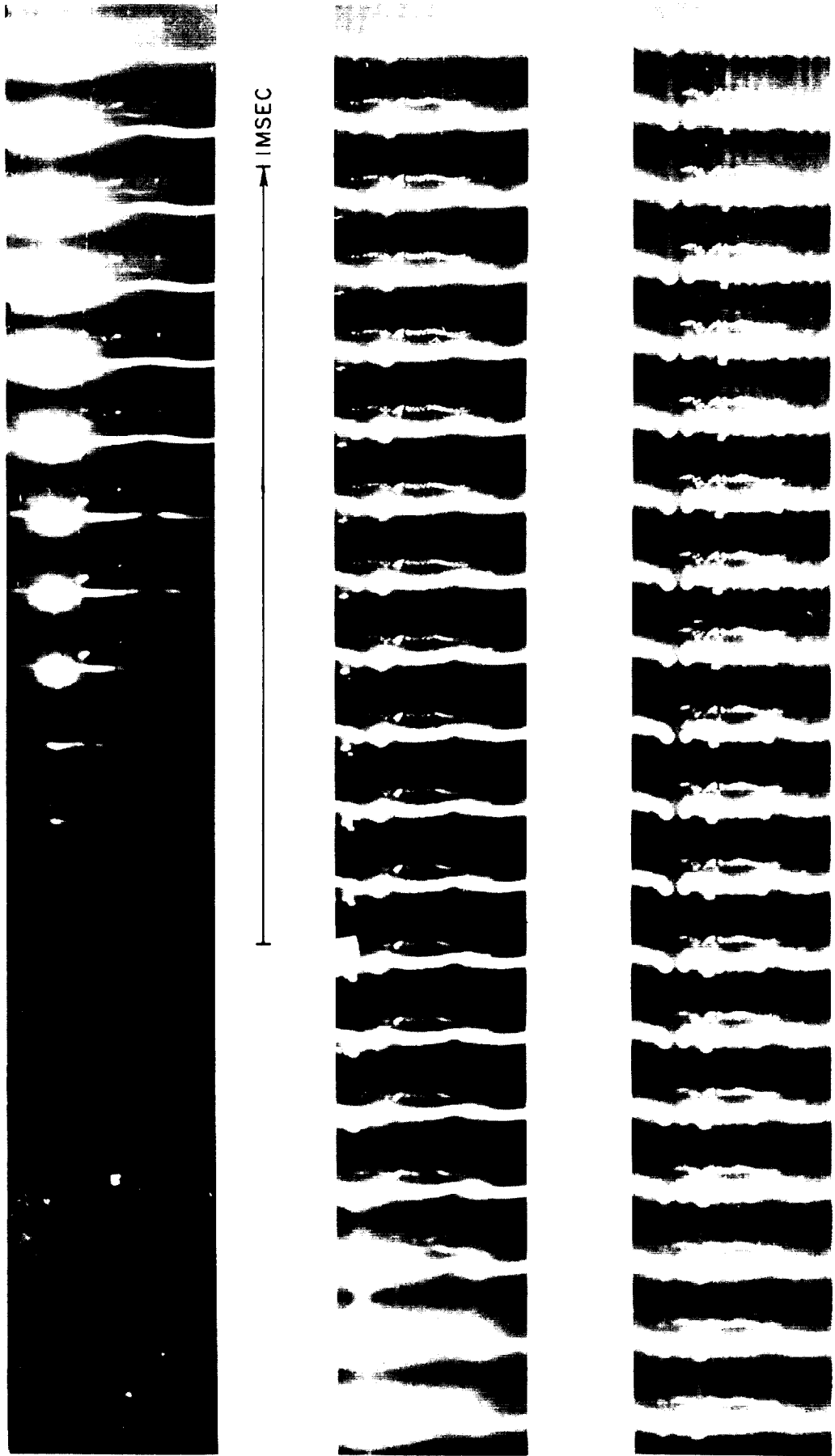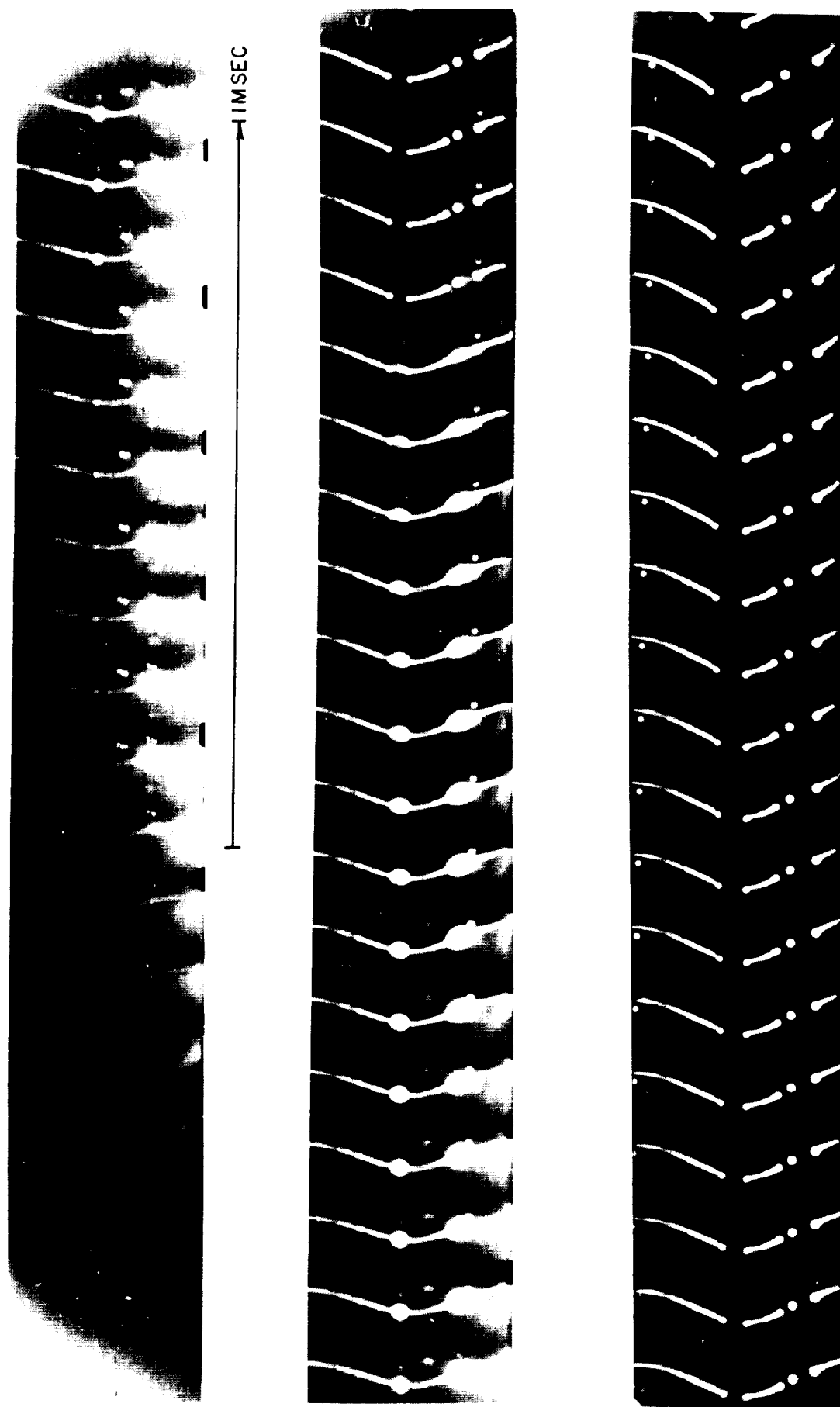
1 MSEC

FIG 54

F910336-24
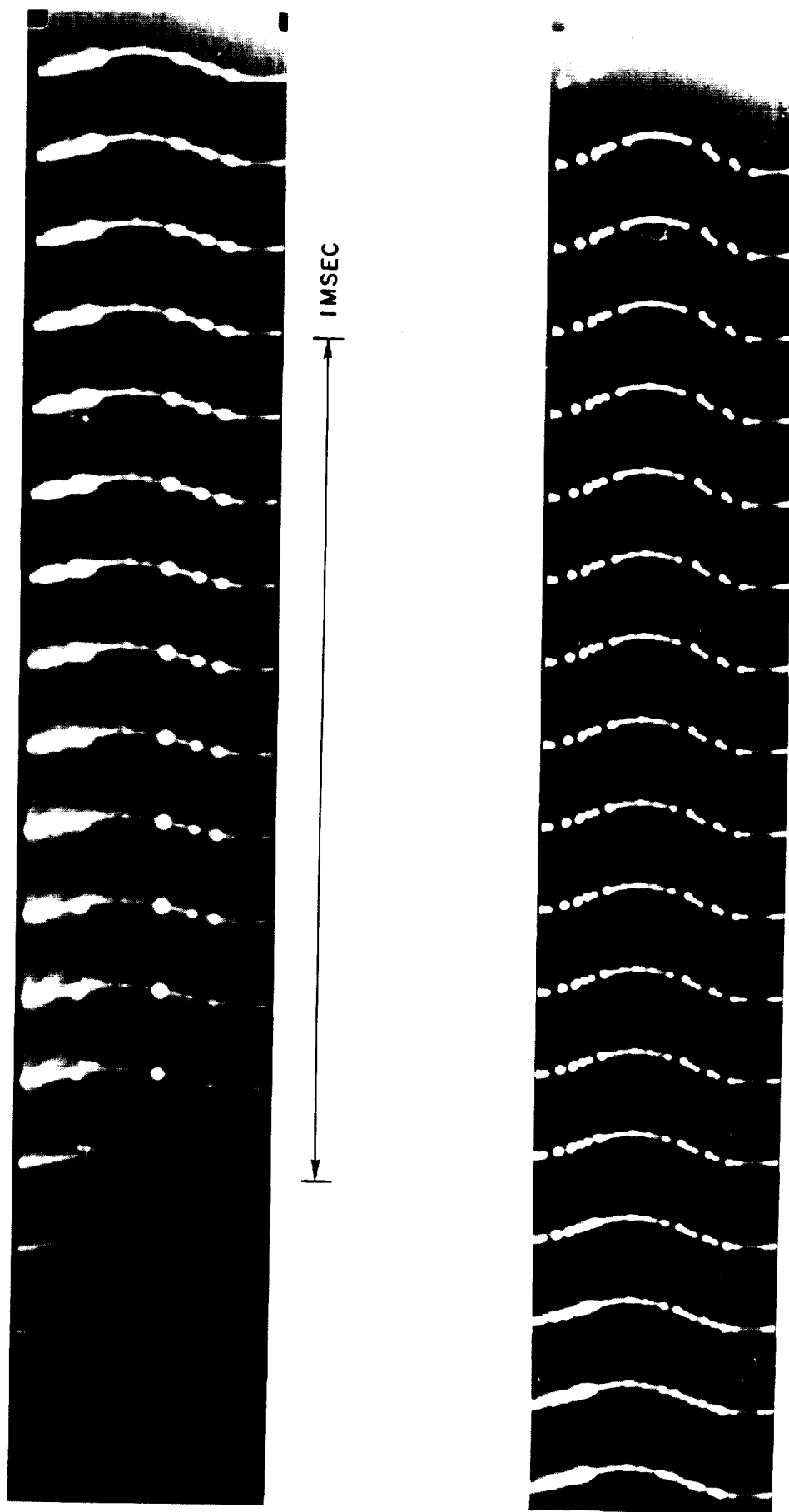
COMBUSTION OF 10-MIL Zr WIRE IN 1 ATM O_2
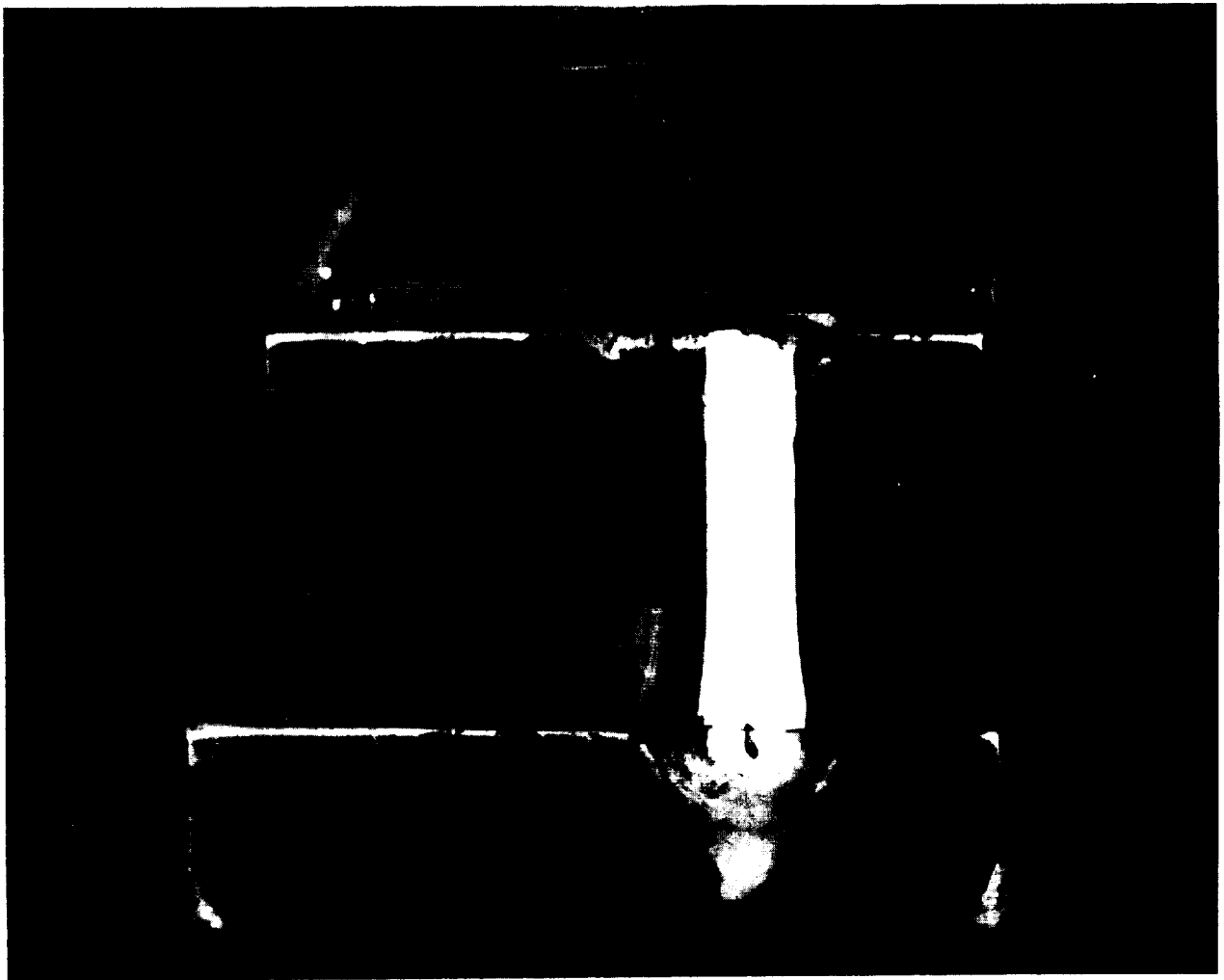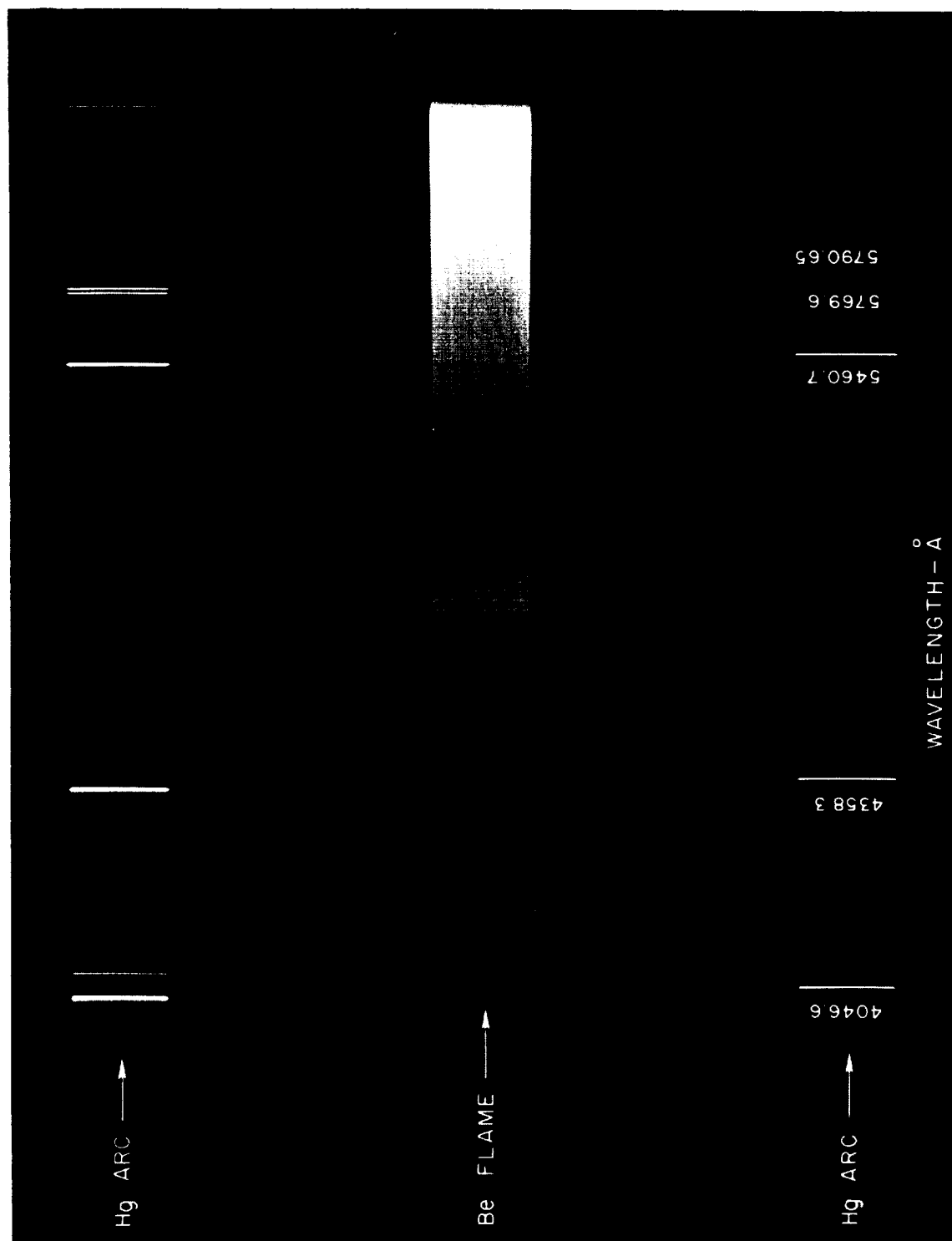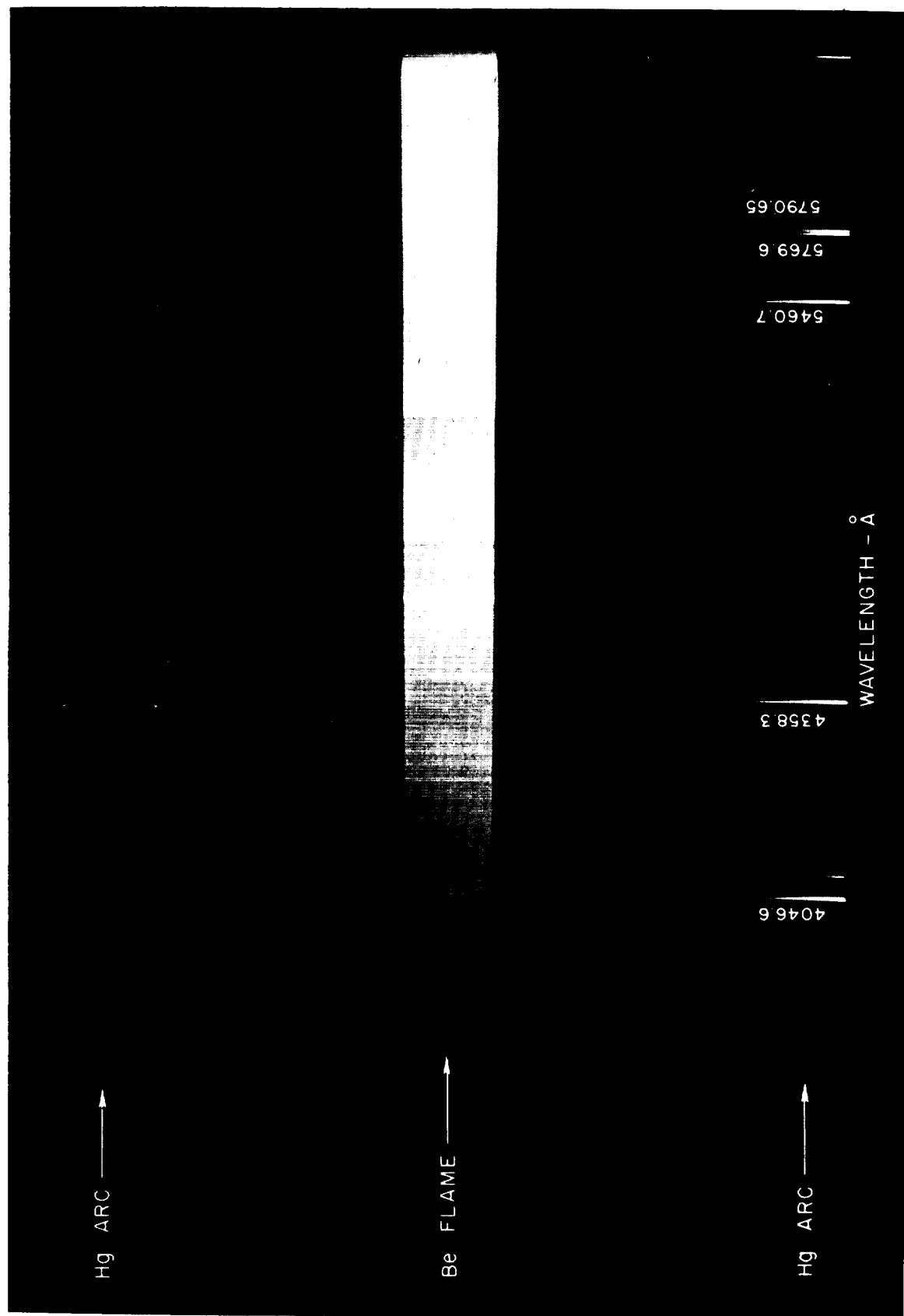10,000 FRAMES PER SECOND, 150V, PULSE IGNITION

1 MSEC

FIG.55

COMBUSTION OF 10-MIL Zr WIRE IN 1 ATM AIR

10,000 FRAMES PER SECOND, 150V, PULSE IGNITION

1 MSEC

RESIDUE OF BORON COMBUSTION IN AIR AT I ATM

FIG.57

FLAME SPECTRUM OF Be IN O_2 AT 64 PSIA

15-MIL WIRE HEATED AT 10^2 DEG K/SEC

Hg ARC

Be FLAME

Hg ARC

4046.6

4358.3

5460.7

5769.6

5790.65

WAVELENGTH – $\overset{\circ}{A}$

FIG.58

FLAME SPECTRUM OF Be IN O_2 AT 64 PSIA

15-MIL WIRE HEATED AT 5×10^5 DEG K/SEC

Hg ARC

Be FLAME

Hg ARC

4046.6

4358.3

WAVELENGTH - Å

5460.7

5769.6

5790.65

FIG.59

FLAME SPECTRA OF Al AND Be IN O_2 64 PSIA

20-MIL Al WIRE HEATED AT 5×10^5 DEG K/SEC
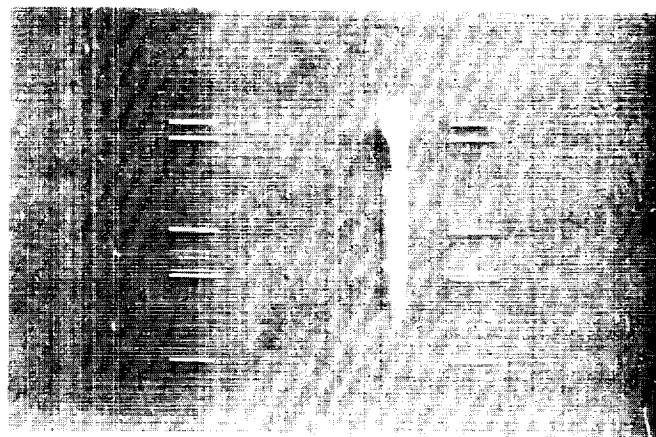15-MIL Be WIRE HEATED AT 5×10^5 DEG K/SEC

Hg ARC

Al FLAME

Be FLAME

Hg ARC

WAVELENGTH—Å

4046.6   4358.3   5460.7   5769.6   5790.65

FIG.60

FLAME SPECTRA OF Be IN O_2 AT 125 PSIA

20 MIL Be WIRE HEATED AT 5×10^5 °K/SEC

EFFECTS OF VARYING CONDENSER VOLTAGE

Hg   Be   Hg

Hg   Be   Hg

240 VOLTS   250 VOLTS   300 VOLTS
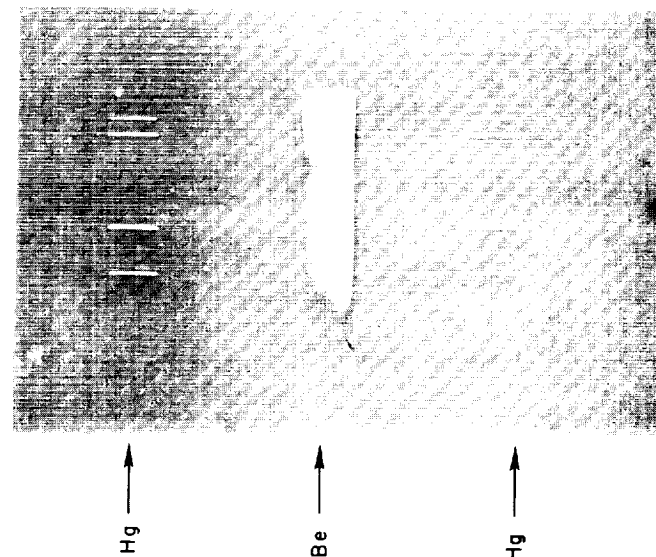
FIG. 61

THEORETICAL COMBUSTION MODEL

FIG.62
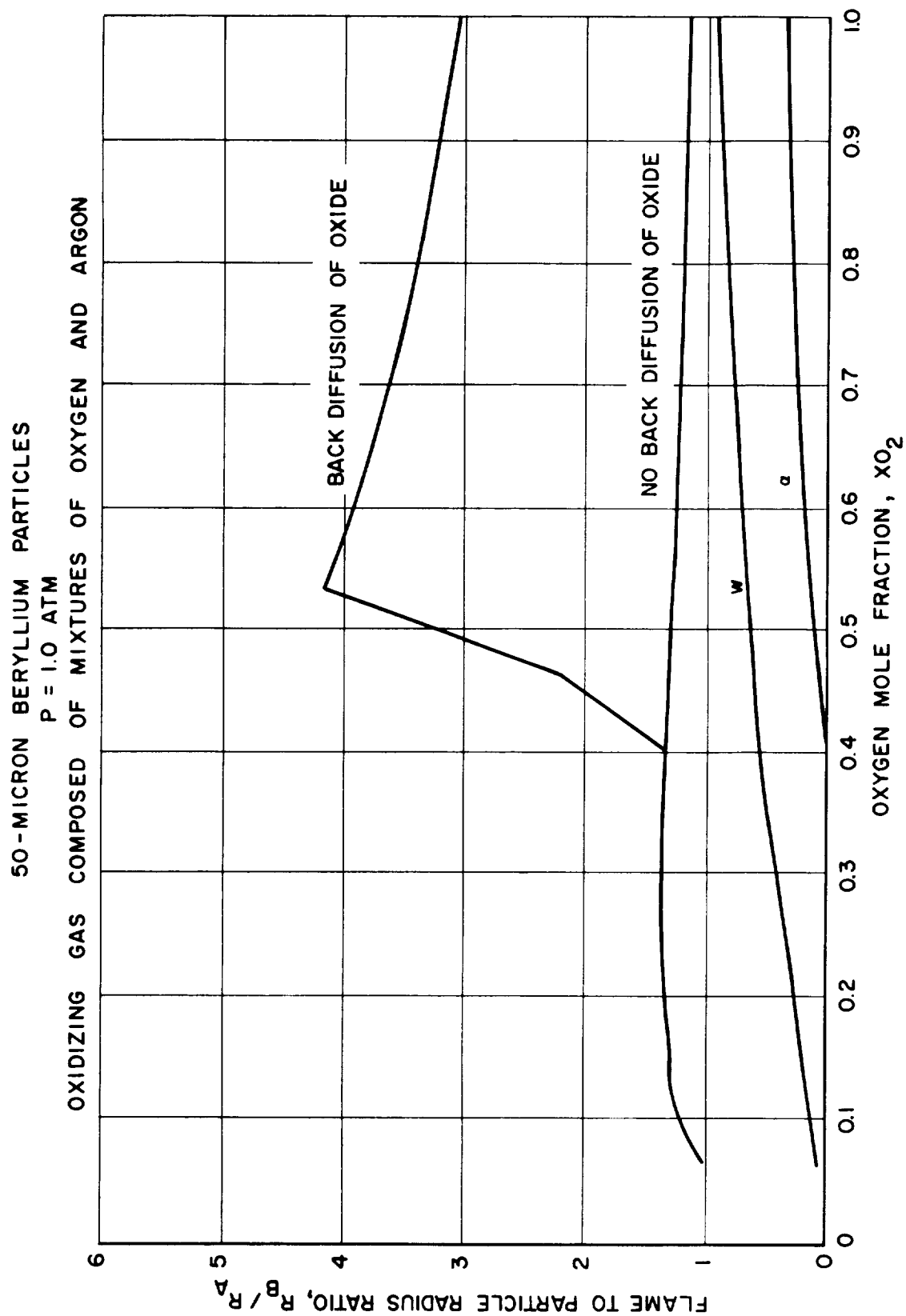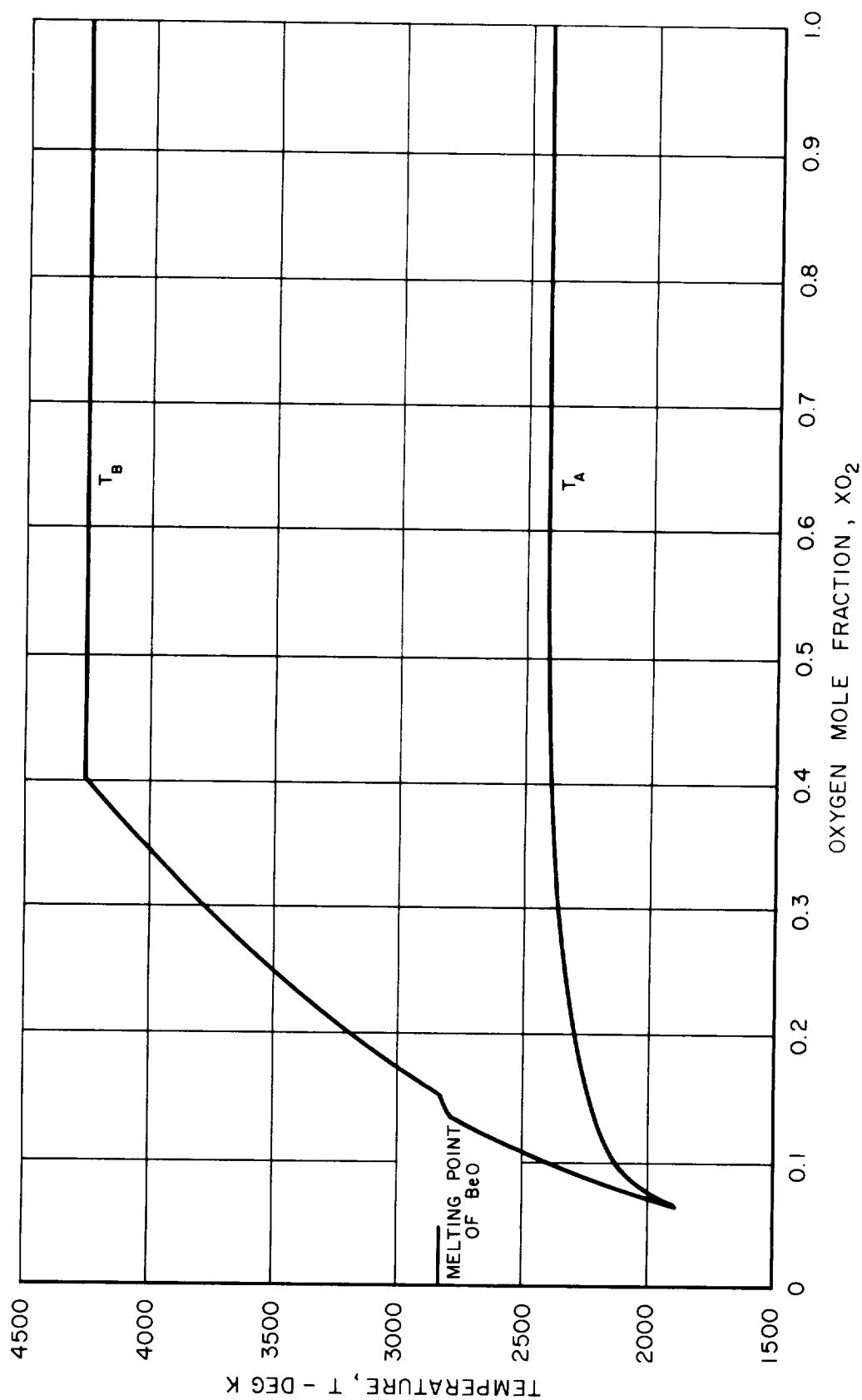

COMPARISON OF FLAME TO PARTICLE RADIUS RATIOS CALCULATED WITH AND WITHOUT BACK DIFFUSION OF METAL OXIDE FROM FLAME FRONT

FIG. 63

THEORETICAL FLAME TEMPERATURE (T_B) AND PARTICLE TEMPERATURE (T_A)
FOR 50-MICRON BERYLLIUM PARTICLES IN 300K OXYGEN-ARGON MIXTURES
AT 1 ATMOSPHERE

FIG. **64**

THE VARIATION OF THEORETICAL CRITICAL OXIDIZER CONCENTRATION (X_o^*) AND MINIMUM OXIDIZER CONCENTRATION (FLAMMABILITY LIMIT) $(X_{o_{MIN}})$ WITH PARTICLE DIAMETER FOR ALUMINUM PARTICLES BURNING IN OXYGEN-ARGON MIXTURES AT 300 K
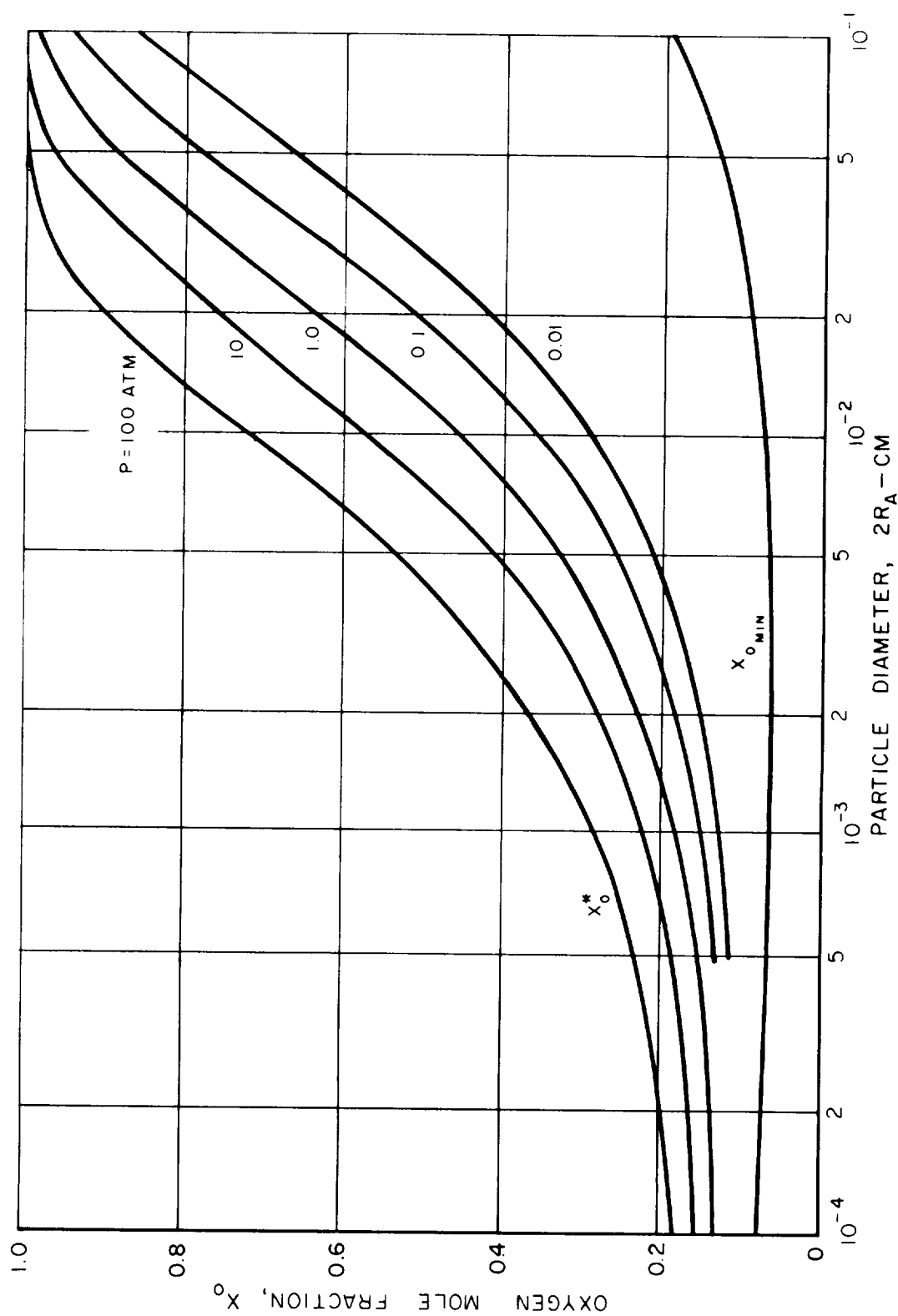
THE VARIATION OF THEORETICAL CRITICAL OXIDIZER CONCENTRATION (X_o^*) AND MINIMUM OXIDIZER CONCENTRATION (FLAMMABILITY LIMIT) $(X_{o_{MIN}})$ WITH PARTICLE DIAMETER FOR BERYLLIUM PARTICLES BURNING IN OXYGEN-ARGON MIXTURES AT 300 K

FIG 66
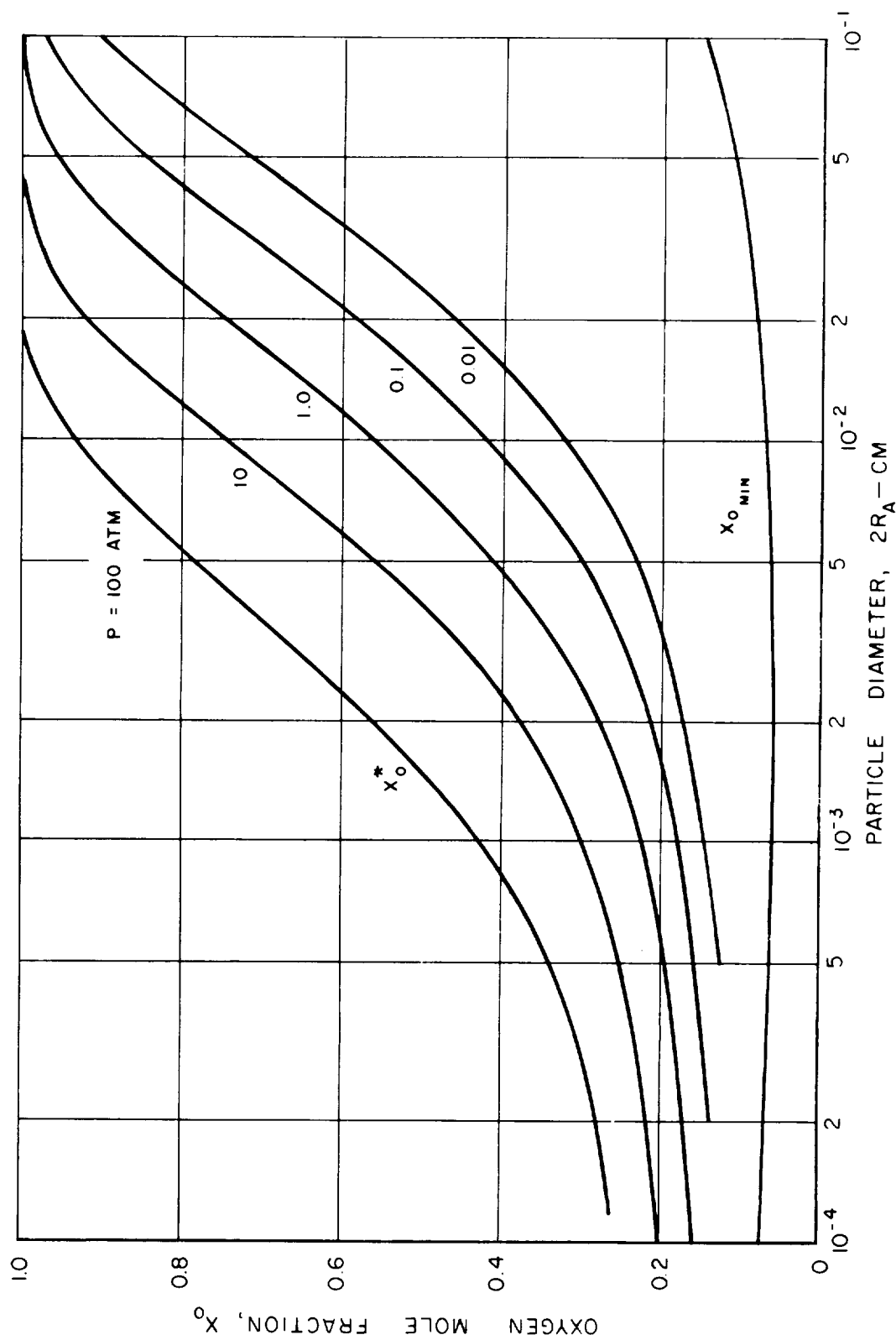
COMPARISON OF CRITICAL OXIDIZER CONCENTRATIONS (x_o^*) OF ALUMINUM AND BERYLLIUM AT 100 AND 0.01 ATMOSPHERES IN OXYGEN-ARGON MIXTURES AT 300 K

FIG. 67
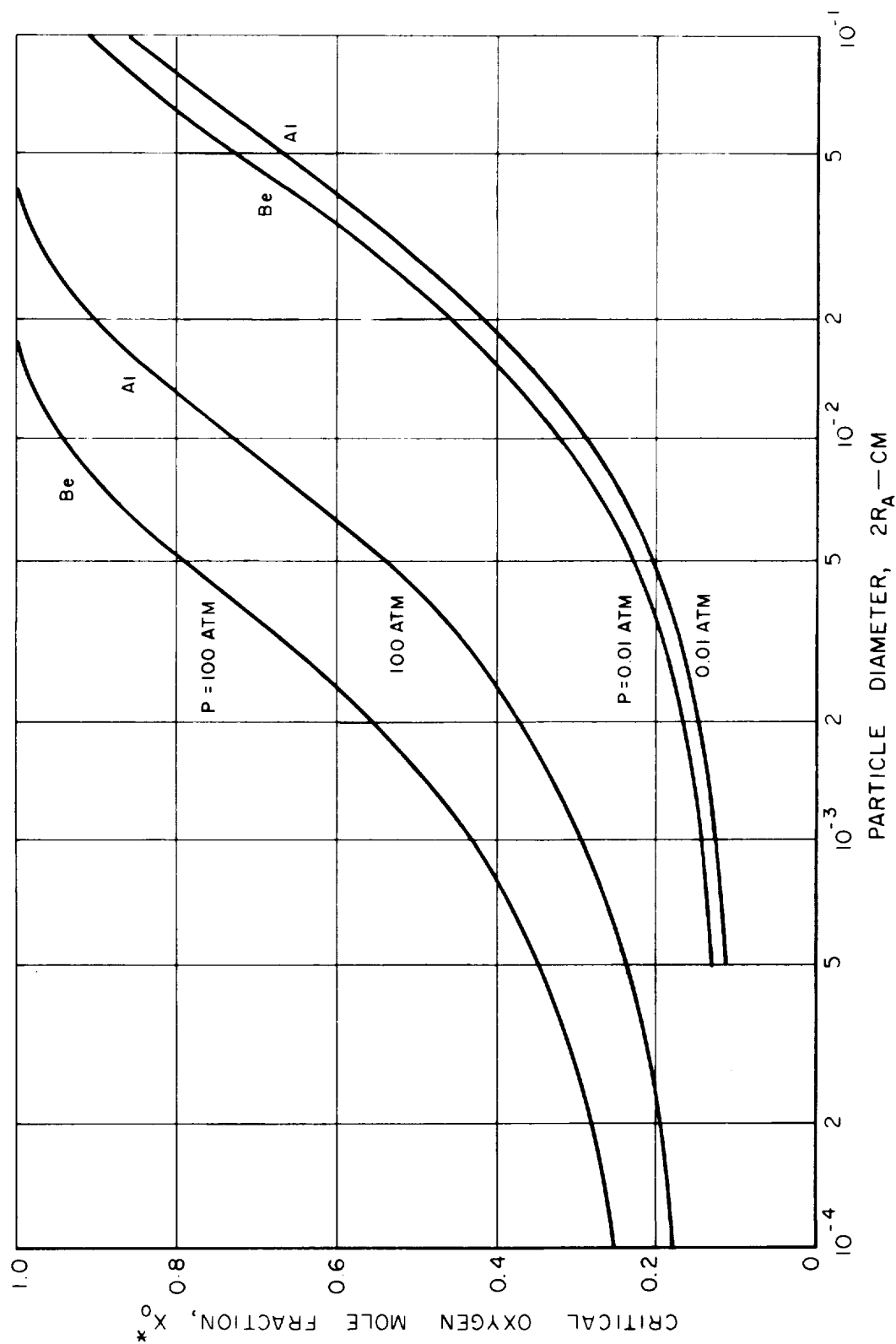
THEORETICAL BURNING RATE OF ALUMINUM DROPLETS IN 100% OXYGEN AND 20% OXYGEN – 80% ARGON AT 300 K FOR A RANGE OF PRESSURES

FIG. 68
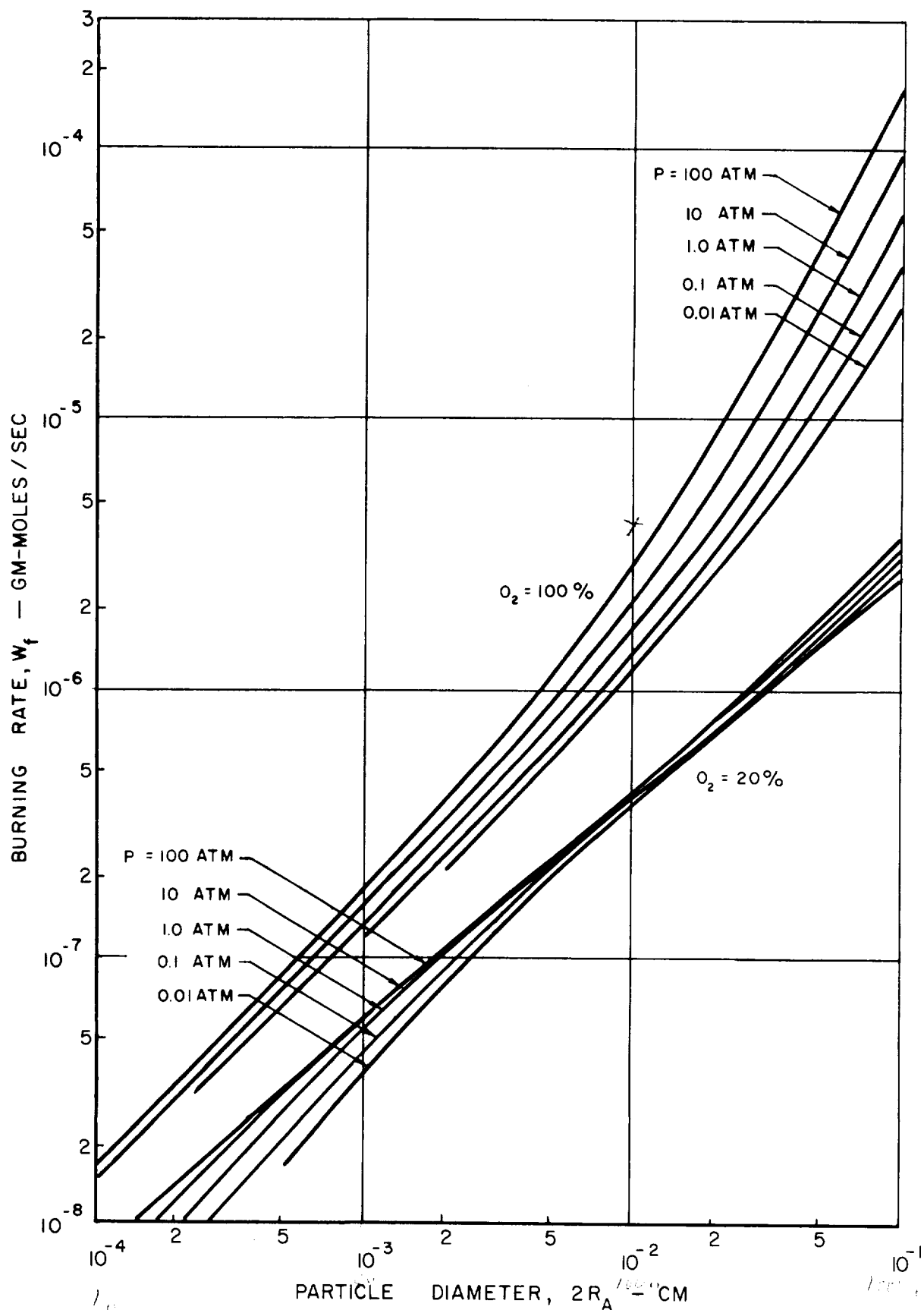
THEORETICAL BURNING RATE OF BERYLLIUM DROPLETS IN 100% OXYGEN AND 20% OXYGEN - 80% ARGON AT 300 K FOR A RANGE OF PRESSURES
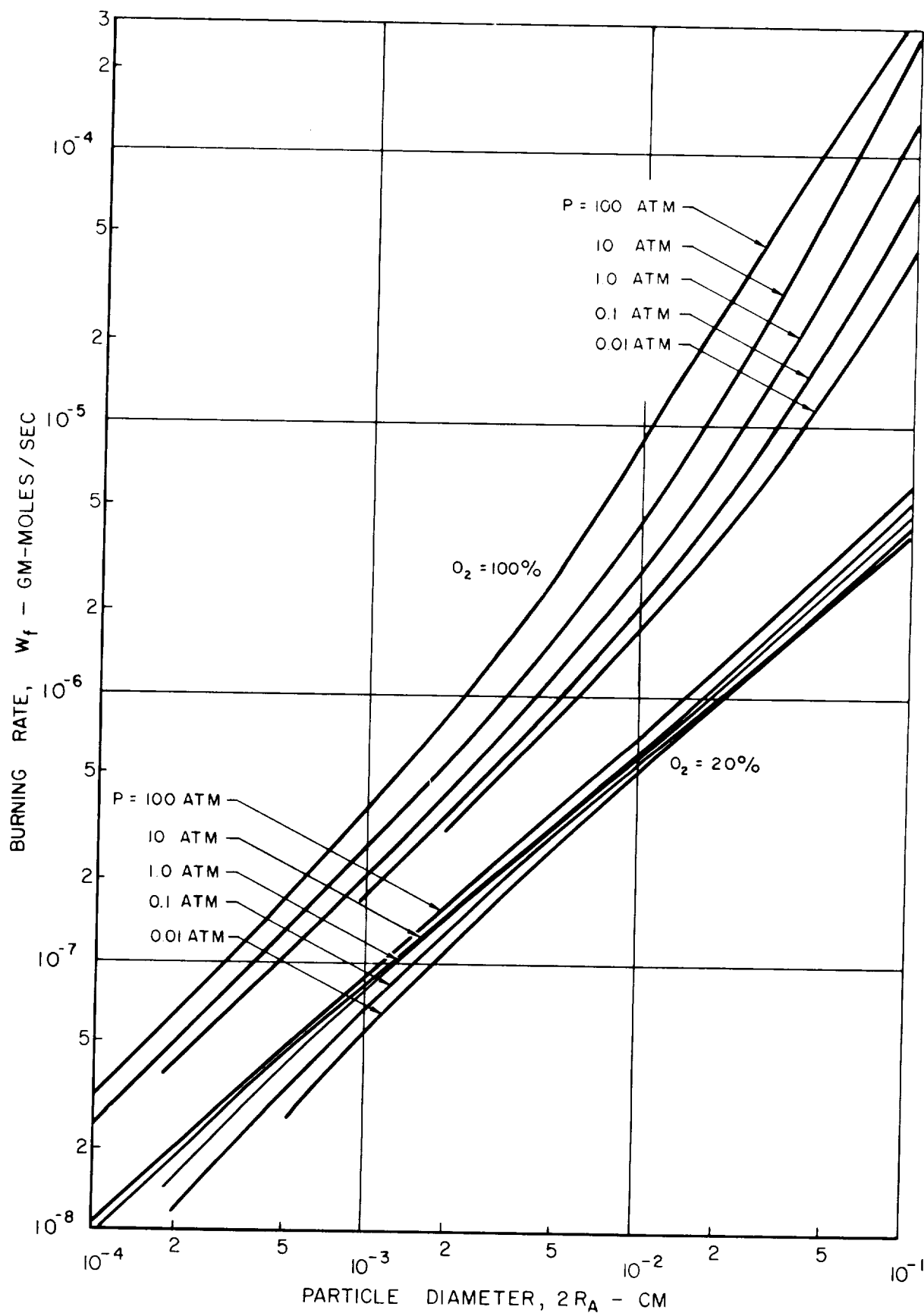
FIG.69

RATIO OF THEORETICAL BURNING RATE TO PARTICLE RADIUS FOR DROPLETS OF BERYLLIUM BURNING IN OXYGEN - ARGON MIXTURES

AMBIENT TEMPERATURE = 300 K

PRESSURE = 1.0 ATM

RATIO OF THEORETICAL BURNING RATE TO PARTICLE RADIUS FOR DROPLETS OF BERYLLIUM BURNING IN OXYGEN – ARGON MIXTURES

FIG. 71

RATIO OF THEORETICAL BURNING RATE TO PARTICLE RADIUS FOR DROPLETS OF BERYLLIUM BURNING IN OXYGEN – ARGON MIXTURES

PRESSURE = 1.0 ATM

AMBIENT TEMPERATURE = 3000 K

FIG.72
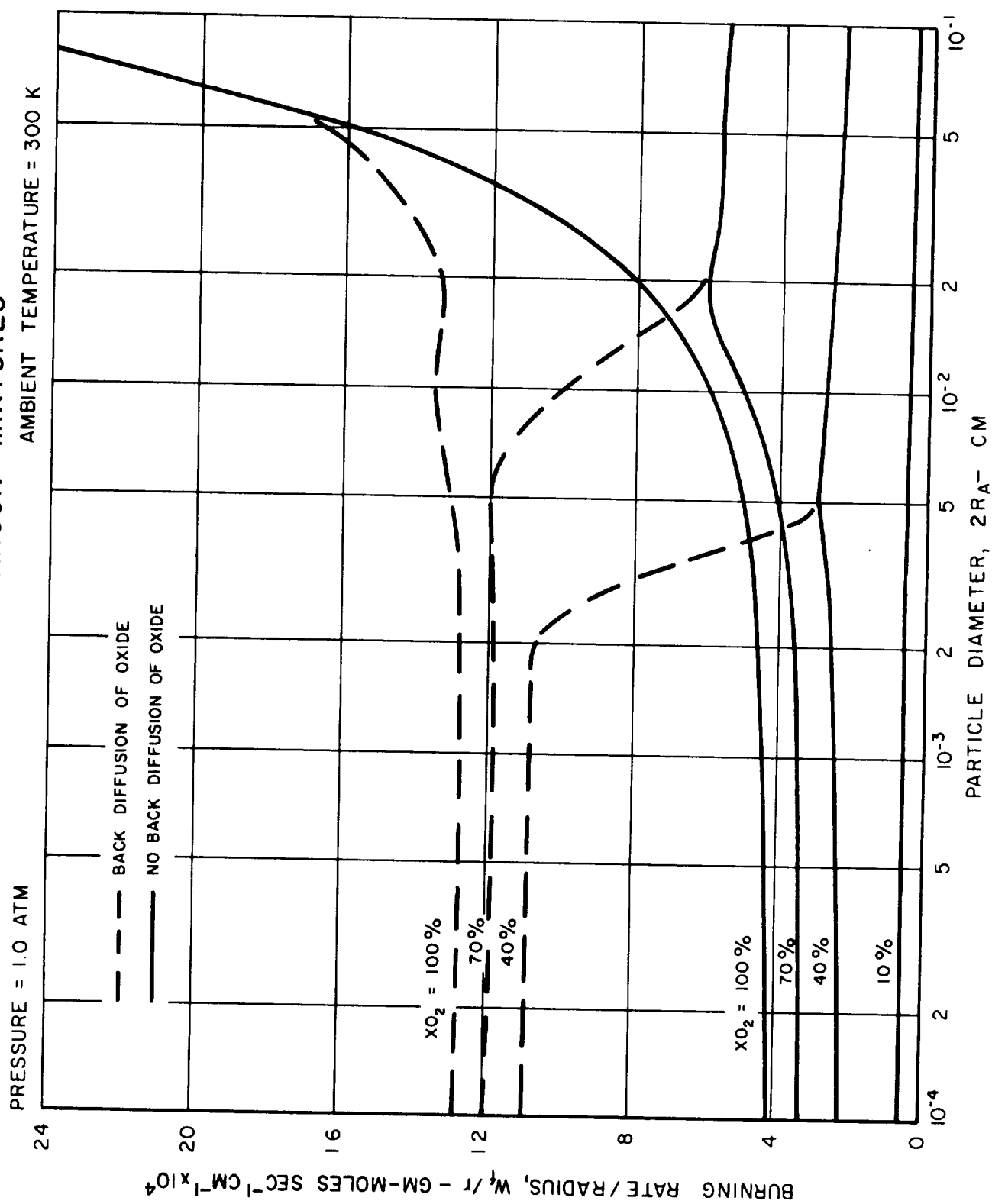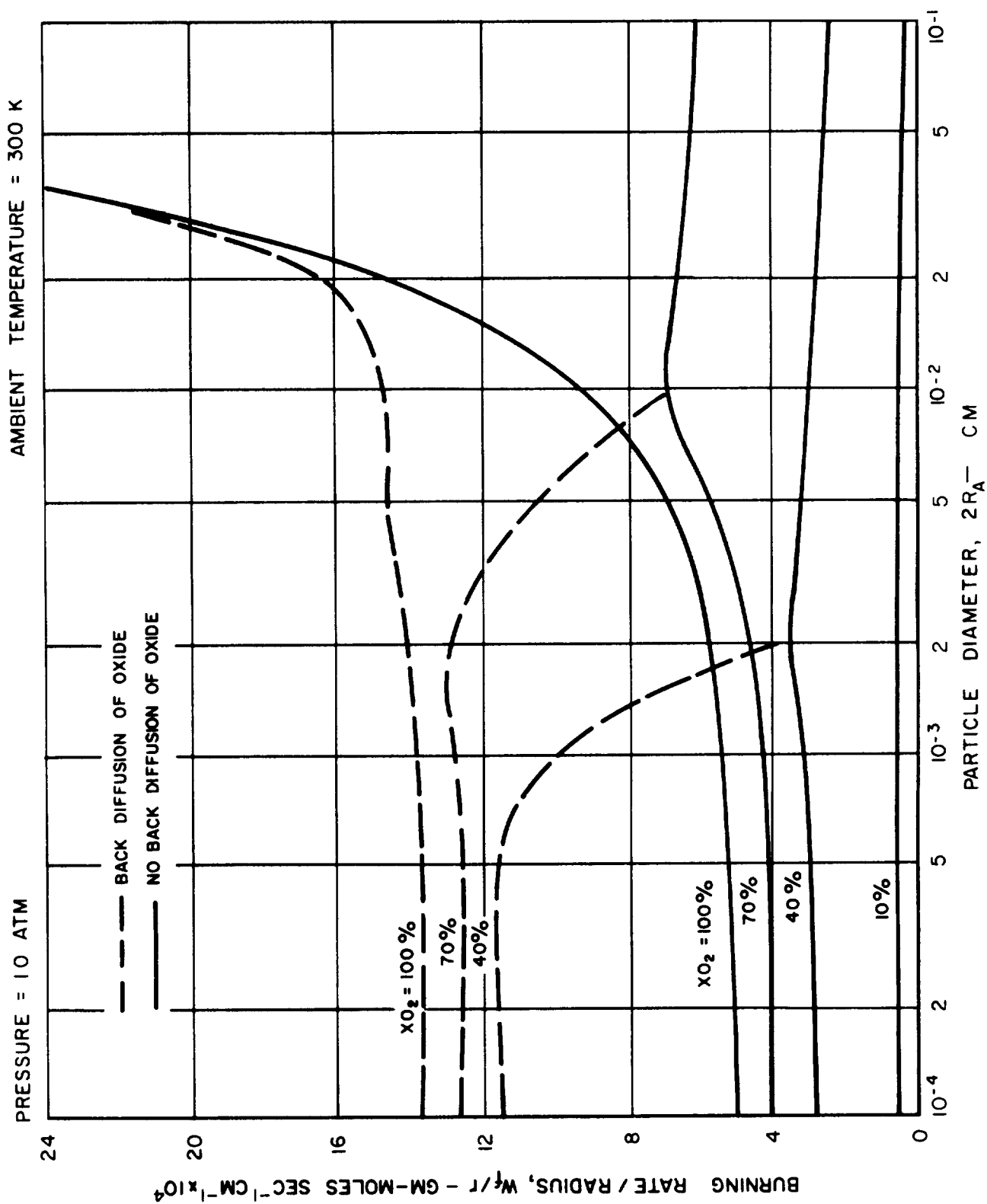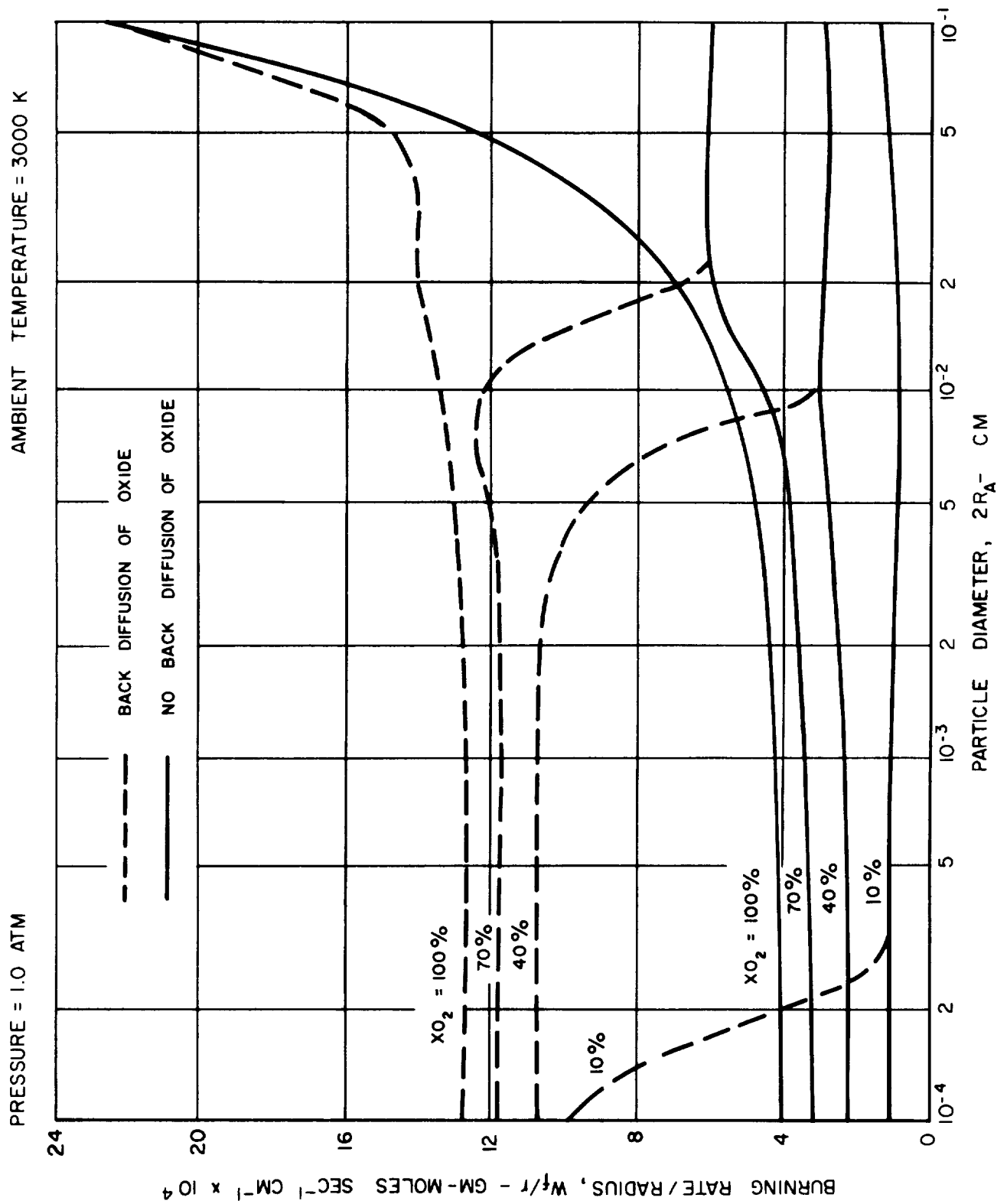
FRACTION (αλ) OF OXIDE DIFFUSING TO METAL PARTICLE FOR
DROPLETS OF BERYLLIUM BURNING IN OXYGEN-ARGON MIXTURES

PRESSURE = 1.0 ATM   AMBIENT TEMPERATURE = 300 K

FIG. 73
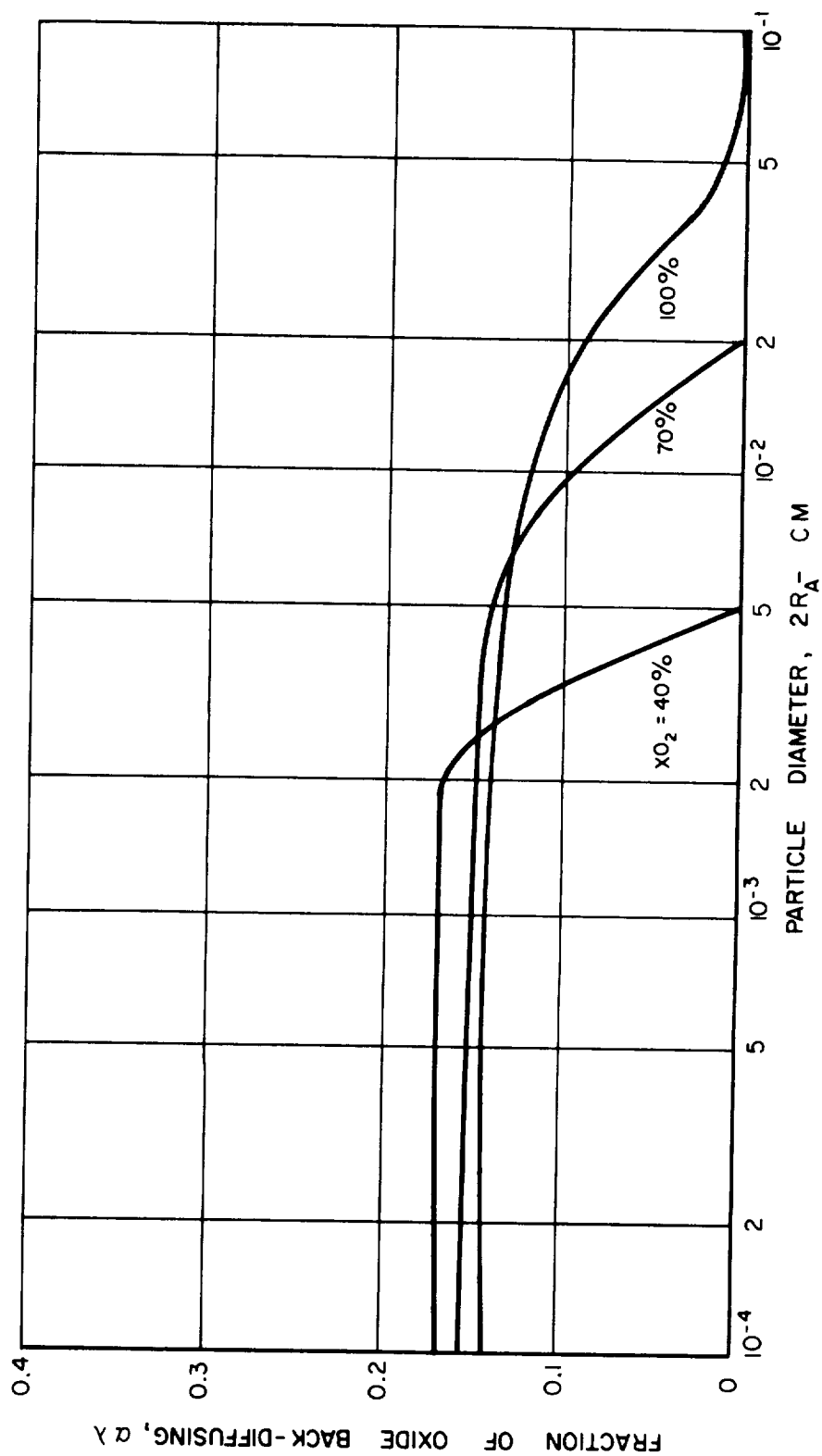
ESTIMATED FINAL DIAMETER OF OXIDE DROPLETS FROM BERYLLIUM BURNING IN OXYGEN-ARGON MIXTURES WITH BACK DIFFUSION

PRESSURE = 1.0 ATM   AMBIENT TEMPERATURE = 300 K
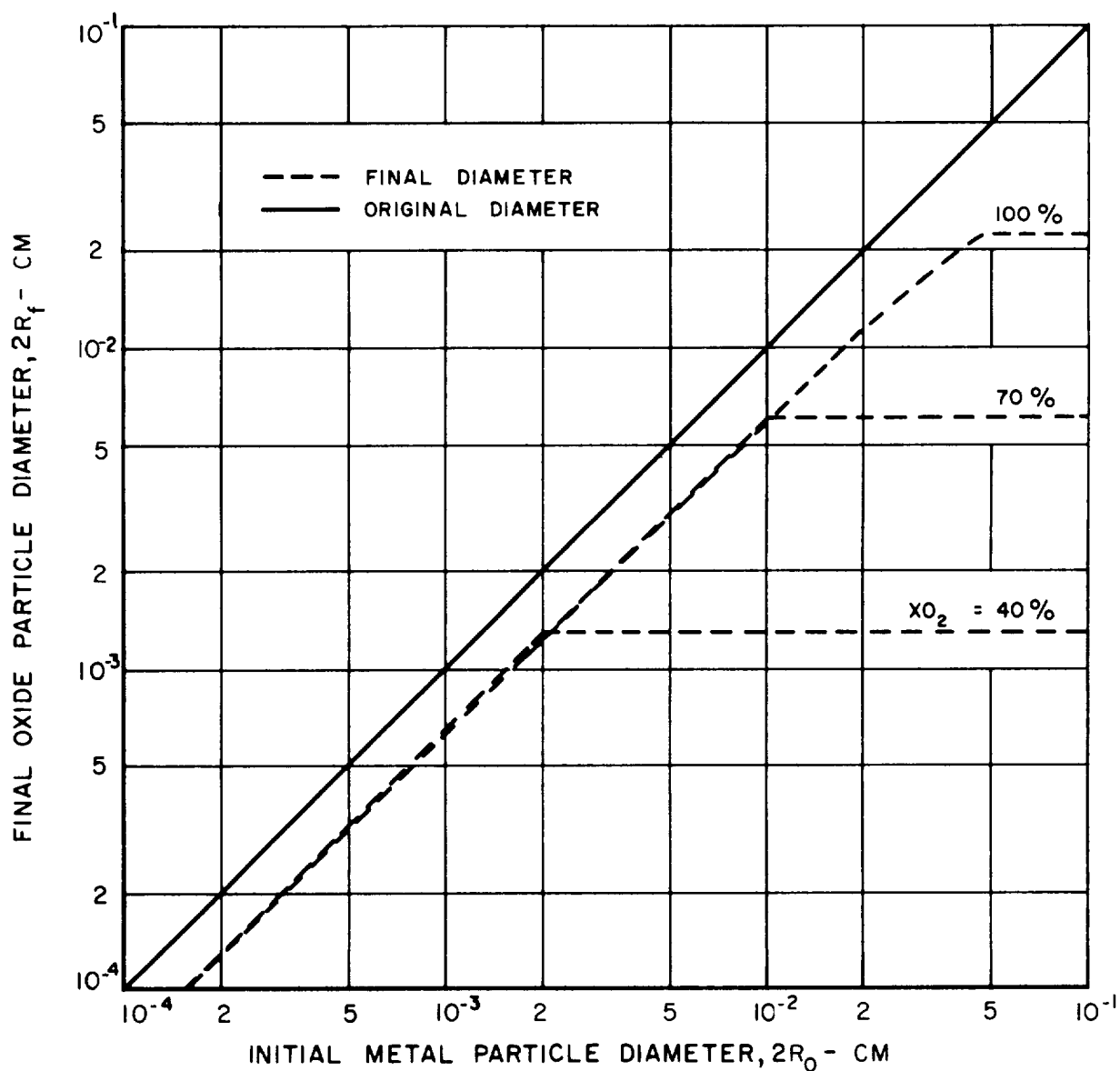
THEORETICAL BURNING TIMES OF DROPLETS OF BERYLLIUM IN OXYGEN-ARGON MIXTURES WITHOUT BACK DIFFUSION OF OXIDE
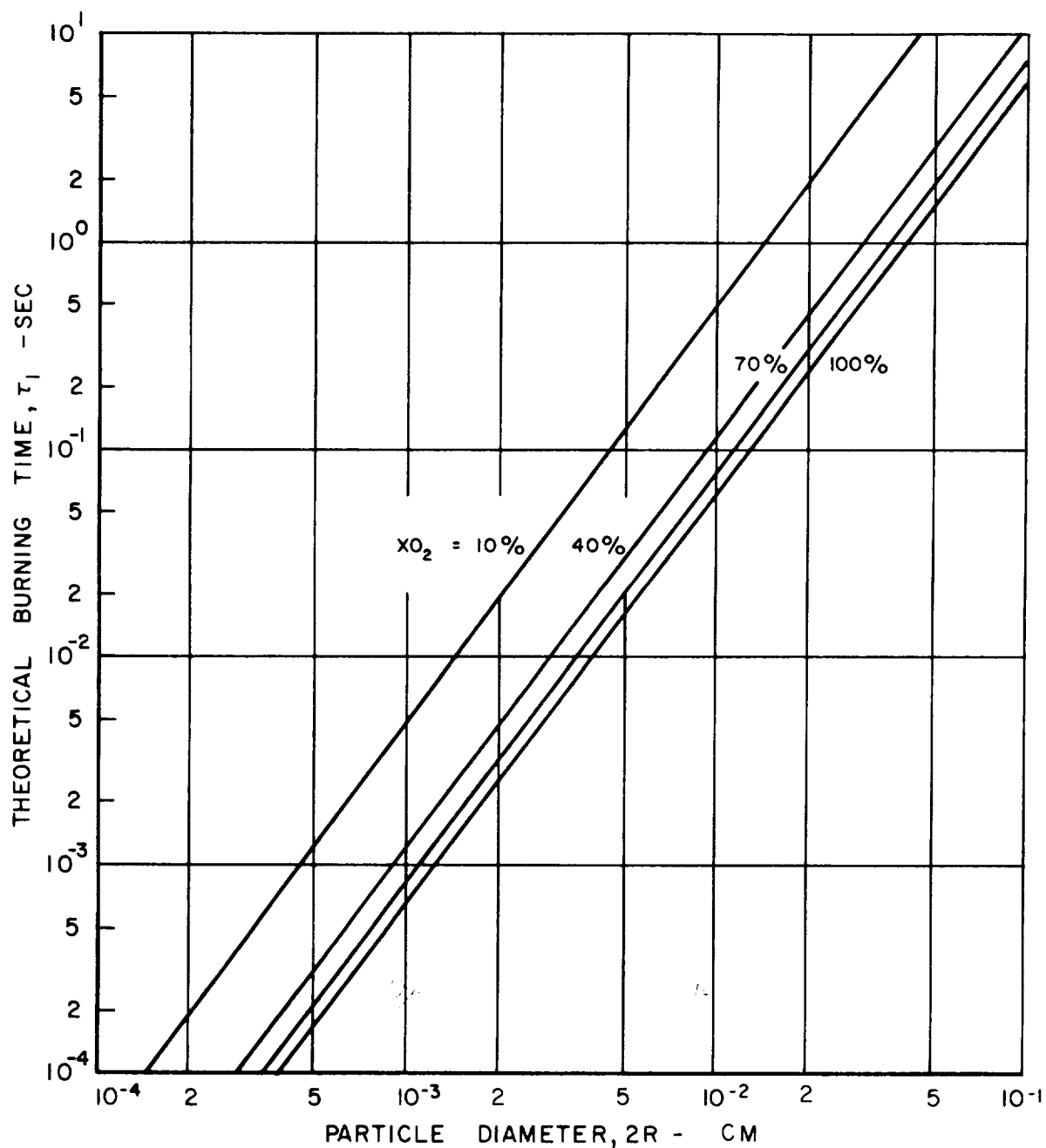
PRESSURE = 1.0 ATM   AMBIENT TEMPERATURE = 300 K

FIG. 75

THEORETICAL BURNING TIMES OF DROPLETS OF BERYLLIUM IN OXYGEN-ARGON MIXTURES WITH BACK DIFFUSION OF OXIDE

PRESSURE = 1.0 ATM   AMBIENT TEMPERATURE = 300 K

FIG. 76
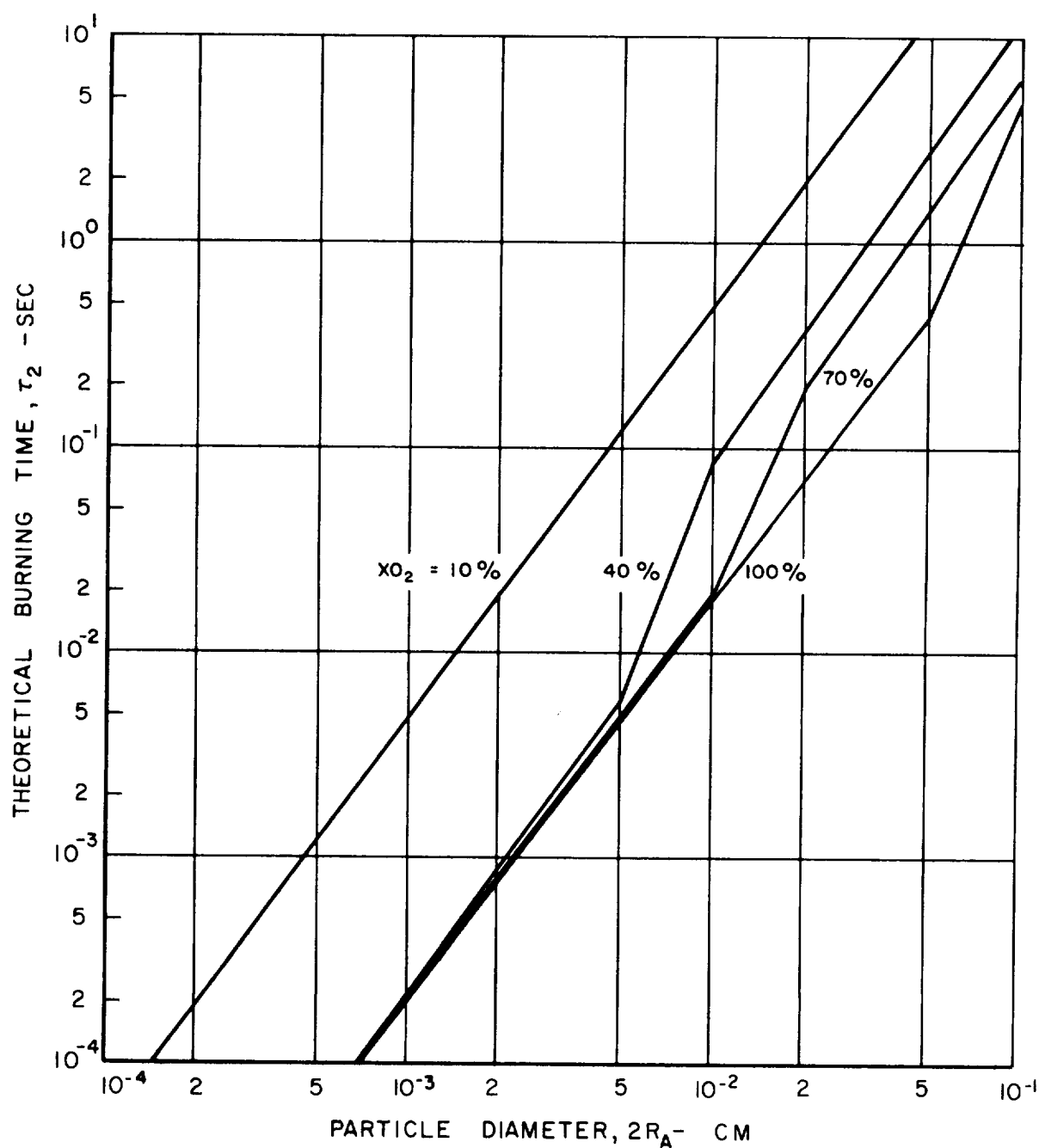
COMPARISON OF FLAME TO PARTICLE RADIUS RATIOS CALCULATED WITH AND WITHOUT BACK DIFFUSION OF METAL OXIDE FROM FLAME FRONT

50-MICRON ALUMINUM PARTICLES
P = 0.1 ATM

OXIDIZING GAS COMPOSED OF MIXTURES OF OXYGEN AND ARGON
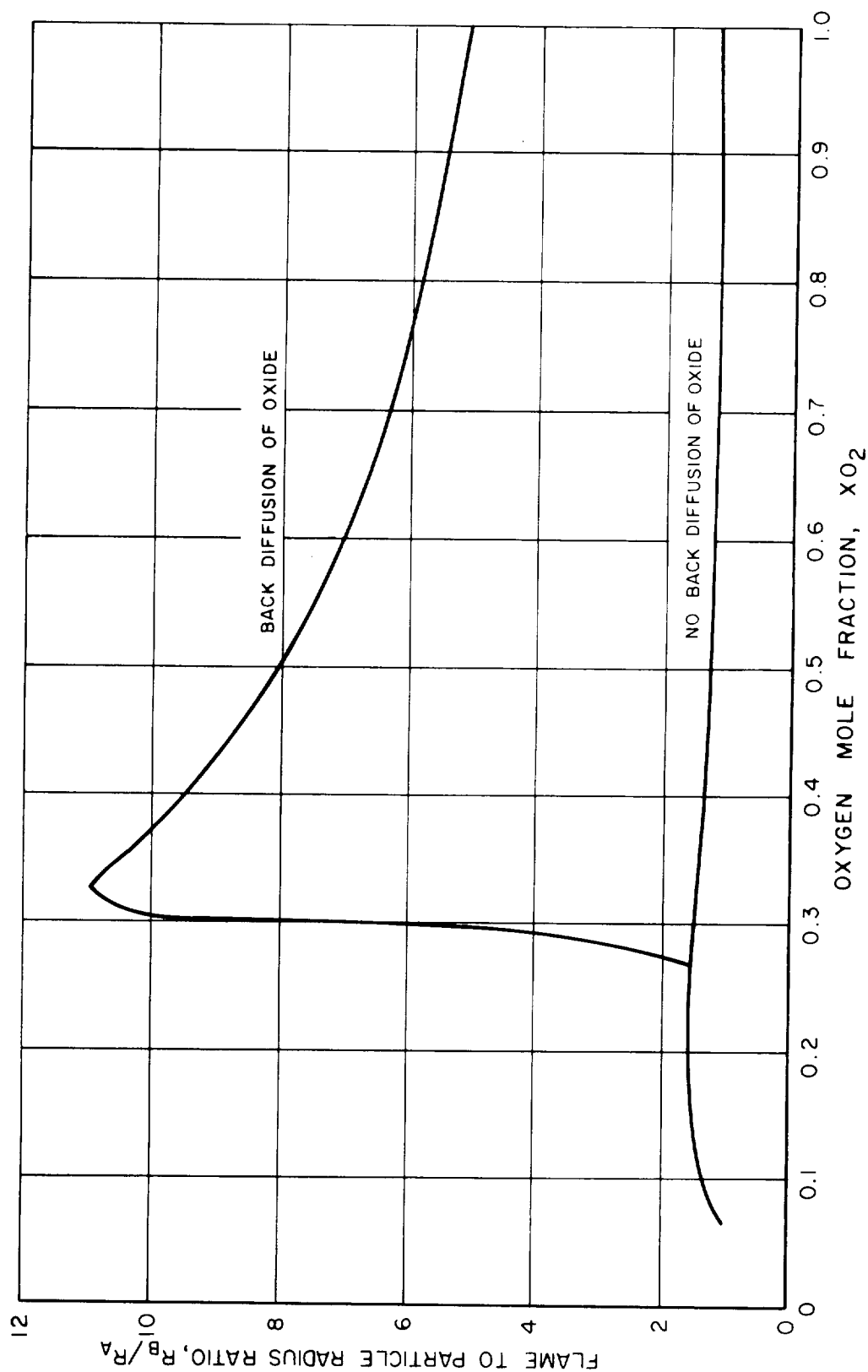
BACK DIFFUSION OF OXIDE

NO BACK DIFFUSION OF OXIDE

FLAME TO PARTICLE RADIUS RATIO, R_B/R_A

OXYGEN MOLE FRACTION, X_{O_2}

COMPARISON OF THE EFFECT OF PRESSURE ON THE RATIO OF FLAME TO PARTICLE RADII CALCULATED FOR ALUMINUM WITH AND WITHOUT BACK DIFFUSION OF METAL OXIDE FROM FLAME FRONT

FIG 78
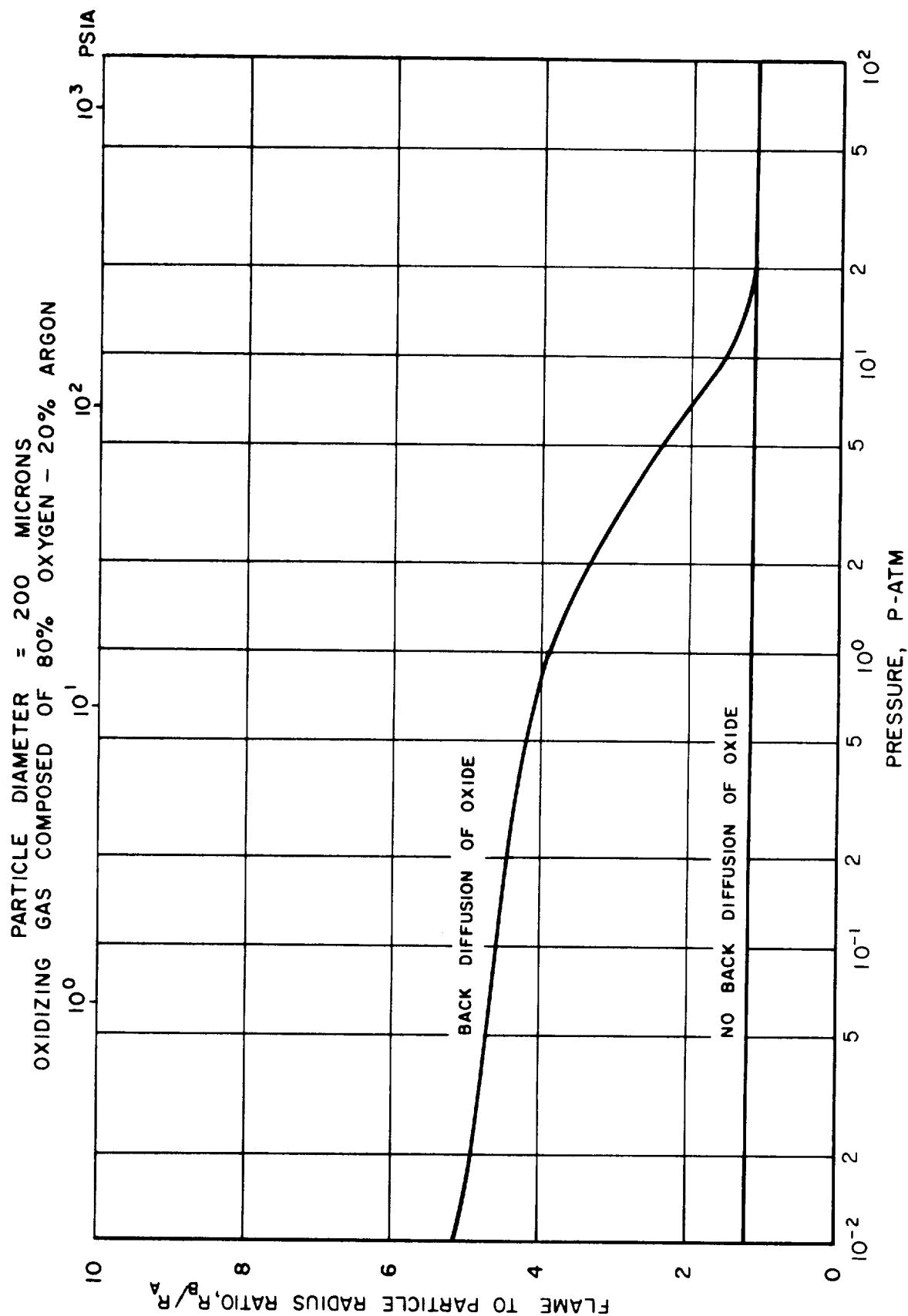
COMPARISON OF THE EFFECT OF ALUMINUM PARTICLE DIAMETER ON THE RATIO OF FLAME TO PARTICLE RADII CALCULATED WITH AND WITHOUT BACK DIFFUSION

P = 0.1 ATM

OXIDIZING GAS COMPOSED OF 90% OXYGEN / 10% ARGON

FIG 79
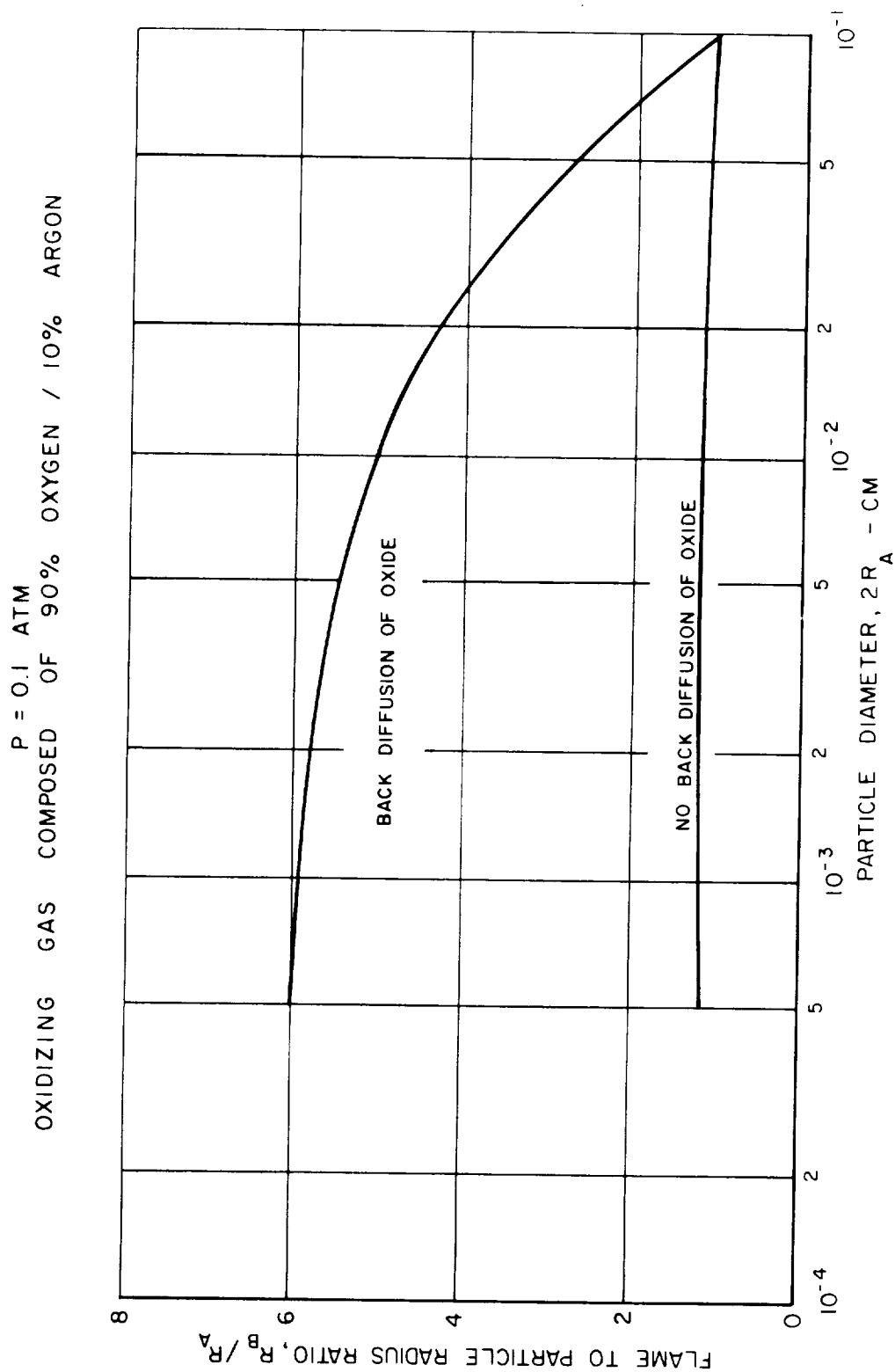
COMPARISON OF CALCULATED FLAME RADII AND FLAME PARTICLE SEPARATION DISTANCES FOR ALUMINUM WITH AND WITHOUT BACK DIFFUSION OF METAL OXIDE FROM FLAME FRONT
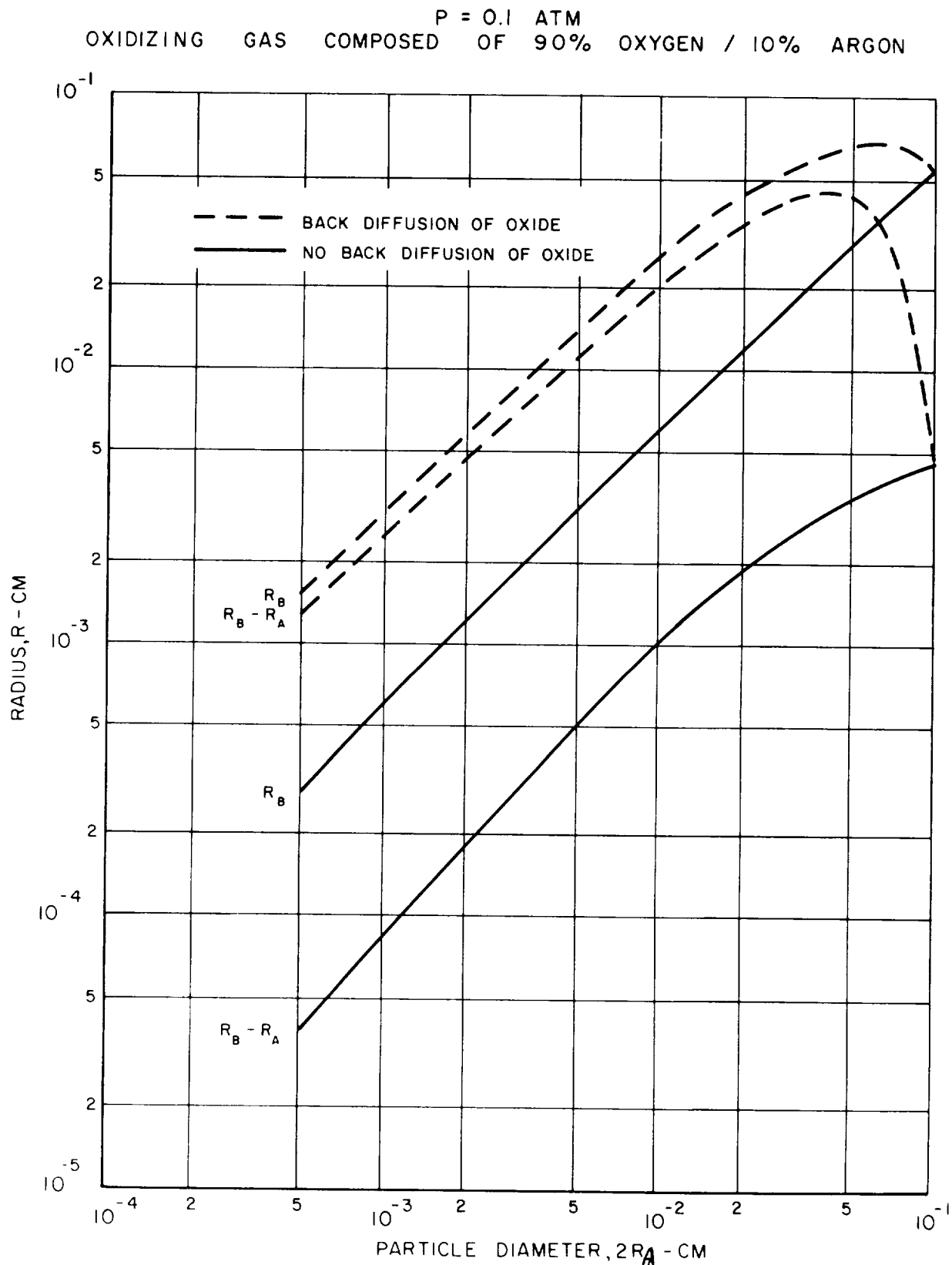
P = 0.1 ATM

OXIDIZING GAS COMPOSED OF 90% OXYGEN / 10% ARGON

FIG. 80

COMPARISON OF FLAME TO PARTICLE RADIUS RATIOS CALCULATED
WITH AND WITHOUT BACK DIFFUSION OF METAL OXIDE FROM
FLAME FRONT

50-MICRON BERYLLIUM PARTICLES
P = 1.0 ATM

OXIDIZING GAS COMPOSED OF MIXTURES OF OXYGEN AND ARGON

FIG. 81
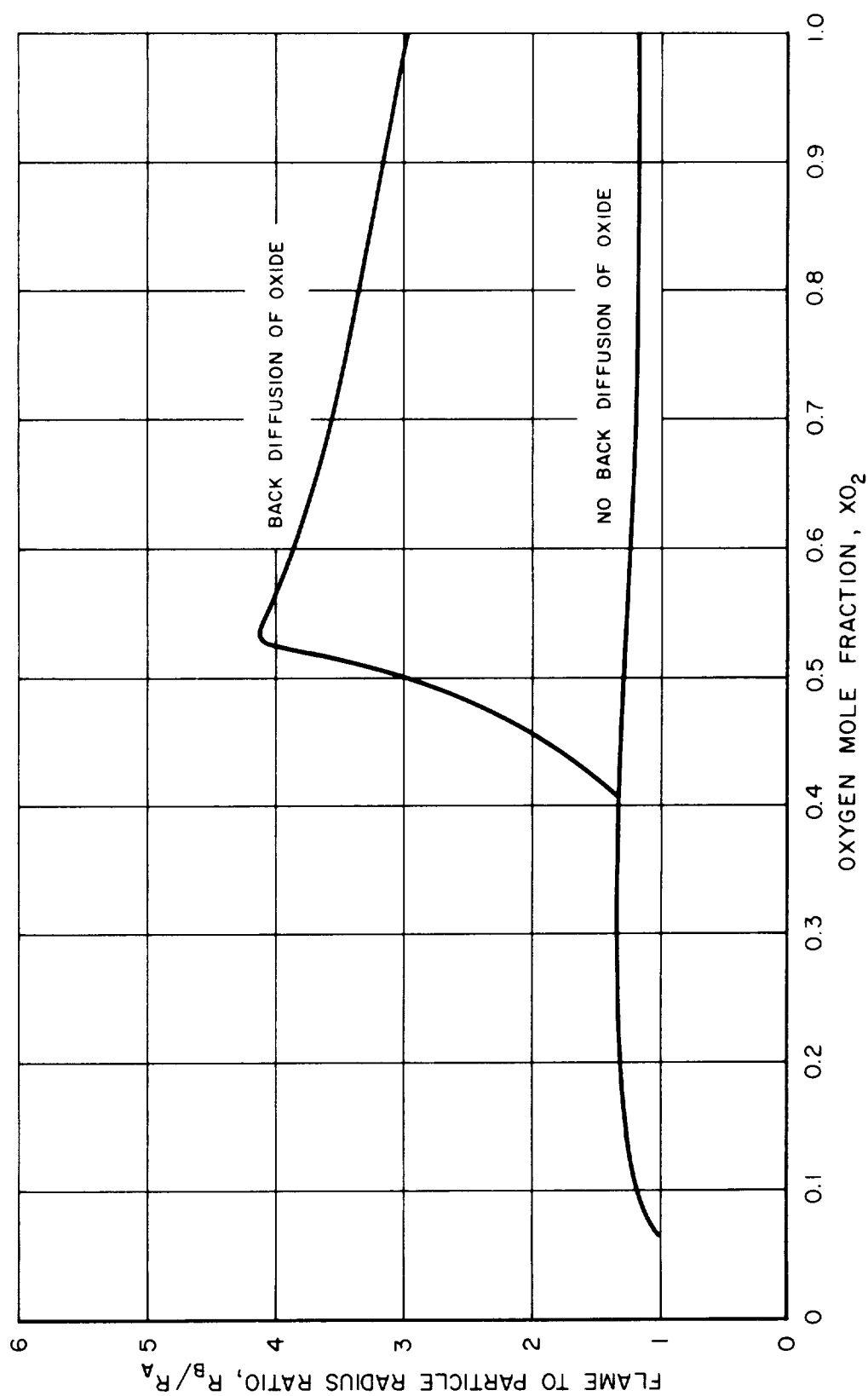
COMPARISON OF THE EFFECT OF BERYLLIUM PARTICLE DIAMETER ON THE RATIO OF FLAME TO PARTICLE RADII CALCULATED WITH AND WITHOUT BACK DIFFUSION

FIG. 82
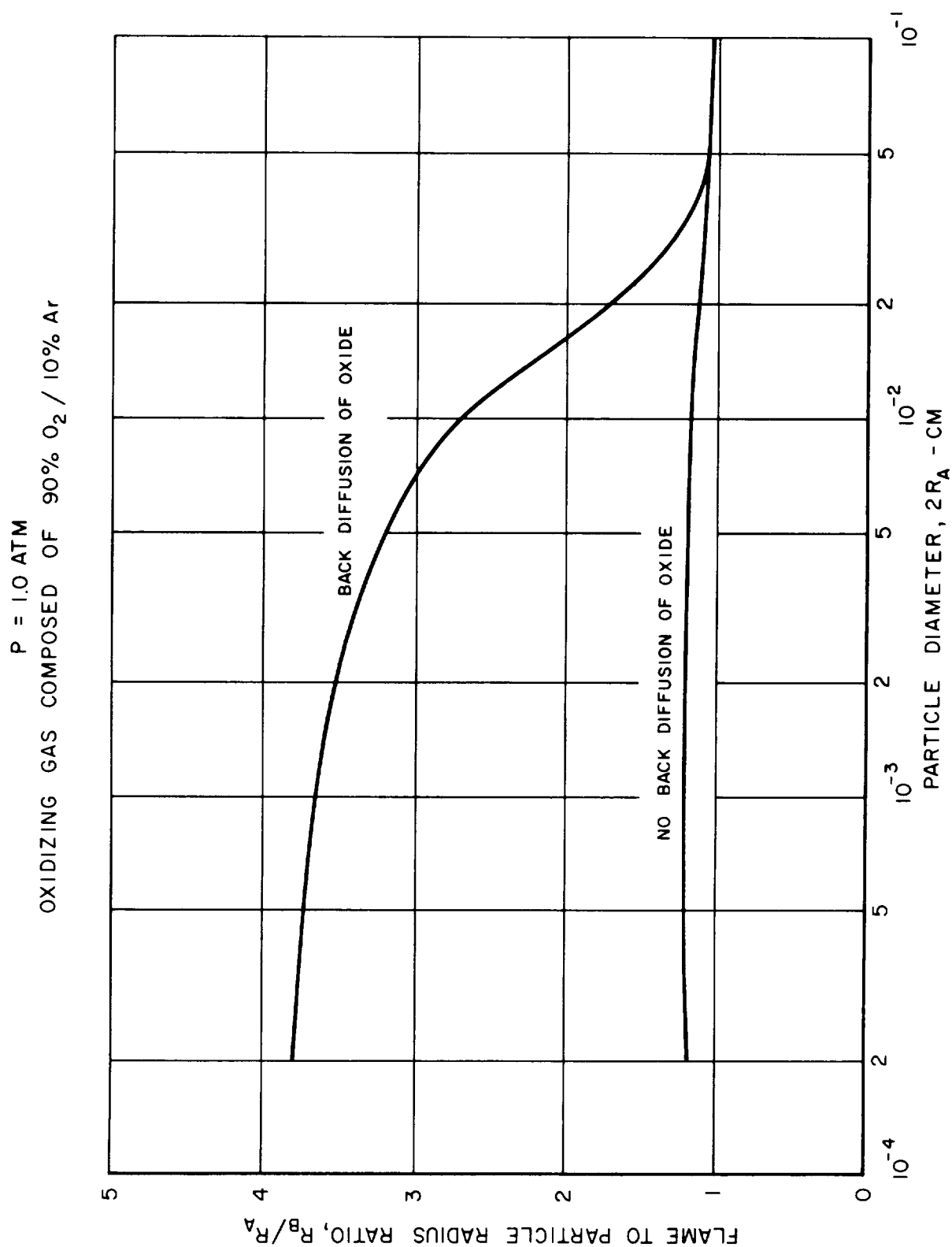
COMPARISON OF CALCULATED FLAME RADII AND FLAME-PARTICLE SEPARATION DISTANCES FOR BERYLLIUM WITH AND WITHOUT BACK DIFFUSION OF METAL OXIDE FROM FLAME FRONT

P = 1.0 ATM

OXIDIZING GAS COMPOSED OF 90% O_2 / 10% Ar

FIG. 83
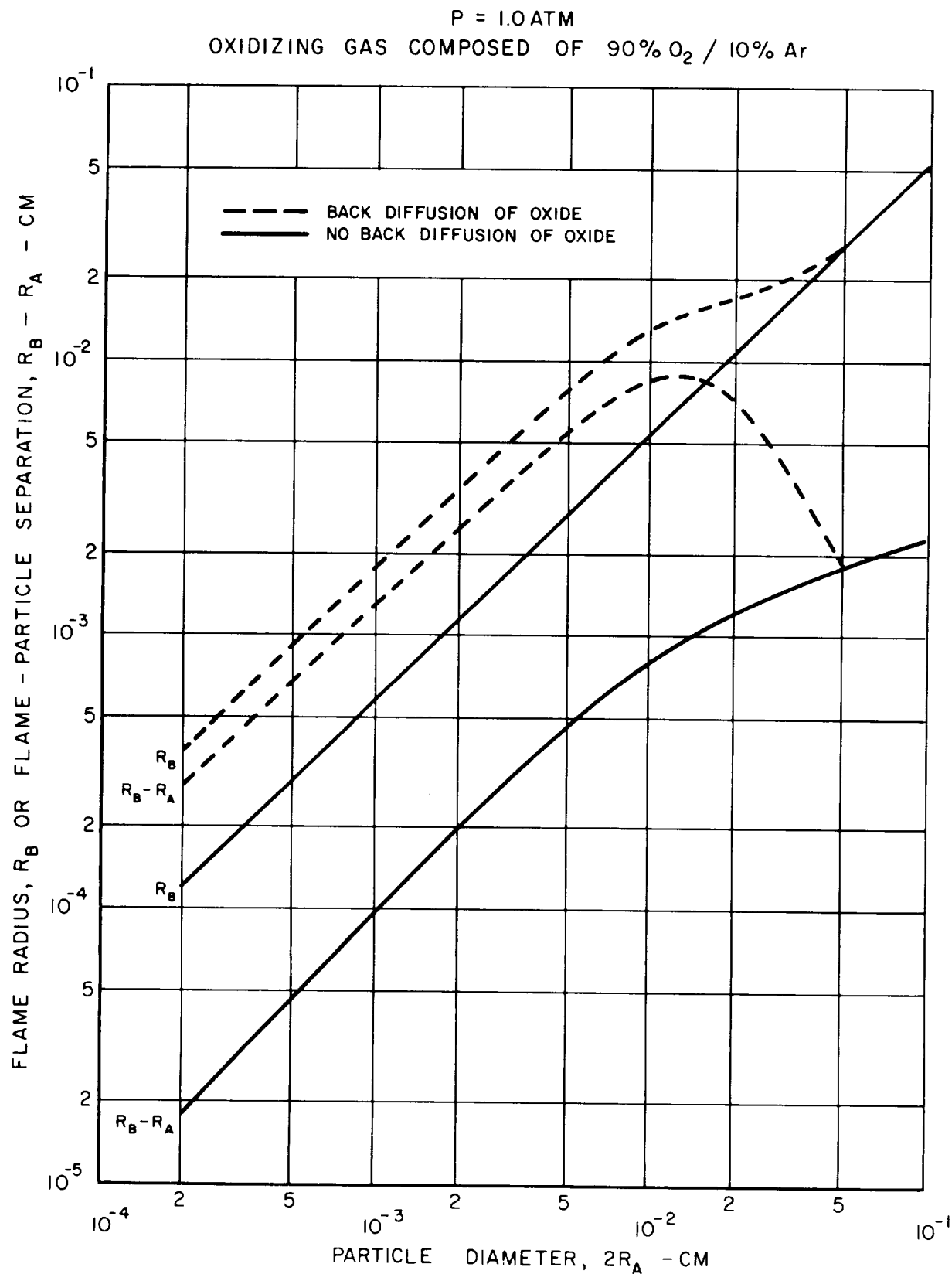
COMPARISON OF CALCULATED PARTICLE DIAMETER DURING BURNING FOR 20-MICRON BERYLLIUM PARTICLES WITH AND WITHOUT BACK DIFFUSION OF METAL OXIDE FROM FLAME FRONT

P = 1.0 ATM

OXIDIZING GAS COMPOSED OF 90% O_2 / 10% Ar

FIG. 84

COMPARISON OF THE EFFECT OF PRESSURE ON THE RATIO OF FLAME TO PARTICLE RADII CALCULATED FOR BERYLLIUM WITH AND WITHOUT BACK DIFFUSION OF METAL OXIDE FROM FLAME FRONT

FIG 85
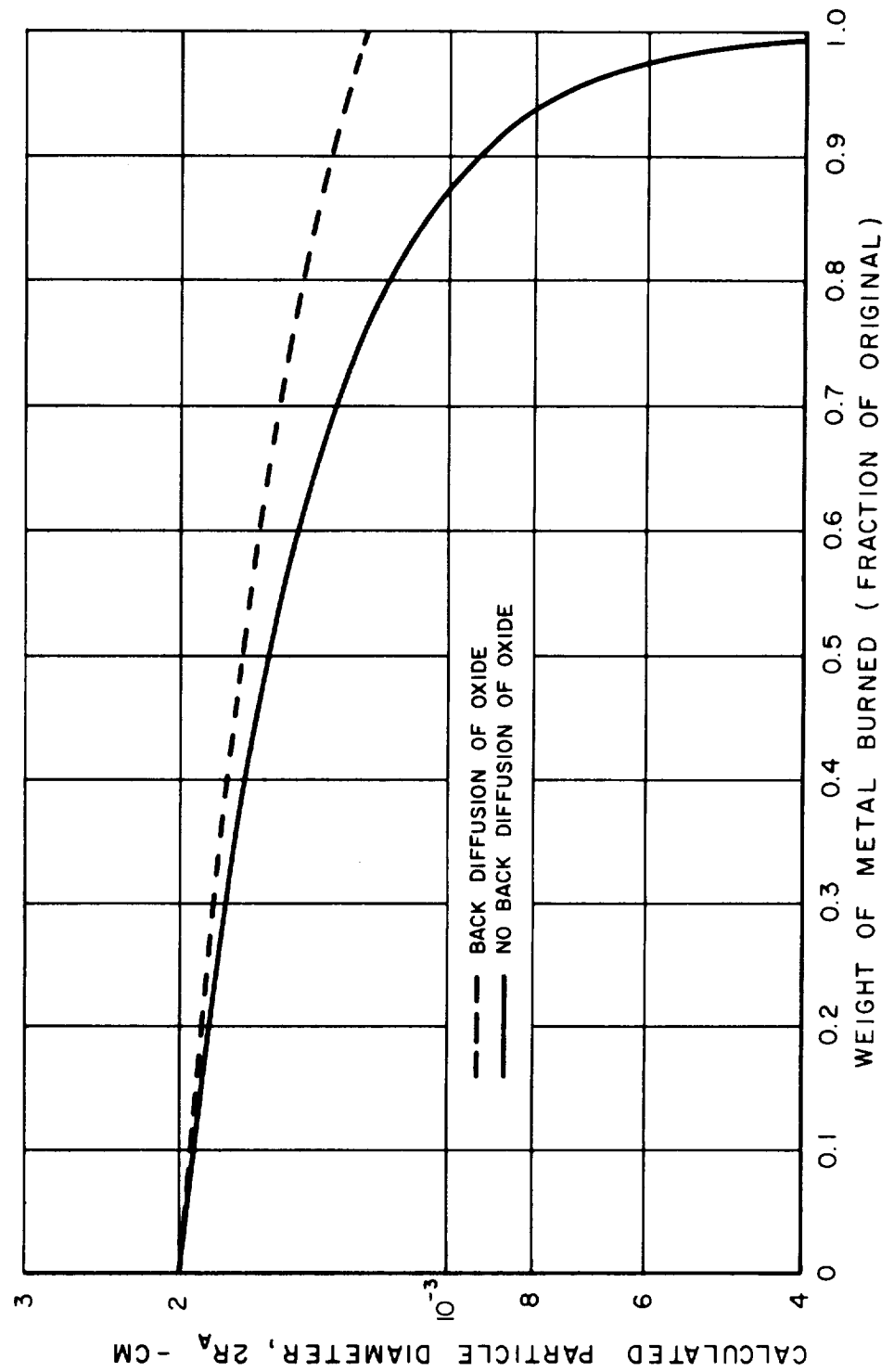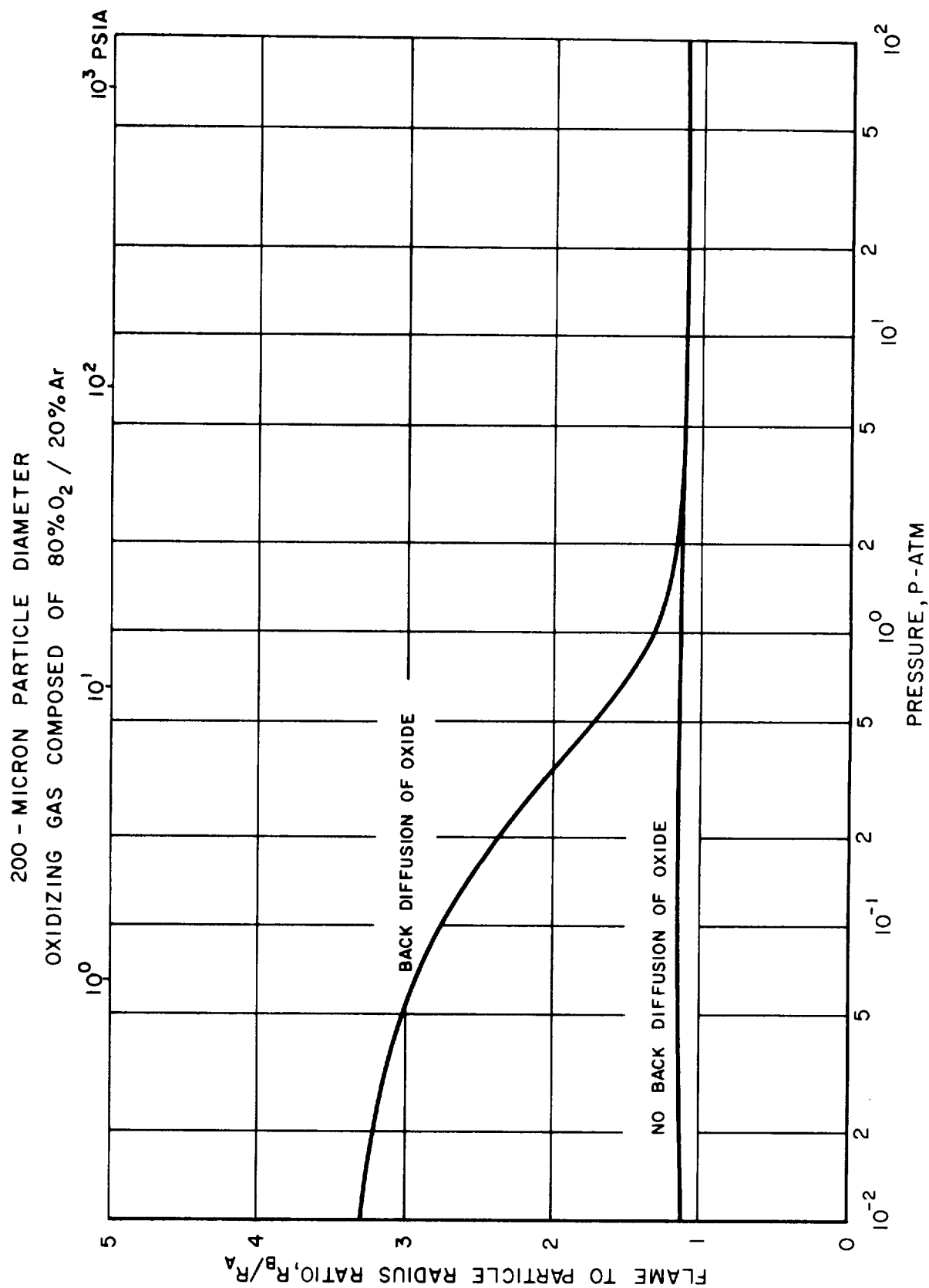
VARIATION OF CALCULATED FLAME TO PARTICLE RADIUS RATIO (R_B/R_A) WITH PARTICLE DIAMETER FOR ALUMINUM WITH DIFFERENT OXIDIZER-INERT MIXTURES

TOTAL PRESSURE: 0.01 ATM

OXIDIZER MIXTURE COMPOSITION: 20% O_2 - 80% INERT
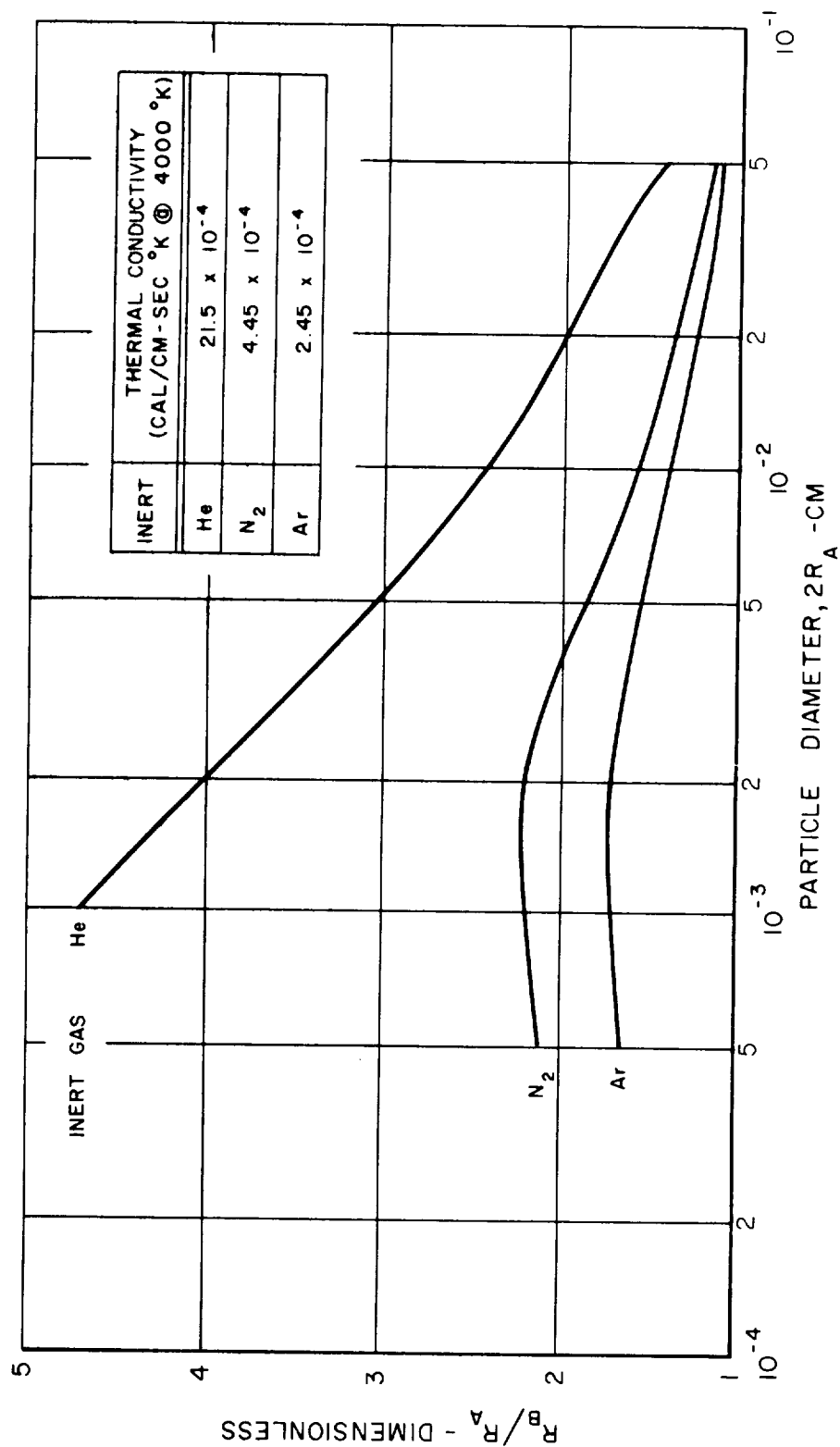
VARIATION OF CALCULATED FLAME TO PARTICLE RADIUS RATIO $\left(R_B/R_A\right)$ WITH FLAME EMISSIVITY (EM2) FOR ALUMINUM PARTICLES

TOTAL PRESSURE : 0.01 ATM
OXIDIZER MIXTURE COMPOSITION : 20% O_2 - 80% Ar
PARTICLE DIAMETER : 5 x 10^{-2} CM (500 MICRONS)

FLAME EMISSIVITY, EM2

FIG.87

ADIABATIC COMBUSTION TEMPERATURE
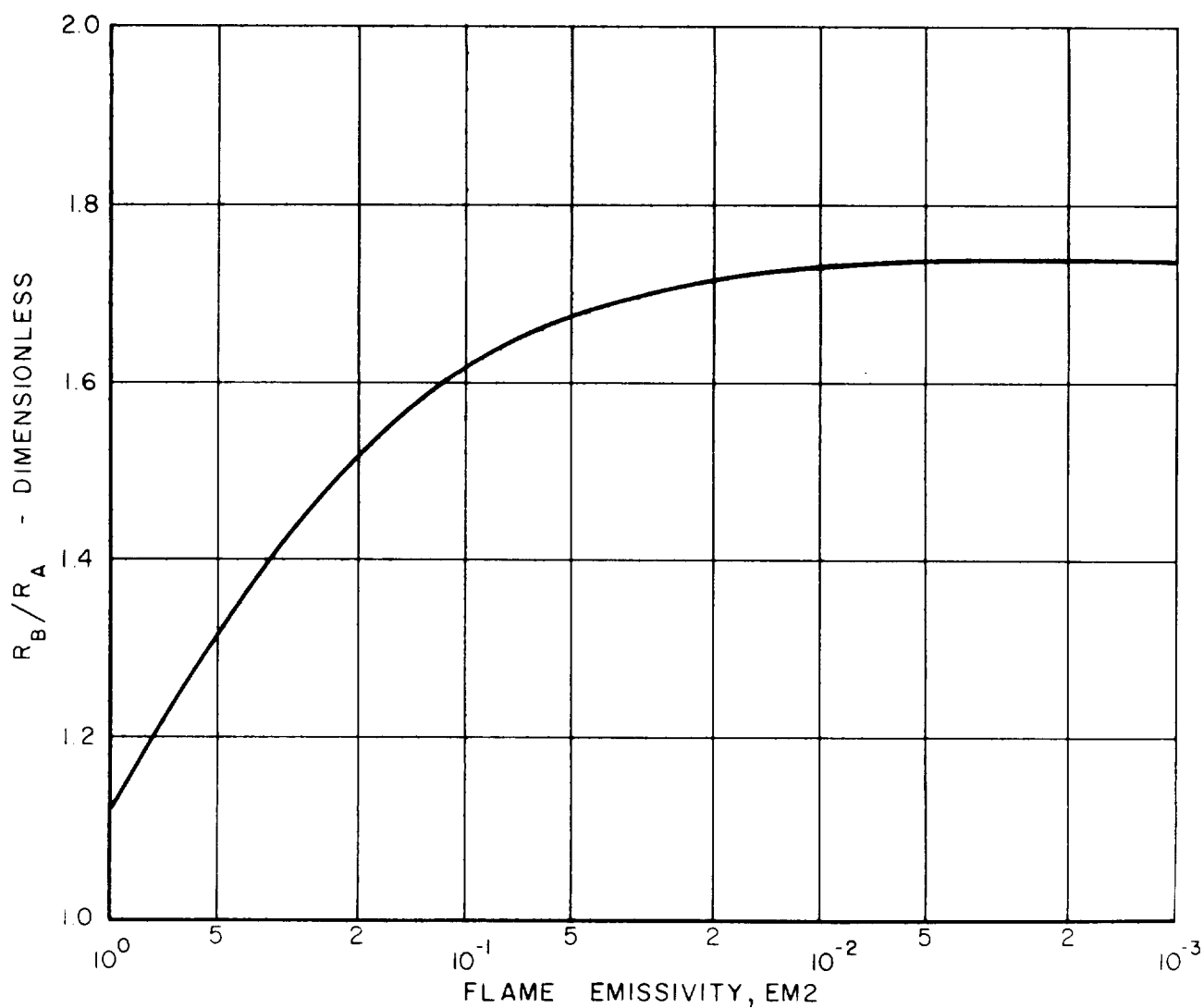
—— Be / 39.9% HCl , 39.7% CO_2 , 20.4% N_2

– – – Be / 21.5% HCl , 21.4% CO_2 , 11.0% N_2 , 46.1% H_2O
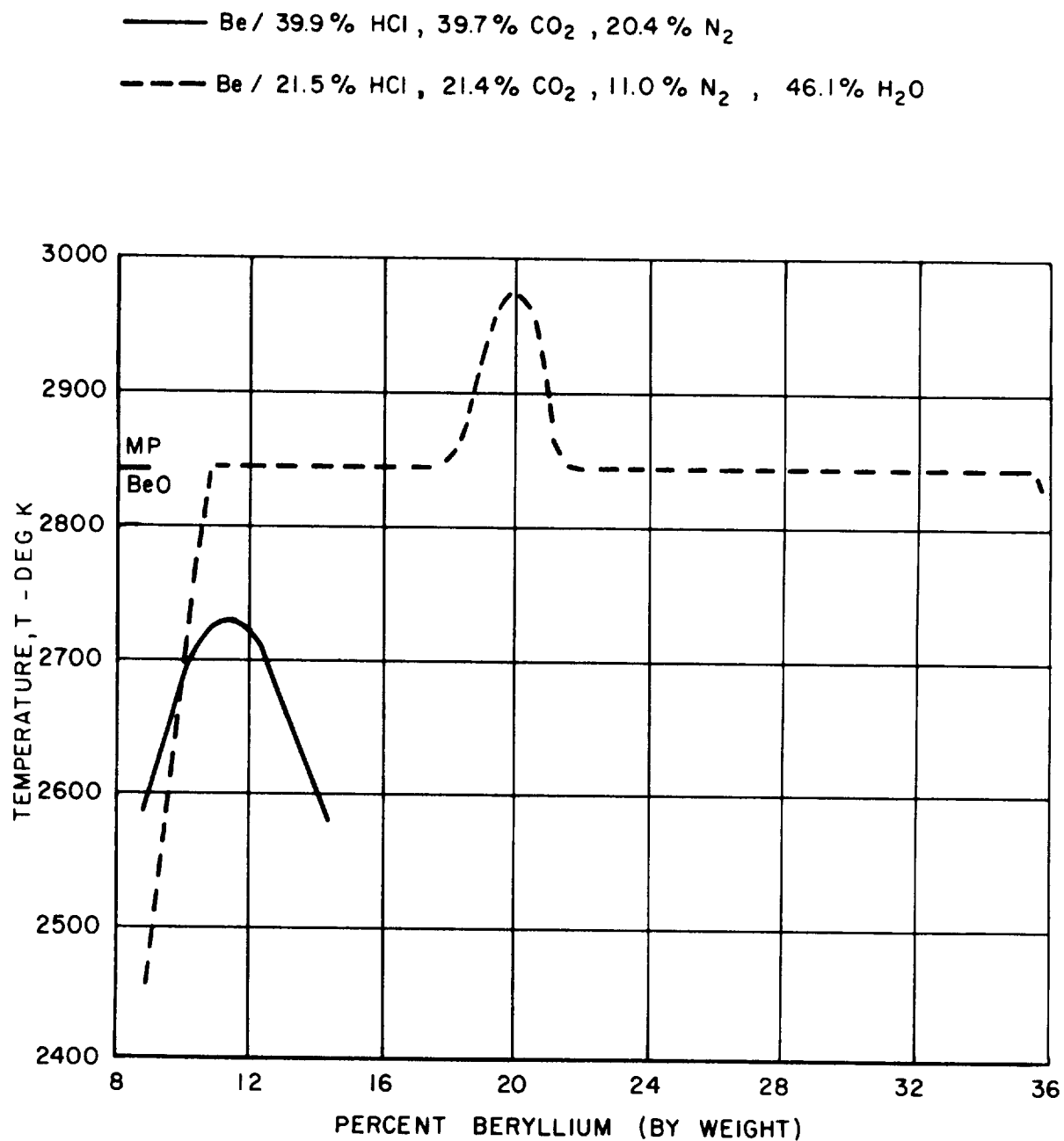
EQUILIBRIUM PRODUCTS OF ADIABATIC COMBUSTION OF
Be / 39.9 % HCl, 39.7 % CO$_2$, 20.4 % N$_2$

P = 500 psia

MOLE FRACTION OF PRODUCT

BeO(s)
CO
BeCl
N$_2$
H$_2$
BeCl$_2$
HCN
HCl
C$_2$H$_2$
C(s)
H
Cl
H$_2$O
Be(g)
CO$_2$

EQUIVALENCE RATIO, $\dfrac{O/F}{(O/F)_{ST}}$

FIG. 89
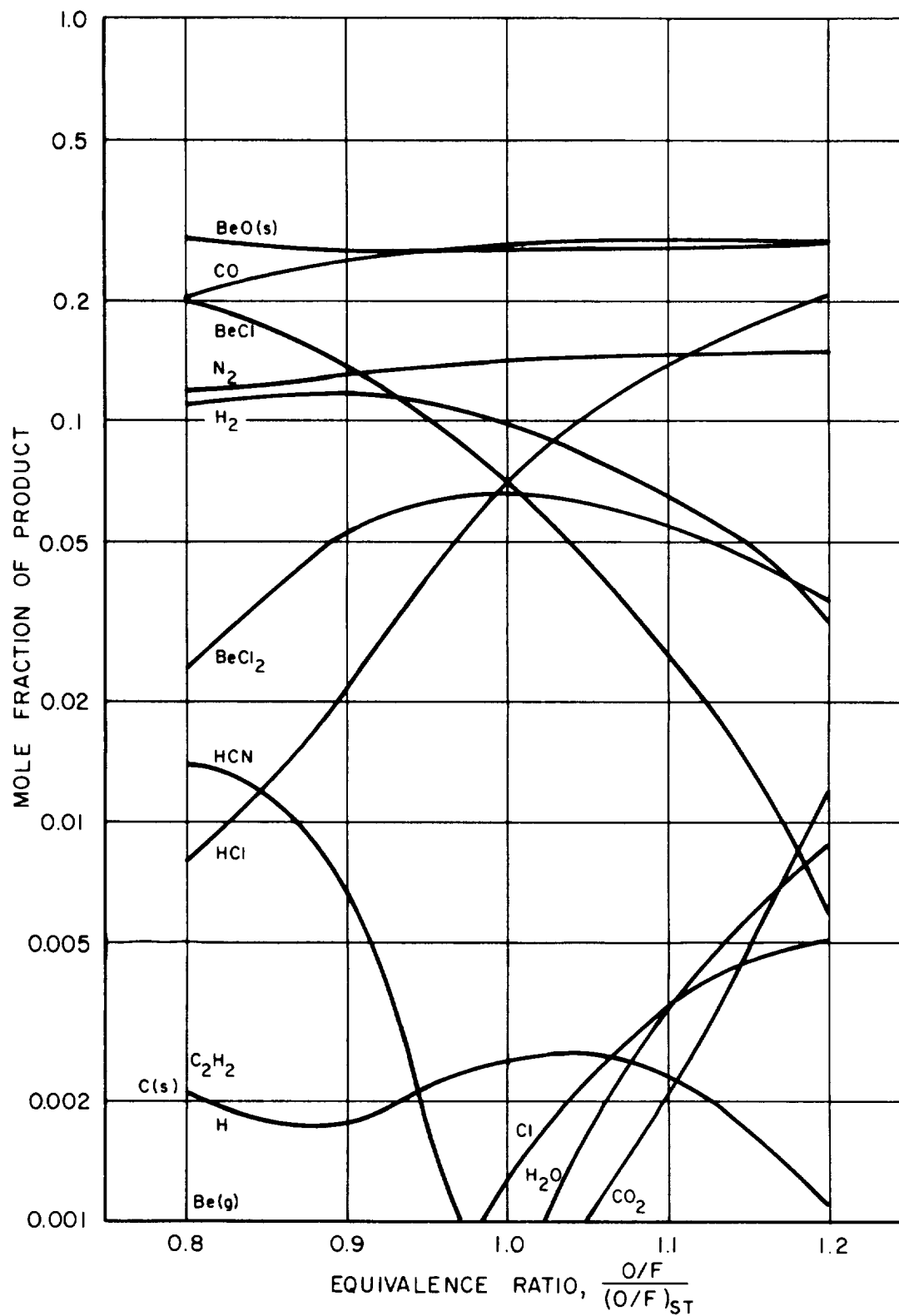
EQUILIBRIUM PRODUCTS OF ADIABATIC COMBUSTION OF
Be/21.5% HCl, 21.4% CO_2, 11.0% N_2, 46.1% H_2O

P = 500 psia
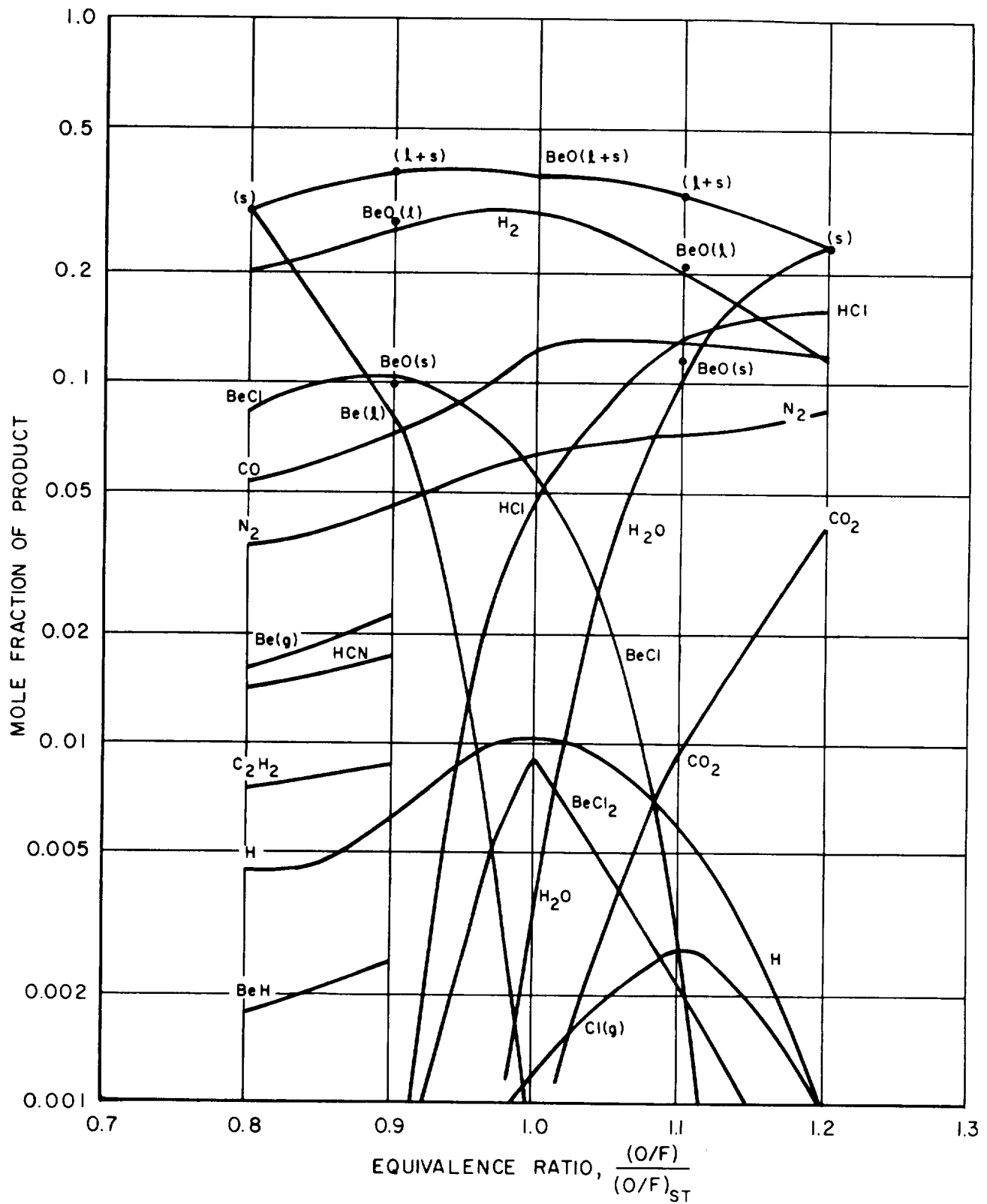
FIG. 90

EFFECT OF EXIT TEMPERATURE ON EQUILIBRIUM EXHAUST PRODUCT COMPOSITION FROM A SOLID ROCKET PROPELLANT CONTAINING 10% PBAN – 90% AP

P_c = 1000 PSIA
T_c = 5305 R
       2950 K
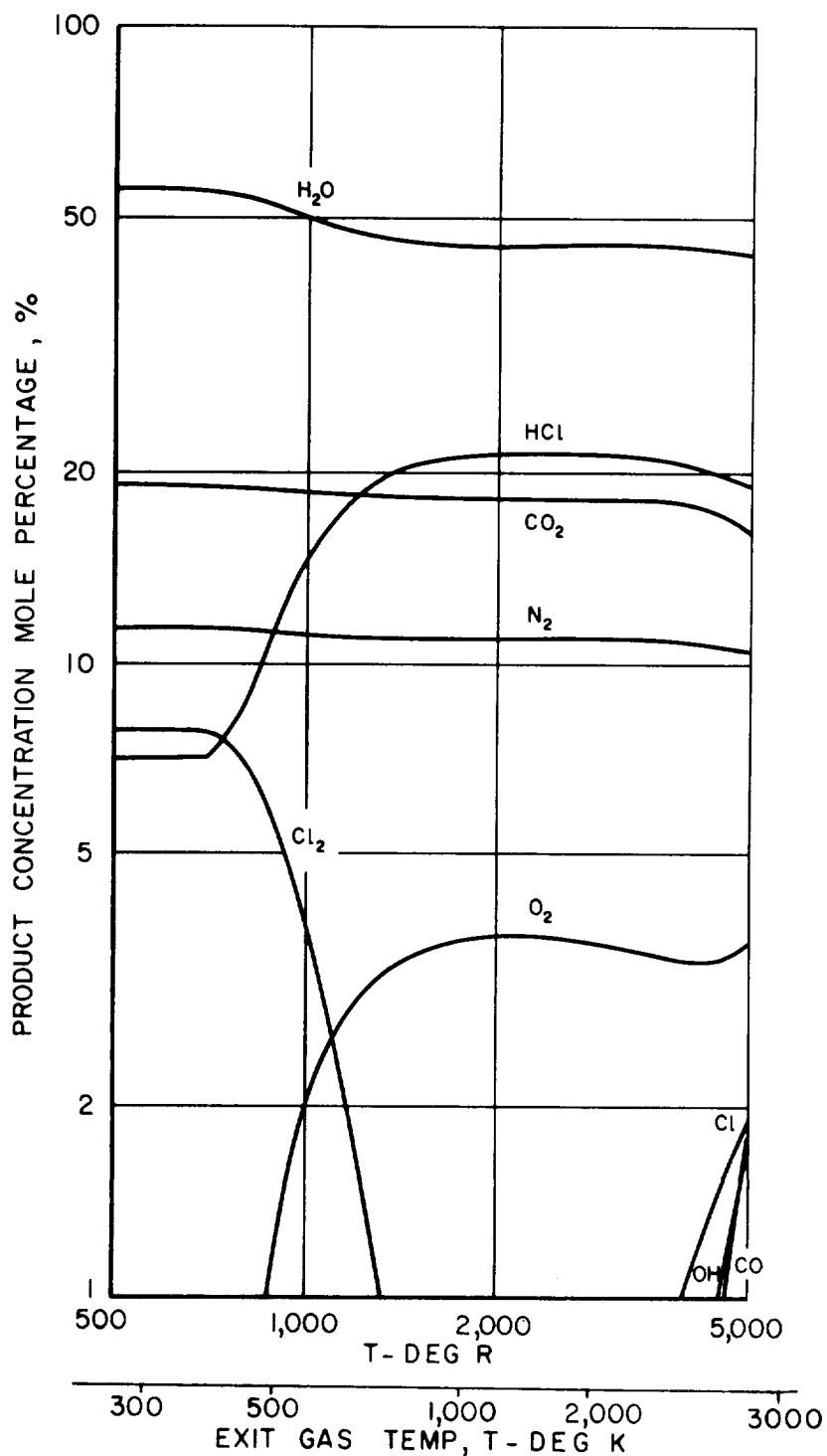
FIG. 91

EFFECT OF EXIT TEMPERATURE ON EQUILIBRIUM EXHAUST PRODUCT COMPOSITION FROM A SOLID ROCKET PROPELLANT CONTAINING 12% PBAN - 88% AP

P_c = 1000 PSIA
T_c = 5461 R
3035 K
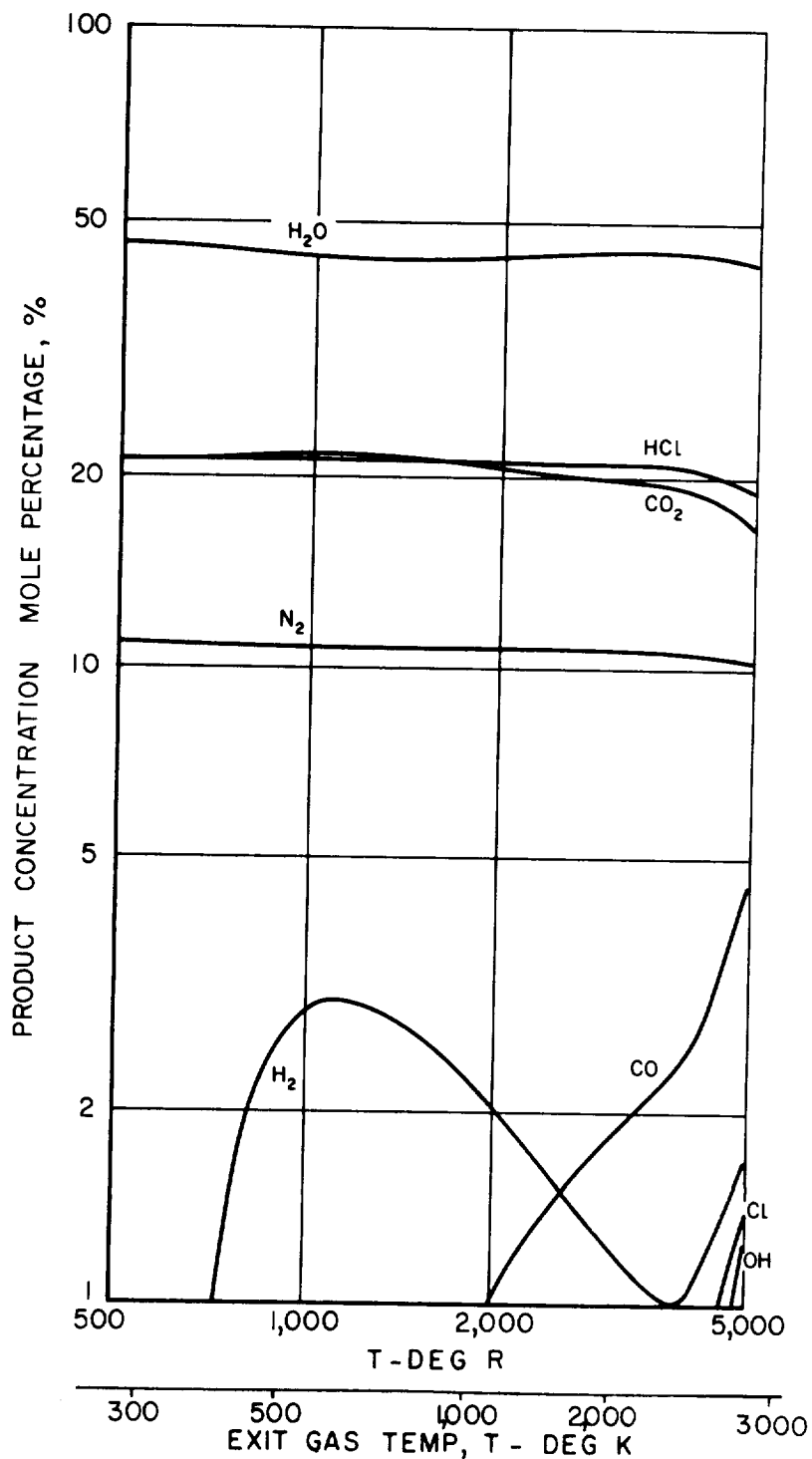
FIG. 92

EFFECT OF EXIT TEMPERATURE ON EQUILIBRIUM EXHAUST PRODUCT COMPOSITION FROM A SOLID ROCKET PROPELLANT CONTAINING 13% PBAN - 87% AP
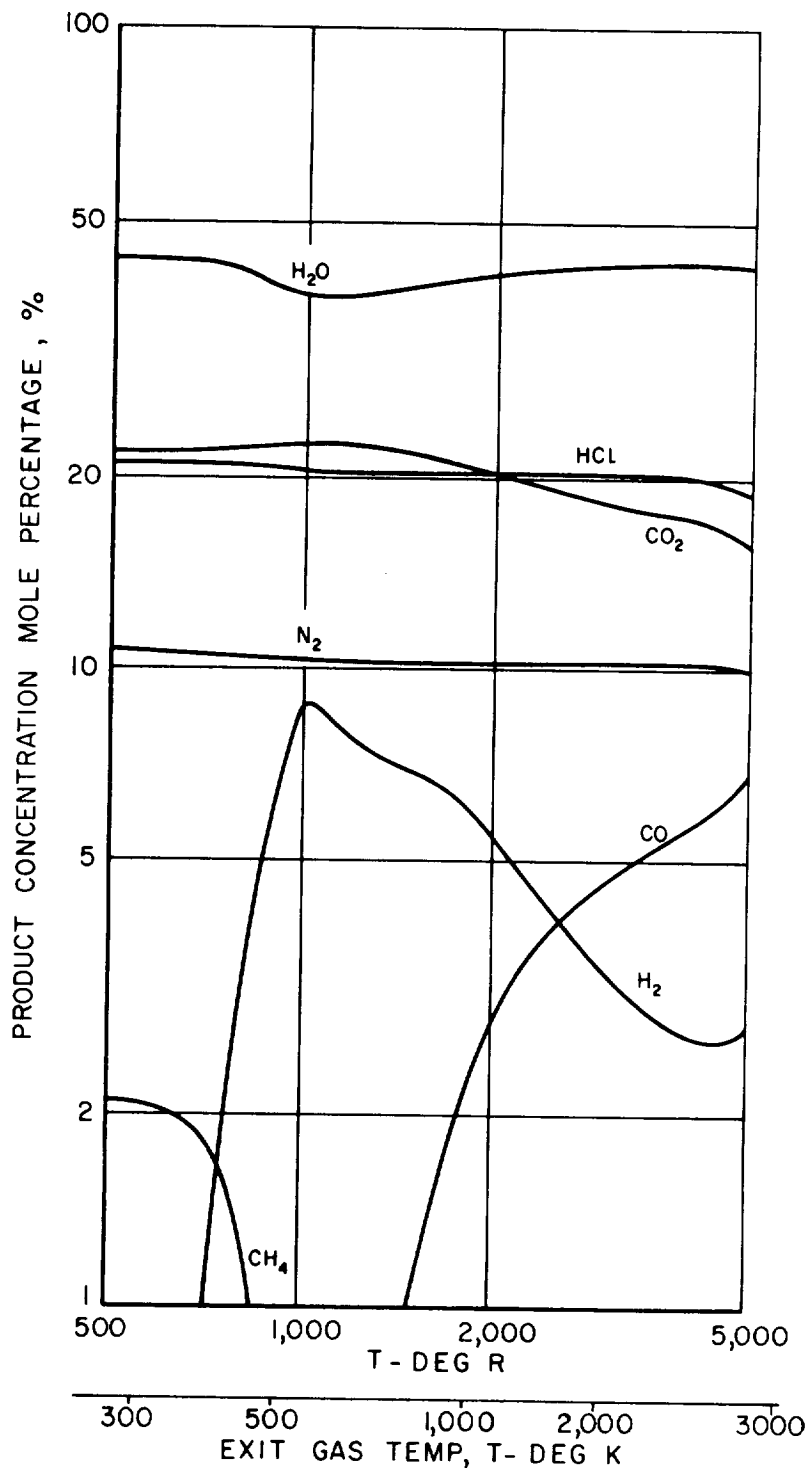
APPENDIX I

SELECTION OF SIMULATED COMBUSTION PRODUCTS

In order to select the composition of gases to simulate the environment of metals in a solid propellant rocket at the point of metal ignition, calculations were made of the equilibrium composition, both in the chamber and in the nozzle during expansion to room temperature, of mixtures of PBAN/AP with PBAN concentrations of 10 to 20 percent. Selected results indicating the effect of temperature on the equilibrium product concentration for PBAN concentrations of 10, 12, and 13 percent are shown in Figs. 90 through 92. The most desirable situation would permit the introduction to the test chamber at room temperature of gases which are stable up to the ignition temperature of the metal, with no intermediate changes in the composition as the metal wire sample temperature is raised. To achieve at 2800 K the composition resulting from the combustion of 10 percent PBAN, 90 percent AP (Fig. 90) would require starting with Cl_2, HCl, N_2, CO_2 and H_2O at room temperature, and heating through the range of composition changes shown in Fig. 90. However, the use of a reference composition containing Cl_2 is undesirable since it would prevent the attainment of one of the program objectives, i.e., prevent showing the effect of halogens on metal ignition and combustion. To simulate combustion products of solid propellants composed of PBAN/AP with PBAN concentrations of 12 percent or higher, the room temperature gas mixture should contain H_2O, HCl, CO_2, N_2 and CH_4 (Figs. 91 and 92; note CH_4 is below 1 percent for the conditions shown in Fig. 91). To achieve equilibrium with these gaseous mixtures at 2800 K, a series of sequential reactions must occur. These are:

$$(1) \quad 2H_2 + CH_4 \longrightarrow CO_2 + 4H_2 \quad \text{occurring below 600 K}$$

$$(2) \quad H_2 + CO_2 \longrightarrow CO + H_2O \quad \text{occurring above 600 K}$$

$$(3) \quad \text{dissociation of HCl, } H_2O, \text{ and } CO_2 \quad \text{occurring above 2200 K}$$

By starting with the basic composition shown in Fig. 91 for 12 percent PBAN and deleting the methane (ca. 0.7 percent), the resulting combination of 46.1 percent H_2O, 21.5 percent HCl, 21.4 percent CO_2, and 11.0 percent N_2 would be stable up to about 2200 K where the dissociation reactions are initiated. The use of this mixture in the experimental program is advantageous for several reasons. The gaseous mixtures which are in equilibrium in the calculated nozzle exhaust at room temperature cannot be in equilibrium throughout the entire chamber while the wire is heated since intermediate reactions must take place in the narrow zone around the wire where a high thermal gradient exists. By use of the suggested gas mixture not containing methane, these intermediate reactions will not occur. In other words, up to 2200 K at the wire, the equilibrium gas composition at the wire surface will be the same as that throughout the chamber, and dissociation near

134

the wire will occur only above 2200 K and to only a slight extent. If no methane is present, then from room temperature to 2200 K, the concentration of water is not critical in maintaining equilibrium. For this reason initial tests were made with dry HCl, CO_2 and N_2 in the ratio 39.9/39.7/20.4, with subsequent tests containing 0.07 and 46.1 percent H_2O together with HCl, CO_2 and N_2 in the above ratio or with CO_2 and N_2 in the ratio 39.7/20.4. All of these mixtures should be stable up to 2200 K.

Calculations were made of the theoretical equilibrium temperatures and reaction products of the adiabatic combustion of beryllium at 500 psia pressure in 39.9 HCl/39.7 CO_2/20.4 N_2 and 21.5 HCl/21.4 CO_2/11.0 N_2/46.1 H_2O mixtures. The calculated product concentrations are shown as a function of equivalence ratio in Figs. 88 and 89 and the calculated temperatures as a function of beryllium concentration in Fig. 87. Figures 88 and 89 show that the oxidizers are preferentially consumed in the order CO_2, H_2O, HCl, with N_2 being inert with respect to beryllium. The predominant reaction products are (in order of decreasing concentration) BeO, CO, and H_2 for the dry gaseous mixture and BeO, H_2, CO for the water-containing gas mixture. The horizontal sections of the temperature curve (Fig. 87) for H_2O-containing mixtures, correspond to the melting point of BeO. Note that the presence of large amounts of water not only raises the reaction temperature but extends the range of beryllium concentrations over which the temperature is maintained. The experimental (Therm-O-Scope) values of reaction temperature in no case exceeded the theoretical values for dry gases (see section of this report on Experimental Results).

APPENDIX II

DISTRIBUTION LIST

Addressee	Copies	Addressee	Copies

National Aeronautics & Space Administration
Western Operations Office
Jet Propulsion Laboratory
4800 Oak Grove Drive
Pasadena, California 91103
  Attn: (1) Robert McGill, Contracting Officer   1
        (2) Warren Dowler, Technical Manager   1

National Aeronautics & Space Administration
Washington, D. C. 20546
  Attn: (1) RPS/Robert W. Ziem   5
        (2) RPM/William Cohen   1
        (3) ATSS-AC/Technical Library   2
        (4) SV/V. L. Johnson   1
        (5) RV-1/C. Wood   1
        (6) RV/M. B. Ames   1
        (7) RC/J. L. Sloop   1
        (8) RP/A. O. Tischler   1
        (9) RTA/R. V. Hensley   1
     (10) RTP/J. J. Phillips   1
     (11) MGS/E. Hall   1
     (12) MTA/M. C. Waugh   1

National Aeronautics & Space Administration
Western Operations Office
1320 Pico Boulevard
Santa Monica, California 90405
  Attn: Eugene F. Wysocki   1

National Aeronautics & Space Administration
Langley Research Center
Langley Station
Hampton, Virginia 23365
  Attn: (1) Robert L. Swain   1
        (2) Technical Library   1
        (3) A. Saunders

National Aeronautics & Space Administration
George C. Marshall Space Flight Center
Redstone Arsenal
Huntsville, Alabama 35812
  Attn: (1) Alton L. Wheeler   1
        (2) Technical Library   1
        (3) R-PVE-PP/R. R. Eilerman   1

National Aeronautics & Space Administration
Manned Spacecraft Center
Houston, Texas 77058
  Attn: (1) Technical Library   1
        (2) J. G. Thibodaux   1

National Aeronautics & Space Administration
Lewis Research Center
21000 Brookpark Road
Cleveland, Ohio 44135
  Attn: (1) James J. Kramer   1
        (2) Technical Library   1
        (3) Dr. Richard J. Priem   1
        (4) Dr. Louis A. Provinelli   1

National Aeronautics & Space Administration   1
Goddard Space Flight Center
Greenbelt, Maryland 20771

Chemical Propulsion Information Agency
8621 Georgia Avenue
Silver Spring, Maryland 20910
  Attn: (1) Applied Physics Laboratory   1
        (2) T. W. Christian   1
        (3) Dr. R. H. Cantrell,
           The Johns Hopkins University   1
        (4) Dr. F. T. McClure,
           The Johns Hopkins University   1

Jet Propulsion Laboratory
California Institute of Technology
4800 Oak Grove Drive
Pasadena, California 91103
  Attn: (1) Technical Library   1
        (2) Winston Gin   1
        (3) L. Strand   1

Science and Technical Information Facility
NASA Representative
Box 5700
Bethesda, Maryland 20014
  Attn: CRT

Army Ballistic Missile Agency
Redstone Arsenal
Huntsville, Alabama
  Attn: Commander, ORDAB-HSI

Advanced Research Projects Agency
The Pentagon, Room 3D154
Washington, D. C. 20301
  Attn: Director, Technical Information Office   1

Department of the Air Force
Headquarters, USAF, DCS/D
Washington, D. C. 20545
  Attn: AFDRT-AS   1

Air Force Systems Command
Space Systems Division
Air Force Unit Post Office
Los Angeles, California 90045
  Attn: Col. H. Robbins   1

Air Force Systems Command
HQ 6593 Test Group (Development)
Edwards Air Force Base, California 93523
  Attn: Mr. Don Hart, Commander   1

Research and Technical Division (AFSC)
Bolling Air Force Base
Washington, D. C. 20332
  Attn: Dr. Leon Green Jr.   1

Air Force Ballistic Missile Division
HQ Air Research and Development Command
P. O. Box 262
San Bernardino, California
  Attn: Commander, WDSOT   1

Department of the Army
Office, Chief of Ordnance
Washington, D. C. 20545   1
  Attn: ORDTB

Addressee	Copies
Army Rocket and Guided Missile Agency U. S. Army Ordnance Missile Command Redstone Arsenal Huntsville, Alabama Attn: (1) Commander, ORDXR-OTL (2) Mr. Frank James	 1 1
Bureau of Naval Weapons Department of the Navy Washington, D. C. 20545 Attn: (1) Code RMMP-2 (2) Dr. O. H. Johnson (3) Mr. Richard F. Gott	 1 1 1
U. S. Naval Ordnance Test Station China Lake, California 93557 Attn: (1) Mr. Edward Price, Code 5008 (2) Technical Library	 1 1
Naval Ordnance Laboratory White Oak Silver Spring, Maryland Attn: (1) Mr. Carl Boyars (2) Technical Library	 1 1
U. S. Naval Ordnance Station Indian Head, Maryland 20640 Attn: (1) Technical Library (2) Lionel A. Dickenson (3) A. Camp, Commanding Officer	 1 1 1
Picatinny Arsenal Dover, New Jersey 07801 Attn: (1) Technical Library (2) J. Picard, Commanding Officer	 1 1
Institute for Defense Analyses 1666 Connecticut Avenue, N. W. Washington, D. C. Attn: Technical Library	 1
Aerojet-General Corporation P. O. Box 296 Azusa, California Attn: Librarian	 1
Aerojet-General Corporation P. O. Box 1168 Sacramento, California 95806 Attn: R. G. Weitz, Head Technical Information Center	 1
Aerojet-General Corporation P. O. Box 15847 Sacramento, California 95813 Attn: Mr. J. Wiegand	 1
Amcel Propulsion Company Subsidiary of Celanese Corporation of America 1026 17th Street, N. W. Washington, D. C.	1
Hercules Powder Company Allegany Ballistics Laboratory P. O. Box 210 Cumberland, Maryland Attn: Librarian	 1
Lockheed Propulsion Company P. O. Box 111 Redlands, California Attn: (1) Helen Ashman, Librarian (2) Dr. Ralph L. Coates	 1 1

Addressee	Copies
Rohm and Haas Company Redstone Arsenal Research Division Huntsville, Alabama Attn: (1) Librarian (2) Dr. William A. Wood	 1 1
Space Technology Laboratories, Inc. 5730 Arbor Vitae Street Los Angeles, California 90045 Attn: Mr. Robert C. Anderson	 1
Thiokol Chemical Corporation Elkton Division P. O. Box 241 Elkton, Maryland 21921 Attn: (1) Librarian (2) E. E. Hackman	 1 1
Thiokol Chemical Corporation P. O. Box 524 Brigham City, Utah 84302 Attn: (1) Librarian, Utah Division (2) R. Reed, Jr., Wasatch Division	 1 1
Thiokol Chemical Corporation Huntsville, Alabama 35807 Attn: (1) Technical Director, Redstone Division (2) L. A. Caveny, Huntsville Division	 1 1
Aerospace Corporation 2400 East El Segundo Boulevard El Segundo, California Attn: Librarian	 1
Hercules Powder Company Bacchus Works Magna, Utah Attn: Librarian	 1
Rocketdyne, Div. of North American Aviation, Inc. 6633 Canoga Avenue Canoga Park, California 91304 Attn: (1) Library, Department 596-306 (2) Dr. Robert B. Lawhead (3) R. V. Golding	 1 1 1
Rocketdyne, Div. of North American Aviation, Inc. Solid Propellant Operations P. O. Box 548 McGregor, Texas Attn: (1) Librarian (2) S. C. Britton	 1 1
Marquardt Corporation 16555 Saticoy Street Van Nuys, California Attn: Librarian	 1
Rocket Power/TALCO A Division of Gabriel Falcon Field Mesa, Arizona Attn: Librarian	 1
Atlantic Research Corporation Shirley Highway at Edsall Road Alexandria, Virginia 22314 Attn: (1) Librarian (2) R. Friedman	 1 1
Rocket Research 233 Holden Street Seattle, Washington Attn: Librarian	 1

137

Addressee	Copies	Addressee	Copies

Stanford Research Institute
Menlo Park, California 94025 — 1

University of California
Aerospace Engineering Department
P. O. Box 109
La Jolla, California   92038
  Attn: Mr. F. A. Williams — 1

Stanford Research Institute
333 Ravenswood Avenue
Menlo Park, California   94025
  Attn: M. Evans — 1

University of California
Chemistry Department
Berkeley, California   94620
  Attn: Mr. E. Peterson — 1

Olin Mathieson Chemical Corporation
Solid Propellant Operations
P. O. Drawer G
Marion, Illinois
  Attn: Librarian — 1

University of Utah
Department of Chemical Engineering
Salt Lake City, Utah   84112
  Attn: Dr. Norman W. Ryan — 1

Army Ballistics Research Laboratories
Aberdeen Proving Ground, Maryland   21005
  Attn: (1) Dr. Leland A. Watermeier, C.O.
       AMXBR-XAS — 1
      (2) Technical Library — 1

Princeton University
James Forrestal Campus Library
P. O. Box 710
Princeton, New Jersey   08540
  Attn: (1) Dr. Martin Summerfield — 1
      (2) I. Glassman — 1

Office of Naval Research
Navy Department
Washington, D. C.   20360
  Attn: Mr. Roland D. Jackel, 429 — 1

Martin Company
Denver Division
P. O. Box 179
Denver, Colorado   80201
  Attn: Mr. R. Knoll — 1

Air Force Rocket Propulsion Laboratory
Edwards Air Force Base, California   93523
  Attn: (1) Mr. Richard Spann — 1
      (2) C. E. Payne, RPMCP — 1

Cornell Aeronautical Labs
4455 Genesee Street
Buffalo, New York   14221
  Attn: Mr. G. Markstein — 1

Air Force Office of Scientific Research (OREP)
Propulsion Division
Washington, D. C.   20333
  Attn: Dr. Bernard T. Wolfson — 1

Stevens Institute of Technology
Mechanical Engineering Department
5th & Hudson Streets
Hoboken, New Jersey   07030
  Attn: Mr. R. F. McAlevy, III — 1

Allegany Ballistics Laboratory
Hercules Powder Company
Cumberland, Maryland
  Attn: Mr. T. A. Angelus — 1

Bellcomm, Incorporated
1100 17th Street, N. W.
Washington, D. C.   20036
  Attn: Mr. R. Sehgal — 1

Thayer School of Engineering
Dartmouth College
Hanover, New Hampshire   03755
  Attn: Dr. Alvin O. Converse — 1

CETEC Corporation
188 Whisman Road
Mountain View, California   94040
  Attn: Mr. R. Anderson — 1

Bolt, Beranek and Newman, Inc.
50 Moulton Street
Cambridge, Massachusetts
  Attn: Dr. Ira Dyer — 1

Arthur D. Little, Inc.
Acorn Park
Cambridge, Massachusetts   02140
  Attn: Mr. K. Bastress — 1

Brigham Young University
Provo, Utah   84601
  Attn: Dr. Marvin D. Horton — 1

Litton Systems, Inc.
Guidance & Control Systems Division
5500 Canoga Avenue
Woodland Hills, California   91364
  Attn: Mr. Robert O. Fleming, Jr. — 1

California Institute of Technology
1201 East California Boulevard
Pasadena, California   91109
  Attn: (1) Dr. Frank E. Marble — 1
      (2) Prof. B. H. Sage — 1
      (3) F. E. Culick — 1

Purdue University
School of Mechanical Engineering
Lafayette, Indiana   47907
  Attn: Dr. John R. Osborn — 1

University of California
Department of Aerospace Engineering
San Diego, California
  Attn: Dr. Stanford S. Penner — 1